

# POLITECNICO DI TORINO

Collegio di Ingegneria Meccanica e Aerospaziale

**Corso di Laurea Magistrale  
in Ingegneria Meccanica**

Tesi di Laurea Magistrale

MODELING AND OPTIMISATION OF ENERGY  
HARVESTING SYSTEM BASED ON  
PIEZOELECTRIC MATERIALS



**Relatori**

prof. BRUSA EUGENIO

**Candidato**

DONGMO TSIMI STEVE

Aprile 2020

## Introduction

Nowadays, microsystems are used in all equipment and in various fields. For example, we can use microsystems as sensors to place them in areas that are difficult to access when operating the equipment. From this context emerged the need to use energy-autonomous systems. These systems must be intelligent (intelligent hardware). Once mounted, they will no longer need human intervention for energy supply given their location. These systems will have to use energy in their immediate environment to be able to feed themselves.

In the environment, we can use several sources of energy, such as light energy that can be recovered by solar panels or mechanical energy recovered by the flow of material in a turbine. We can also recover vibratory energy thanks to the properties of piezoelectric materials. During their deformations, the piezoelectric materials produce electric charges and it is possible to recover these charges with a suitable circuit. For this work, the goal is to find a good circuit using the right method of condensation to optimize the recovery of car tires using a piezoelectric material. Use these powers to provide a powerful TPMS (Tire Pressure Monitoring System) battery to: send a signal to the smartphone.

Many microsystems use piezoelectric materials to dampen vibrations in SSD (Synchronized Switch Amorting) techniques and even for energy accumulation with SSH (Synchronized Switch Harvesting) techniques. These techniques are very interesting because they are energy independent. However, given the best conditions, they need optimization to be more profitable. To perform this modeling work and optimization of the energy recovery system from piezoelectric material, we will first perform a general study on energy recovery, why recover energy? Why vibratory energy? why use piezoelectric materials? On what principle does this energy recovery work? What are the sets that constitute a system of energy recovery by piezoelectric materials? Answering these questions will be the subject of our first chapter.

In the second chapter, we will focus on the circuits such as the optimal circuit to use to recover the vibratory energy with piezoelectric materials. By using a good circuit, the right material and a good method of condensation to minimize errors in our calculations, we will get a good result an optimal circuit. We begin this part of the operating principle of an RC circuit powered by an AC voltage source via a diode. At this circuit, we then add a coil, a diode bridge or a capacitor, to understand the role of all these elements in our circuit and their impact on the energy accumulated during the operation of the system. Then, we will replace our voltage source with an alternating current source connected in parallel with a capacitance, the latter being a representation of our piezoelectric element, doing the comparative studies we will see which circuit is adapted for the energy recovery. After having determined the optimal circuit, under the software COMSOL and thanks to the dynamic condensation technique proposed by M. Collet and KA Cunefare [1] using the good material, we will represent our piezoelectric element in which we will extract the necessary matrices at simulations on the circuit. Finally, we use our state system in our electrical circuit and it will represent our piezoelectric element on Simulink.

It should also be noted that our state system will have a force that will impose the deformations of our piezoelectric element and the voltage from the electrical recovery circuit connected to

the piezoelectric element via an electrode. That said, there will be a feedback between the electrical circuit and our piezoelectric. The electrical recovery circuit will impose a voltage to the piezoelectric and receive from the latter an electric charge which will then accumulated in the capacitor to supply other sources.

At the end of all, we will study some applications using existing piezoelectric material energy recovery systems in publications such as the pacemaker, shoes, buildings and bridge, TPMS (Tire Pressure Monitoring System) in order to see if our energy recovery at first is of the same order of magnitude as that of existing systems on the market in order to see what needs to be done to optimize it even more.

# Table of Contents

## Introduction

### Chapter I: General information on energy recovery

1. Application areas of energy recovery.
2. Energy Sources.
3. Conversion types.
4. Vibration Energy Harvesters (VEHs) operating principles

### Chapter II: Modelling and optimisation of energy harvesting circuit

1. Simple AC rectifier Circuit
  - 1.1. Diode
  - 1.2. Analytical Study
    - 1.2.1. At initial time  $t=0$ .
    - 1.2.2. For  $t \in ]0, \tau_1[$  The capacitor charge starts.
    - 1.2.3.  $\tau_1 < T/4$  with  $T=2\pi\omega$ .
    - 1.2.4. For  $t= \tau_1$  : The diode is on (Open circuit).
    - 1.2.5. For  $t \in [\tau_1, T/4[$  : Diode voltage decreases.
    - 1.2.6. For  $t=T/4$ : At this moment, the sign of generator voltage changes.
    - 1.2.7. For  $t=3T/4$ : The generator voltage become positive.
    - 1.2.8. For  $t= \tau_2 < T$ : The diode is off.
    - 1.2.9. For  $t \in ]\tau_2, \tau_3[$  : Capacitor charge for the second period ( $\tau_3 < 5/4T$ ).
    - 1.2.10. Energy harvesting calculation.
  - 1.3. AC rectifier circuit Simulation.
    - 1.3.1. Simulation Results of AC rectifier circuit.
    - 1.3.2. Results obtain changing resistance and capacitor values.
2. Modifications of our circuit on Simulink.
  - 2.1. Diode Bridge.
    - 2.1.1. Simulation of an RC circuit with the diode bridge.
  - 2.2. Effect of inductance.
    - 2.2.1. Theoretical study.
    - 2.2.2. Simulation Results.
3. Energy difference between AC Simple Diode Circuit, AC rectifier Circuit.
4. Circuit Synchronised Switch Damping (SSD), Synchronised Switch Harvesting (SSH).
  - 4.1. SSD and SSH presentation.
  - 4.2. SSD circuits.
    - 4.2.1. Results obtained with SSD.
  - 4.3. Recovery with RC Circuit.
  - 4.4. SSDI and SSHI Circuits.
  - 4.5. SSDV Circuit.

5. Energy comparisons between SSHI, SSHV, and RLC Circuits.
6. Mechanical System.
  - 6.1. Mechanical system Presentation.
  - 6.2. Use of the modal synthesis and condensation technique for a precise impedance's calculation.
    - 6.2.1. Technique description.
    - 6.2.2. Comsol procedure description.
  - 6.3. Frequency response function.
7. State system.
8. SSHI simulation With the piezoelectric elements
9. Applications.
  - 9.1. Tire Pressure Monitoring system (TPMS).
  - 9.2. Pacemakers.
  - 9.3. Others application.

References.

## Chapter I:        General information on energy recovery

### Introduction

With time, and a lot of investment in research, scientific evolution has increased in several areas. This evolution is guided by the desire of researchers to provide innovative and promising solutions. In the field of electronics, we see more and more the birth of devices consuming less energy and especially miniaturized. This miniaturization allows the use of electronic devices in all the equipment of the everyday life in order to control them or to receive the physical parameters as it is the case with the sensors. To receive the measured parameters, the researchers were able to develop networks of autonomous sensors communicating wirelessly. These wireless sensor networks find application in many areas of activity. Wireless sensor network (WSN) refers to a group of spatially dispersed and dedicated sensors for monitoring and recording the physical conditions of the environment and organizing the collected data at a central location. A wireless sensor network is made by a radio transceiver with an internal antenna or connection to an external antenna, a microcontroller, an electronic circuit for interfacing with the sensors and an energy source, usually a battery. The devices we want to study in this study have a well-limited power consumption of the order of 10  $\mu\text{W}$  to 100  $\mu\text{W}$  and the bulk of the energy supplied to the device is spent in wireless transmission. The miniaturization of these devices made so that they are used in hard to reach areas and this created a big problem for changing the batteries. It is therefore imperative to find new sources of energy in the immediate environment where microsystems are used to make these microsystems energetically autonomous.

### 1. Application areas of energy recovery

Research at the sensor level, for example, is guided by the need for scientists to know, analyse, measure and control the evolution of our natural environment in order to be able to affect it. Sensors have their applications in several application areas, particularly in the biomedical field where the implantation of autonomous sensors within the human body can collect physiological data, allowing remote monitoring of patients or so to make diagnostics and the disease prevention [1]. In the field of aeronautics where the electronic information capture functions, for the management of the aircraft are gathered under the acronym HUMS 'Health and Usage Monitoring Systems' here we need to measure several parameters such as the speed, the temperature, the state of the metal frame of the device. In the military field which is one of the first to make use of the sensors in order to determine the position of the enemy troops on a field of battle. In the civil field, the desire to know the state of health of the buildings. In the environmental field to determine natural disasters and prevent loss of life and property. In the industry for the control of the operation of industrial machines and the prevention of breakdowns contributing to the continuity of the service and thus to the productivity of

a factory. In the automotive sector, standards are becoming stricter on fuel consumption and manufacturers are turning more and more to other sources of energy consumption, research is focused on renewable energies, future are hybrid, electric. Looking at the number of patents filed in recent years in Europe, we see that car manufacturers are among the first brevet depositories. A car can have more than a hundred sensors; we need to master the parameters to lower fuel consumption. By using the wireless sensors, it saves on the weight of the car therefore the fuel consumption, identifying thanks to the temperature sensor the hot zones it is possible to better organize the cooling of the motor and to close the entrances of air this to a great advantage over fuel consumption. Wireless sensor networks are important for the automotive field and the most common application in the field of transportation is the tire pressure sensor called TPMS (Tire Pressure Monitoring Systems). But the problem of energy management within sensors remains.

## 2. Energy Sources

As an energy source, we can cite electrochemical energy. It is defined as “the energy which converts electrical energy to chemical energy and vice versa.” The electrochemical energy is related to fuel cells, photo electrochemical, and energy storage systems such as batteries, super capacitors or ultra-capacitors. The development of electrochemistry has led to the emergence of portable electronic devices. Several constraints remain to be solved, especially those related to limited autonomy and replacement or regular reloading, sometimes impossible when it comes to power buried appliances or in hostile environments like. To overcome these problems, one solution is to assist the operation of the battery by an energy recovery system that increases its autonomy. The battery then acts as an energy buffer that continuously stores the energy recovered from the surrounding environment and makes it available when necessary or when the stored energy level is sufficient. In the environment, we have several sources of energy; we can recover energy by radiant sources like solar Radiation sources and Radio frequency sources. With regard to the light radiation, we can recover energy with photovoltaic cells. The photovoltaic effect makes it possible to convert the light energy into electricity by means of a semiconductor material carrying the electric charges. Photons from the sun or another light source arrive on the surface of the semiconductor material tearing it out of the electrons. These electrons being excited go from the valence band to the conduction band creating a voltage where an electric current. The main limitation of energy recovery systems bright is its strong sensitivity to lighting conditions. The proliferation of radio transmitters in the current urban landscape allows for solutions where ambient radio frequency signals serve as an energy reservoir for mobile applications. The basic structure of a radio frequency energy harvesting system consists of a receiving antenna, matching circuit, peak detector, and voltage elevator. Where electromagnetic waves are captured by the antenna, voltage is amplified using the matching circuit, signal is converted to a voltage value thanks to the peak detector, and finally this voltage output is adjusted using the voltage elevator. Ambient radio frequency energy recovery systems, are very limited in power and require either a large receiving surface or to be very close to the source emitting. As environmental energy source, it is possible use vibration. Vibration is a mechanical phenomenon whereby oscillations occur about an equilibrium point. In many cases, however, vibration is undesirable, wasting energy and creating unwanted sound. For example, the vibrational motions of engines, electric motors, or any mechanical device in operation are typically unwanted. Such vibrations could be caused by imbalances in the rotating parts, uneven friction, or the meshing of gear teeth. Careful designs usually minimize unwanted vibrations. Vibration Energy Harvesting is the concept of converting vibration energy to electrical energy. It basically is as

simple as it sounds. This is possible through different technologies, like Electromagnetic Conversion, Electrostatic Conversion, and Piezoelectric Conversion.

Tableau 1 ENERGY SOURCES COMPARISONS

ENERGY SOURCES	POWER SUPPLIED
solar radiation	15 000 $\mu\text{W} \cdot \text{cm}^{-3}$
mechanical vibrations	300 $\mu\text{W} \cdot \text{cm}^{-3}$
thermal gradients	40 $\mu\text{W} \cdot \text{cm}^{-3}$

### 3. Types of conversions.

Vibrations of the surrounding medium can be used to recover energy by electromagnetism based on the movement of a permanent magnet inside a coil. This movement creates a current in the coil proportional to the variation of the magnetic flux in the coil, therefore proportional to the speed of the magnet, to the average magnetic field generated by the magnet in the coil and the surface of the turns. In 2008, Kulkarni et al. from the Tyndall National Institute [2] produced 3 prototypes of electromagnetic silicon generators based on slightly different structures for a volume of 0.1 cm<sup>3</sup>. The prototype consists of a magnet attached to a beam able to move between two planar coils figure a. This prototype generates a maximum power of 586 nW at 60 Hz for an acceleration of 8.83 ms<sup>-2</sup>

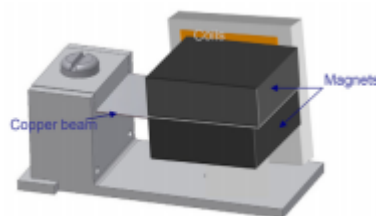


Figure 1. MEMS electromagnetic generators.

Electrostatic converters are capacitive structures made of two plates separated by air, vacuum or any dielectric materials. A relative movement between the two plates generates a capacitance variation and then electric charges. To start the charge cycle we need an external polarization source. In 2005, Despesse et al. Developed a macroscopic device (Figure 23(a)) able to work on low vibration frequencies and able to harvest 1mW for a vibration of 0.2G@50Hz [3]. This prototype has the highest power density of eVEH ever reached. Some other MEMS devices were then developed by Basset et al [4] (Figure 23(b)) and Hoffmann et al. [5].

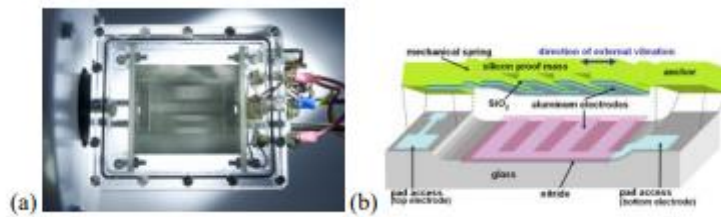


Figure 2. Electrostatic vibration energy harvesters from (a) Despesse et al. [3] and (b) Basset et al.

The piezoelectric converters generally consist of a recessed beam at one end on which are fixed one or more piezoelectric ceramics. The use of a beam makes it possible to improve the mechanical coupling of the structure by causing a high stress on the piezoelectric material. Thanks to the property of piezoelectric materials to electrically polarize under the effect of a stress (direct effect), piezoelectric converters can directly transform vibrations into electrical current. The company Mide technology [76] proposes a range of piezoelectric systems aimed at the supply of autonomous sensors on vehicles (helicopters, tire pressure ...), sensor networks deployed for industrial production monitoring, or implemented in oil and gas extraction and processing operations. For example, the generator "Vulture PEH25w", with a volume of 40.5 cm<sup>3</sup> allows to recover 4.5 mW at 40 Hz for an acceleration vibration 1g.

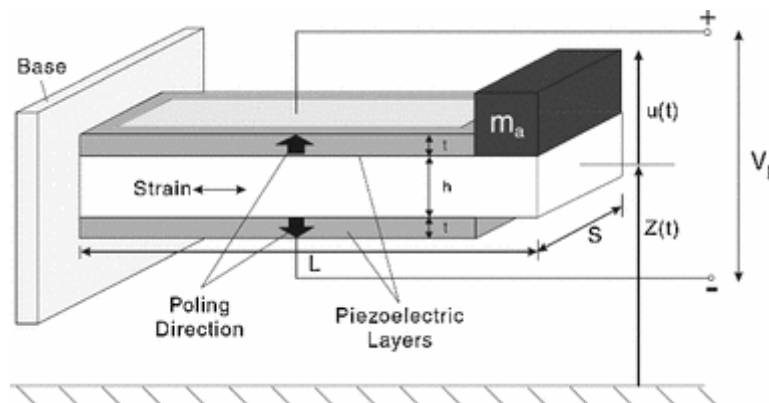


Figure 3. Piezoelectric vibration energy harvester

The table 1 shows us a comparative study of the different conversion systems. In this table, we can note the ease of integration of electrostatic systems, the low voltages produced by electromagnetic generators or the high output impedance of piezoelectric generators.

Table 2: Advantages and drawbacks of converters [7]

	Piezoelectric devices	Electromagnetic devices	Electrostatic devices
Advantages	<ul style="list-style-type: none"> <li>-high output voltages</li> <li>-high capacitances</li> <li>-no need to control any gap</li> </ul>	<ul style="list-style-type: none"> <li>-high output currents</li> <li>-long lifetime proven</li> <li>-robustness</li> </ul>	<ul style="list-style-type: none"> <li>-high output voltages</li> <li>-possibility to build low-cost systems</li> <li>-coupling coefficient easy to adjust</li> <li>-high coupling coefficients reachable</li> <li>-size reduction increases capacitances</li> </ul>
Drawbacks	<ul style="list-style-type: none"> <li>-expensive (material)</li> <li>-coupling coefficient linked to material properties</li> </ul>	<ul style="list-style-type: none"> <li>-low output voltages</li> <li>-hard to develop MEMS devices</li> <li>-may be expensive (material)</li> <li>-low efficiency in low frequencies and small sizes</li> </ul>	<ul style="list-style-type: none"> <li>-low capacitances</li> <li>-high impact of parasitic capacitances</li> <li>-need to control <math>\mu\text{m}</math> dimensions</li> <li>-no direct mechanical-to-electrical conversion for electret-free converters</li> </ul>

Our study will focus on the automotive field in which competition between automaker is becoming more and fiercer and or research patents are being filed more and more to improve comfort, reliability, fuel consumption and reduce the pollution. This is also driven by ever more stringent standards. To comply with these standards, the new cars are equipped with a hundred sensors the purpose being to know what is happening with the direct environment. For example by knowing the hottest areas in the hood of a car we can minimize the air intake and save fuel because the more air intake there is more the car is subject to the resistance of the car. Only to overcome the engine must turn, inducing greater energy expenditure. Our study is not at the hood, but at the car tire, because the pressure in the tire is important because knowing the pressure in the tire reduces fuel consumption and increases the life of the tire. To control the pressure in the tire on the market there is the TPMS module that is installed in the tire, the position of its module in the passenger compartment of the tire makes it is in an area difficult to access and therefore difficult for the replacement of the batteries, moreover it would not be possible to use the wires for this supply of the TPMS inside the tire. The problem with the use of wires to feed the sensors is at the level of the increase in labour costs, the weight of the wires to feed the sensors, and the impossibility of deploying the wires in all areas like in the tire. Because of these limitations, we are therefore obliged to find an autonomous source of energy for recharging batteries or a source in its direct environment that will ensure its power. As we saw earlier in the environment there are several sources of energy, but we should find one that is appropriate. Thus, solar energy and radio frequency energy are not suitable for making a pressure sensor autonomous in a car tire, unlike the energy of mechanical origin available during driving. Vibrations are numerous and present in a wheel, these vibrations are random, and depend on several factors such as centrifugal acceleration, the state of the road, the weight of the car. Although these vibrations are numerous, there are also several ways to transform vibratory energy into electrical energy. The electromagnetic converters, although robust, require a large voltage at the output and the electrostatic converters are difficult to develop as MEMS. Electrostatic converters have a good voltage output, they have a coupling coefficient easy to adjust, but we need to control the dimensions of equipment. We will use piezoelectric converters with a good voltage at the output, whose coupling coefficients depend on the materials already studied.

## 4. Vibration Energy Harvesters (VEHs) operating principles

In order to design and optimize a vibratory energy recovery system based on piezoelectric materials to feed a TPMS sensor of a car, in order to power it or to allow the recharging of the battery, we will study the different components of our recovery system. Our energy recovery system is made up of 2 large subsystems, a mechanical system operating on the principle mass traditional shock absorber spring to which we add a piezoelectric element in which is made the transformation of mechanical energy into electrical energy. And an electrical system consisting of an electric circuit and a battery or a capacitor as can be seen in FIG. 4

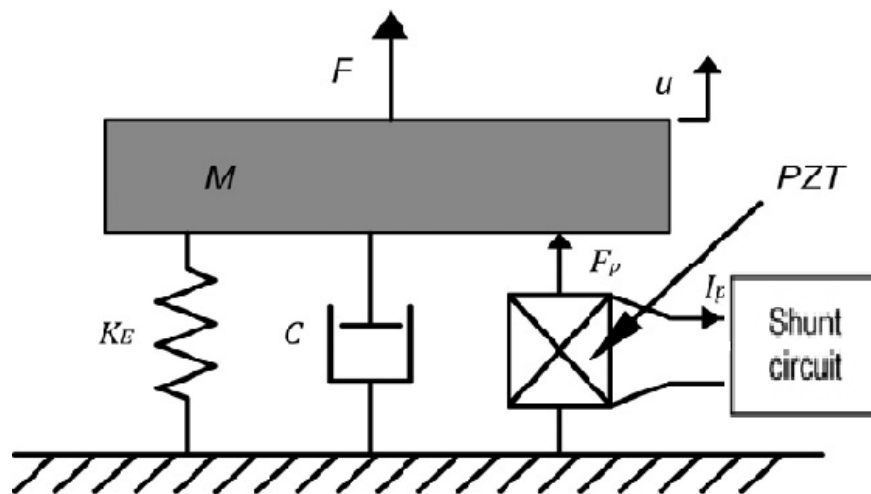
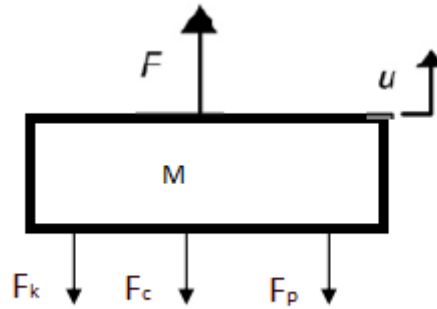


*Figure 4. Schematic representation of the electromechanical model for piezoelectric shunt damping. PZT: piezoelectric patch.[10]*

These inertial systems are conventionally designed by a mass-shock absorber system of the second order, as represented in FIGS. 2.1 (a) composed of a mass  $M$ , a stiffness spring  $K_E$  and a damper  $C$ . It is assumed that the system is excited around its resonance frequency by a force of constant amplitude applied to the frame:  $F = -M\ddot{y}$ . This excitation creates a relative displacement  $u(t)$  between the mass and the support, which will allow the conversion of the energy thanks to the piezoelectric transducer. This simplified model was developed for the first time by Williams and Yates [9].



Equations of motion

$F_p$ : Electric damping Force.

$F_c$ : Mechanical damping Force.

F: Internal acceleration force.

$F_K$ : Spring back force.

By applying the fundamental principle of dynamics, we have the following relation:

$$\sum \vec{F}_{ext} = \vec{0}$$

$$m\ddot{u} + F_K + F_c + F_p = F$$

$$m\ddot{u} + K \cdot u + C \cdot \dot{u} + C_e \cdot \dot{u} = F$$

$$m\ddot{u} + \dot{u}(C + C_e) + K \cdot u = -m\ddot{y} \quad \text{With } F = -m\ddot{y} = m \cdot Y_0 \cdot \sin(\omega t)$$

$$\ddot{u} + \frac{(C + C_e)}{m} \cdot \dot{u} + \frac{K}{m} \cdot u = Y_0 \cdot \sin(\omega t)$$

By integration, we have the steady state solution

$$u(t) = \frac{\omega^2}{\sqrt{\left(\frac{K}{m} - \omega^2\right)^2 + \left(\frac{C_e + C}{m}\right)^2}} Y_0 \cdot \sin(\omega t - \phi)$$

The amplitude of this movement depends on the amplitude of the input signal, the damping, as well as the difference between the resonant frequency and the vibration frequency.

Setting  $C_T = C_e + C$  the total damping coefficient,  $\phi$  is the phase and  $\omega_n$  is natural frequency.

$$\text{With } \phi = \tan^{-1}\left(\frac{C_T \cdot \omega}{K - \omega^2 m}\right), \omega_n = \sqrt{\frac{K}{m}}, C = 2m \cdot \xi_m \cdot \omega_n \text{ and } C_e = 2m \cdot \xi_e \cdot \omega_n$$

Electrical power can be define as:

$$P_e = \frac{1}{T} \int_0^T F_p(t) \cdot \dot{u}(t) \cdot dt = \frac{1}{T} \int_0^T C_e \cdot \dot{u}(t) \cdot \dot{u}(t) dt$$

Solving we have:

$$p = \frac{mY_0^2(\xi_e) \left(\frac{\omega}{\omega_n}\right)^6 \omega^3}{\left(2(\xi_e + \xi_m) \frac{\omega}{\omega_n}\right)^2 + \left(1 - \left(\frac{\omega}{\omega_n}\right)^2\right)^2}$$

The recoverable power depends on the mechanical damping, the electrical damping, the amplitude and the frequency of the ambient vibrations.

$$P_e = \frac{m.A^2.\xi_e}{4(\xi_e + \xi_m)^2 \omega_n} \quad \text{With } A = Y_0 \omega^2$$

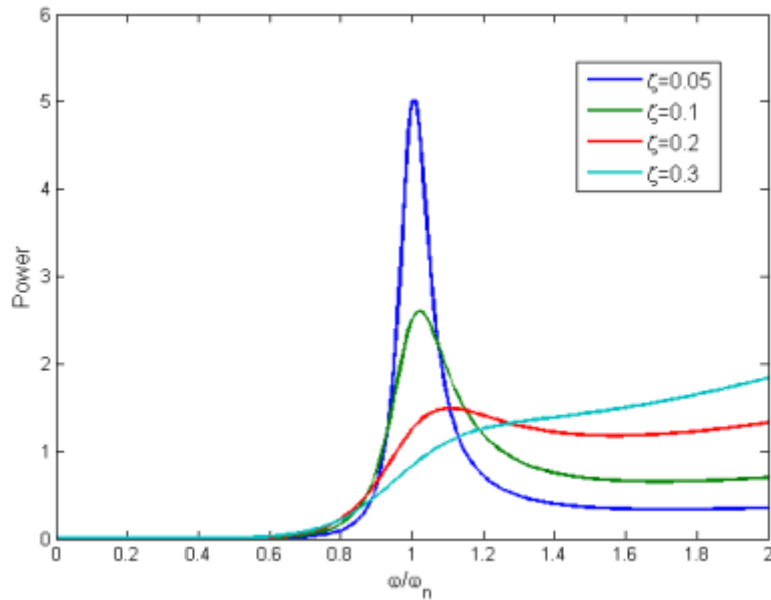


Figure5. Damping system power- frequency diagram

On the Figure 5 we can see that to maximize the output power, it is important to minimize the electrical damping coefficient, so increase the converter quality factor. However, the higher the quality factor of the structure, the narrower the system bandwidth becomes.

Studies on the vibration frequencies available in a car have already been the subject of several researches such as that carried out by Roundy [11] demonstrating that in the engine compartment, we can end up with frequencies close to 200HZ for vibrations having an acceleration of the order of 12 m / s. Tanner [12] studied the vibration frequencies according to the acceleration of 2 car models. From this study, we can see that the vibration frequencies in the car tire are very small for accelerations of 0.2g for example we have frequencies of 13HZ. Overall acceleration frequencies in the car are greater at the hood and do not exceed 1000HZ.

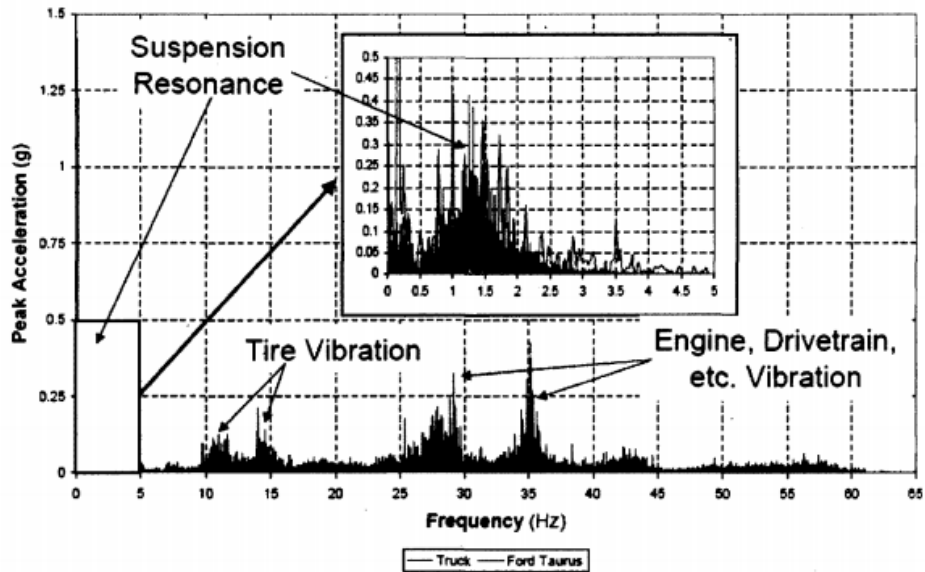


Figure 5. Accelerations spectrum available in two types of vehicles [12]

## Conclusion

At the end of this first chapter we have made a general introduction and a contextualization with regard to energy recovery systems, possible sources of energy recoveries as well as applications in which we can use the systems of energy recoveries. We are part of the general to the specific by making each time see why we chose to work on vibratory energy recovery systems and the difference compared to other systems as well as the physical principle and the equations governing the recovery energy system. In the following we will study in more detail the vibratory energy recovery circuits in order to have an optimal electrical circuit.

- [1] Karami, M.A, and Inman, D.J. (2011). Linear and nonlinear energy harvesters for powering pacemakers from heart beat vibrations. In Active and passive smart structure and Integrated Systems 2011. International Society for Optics and Photonics.
- [2] S Kulkarni, E Koukharenko, R Torah, J Tudor, S Beeby, T O'Donnell, and S Roy. Design, fabrication and test of integrated micro-scale vibration-based electromagnetic generator. Sensors and Actuators A : Physical, 145-146 :336–342, 2008.
- [3] Despesse G, Chaillout J J, Jager T, Léger J M, Vassilev A, Basrour S, Charlot B. High damping electrostatic system for vibration energy scavenging. Proc. sOc-EUSAI 2005:283- 6.
- [4] Basset P, Galayko D, Paracha A, Marty F, Dudka A, Bourouina T. A batch-fabricated and electret-free silicon electrostatic vibration energy harvester. IOP Journal of Micromechanics and Micro engineering 2009;19(115025). <http://dx.doi.org/10.1088/0960-1317/19/11/115025>
- [5] Hoffmann D, Folkmer B, Manoli Y. Fabrication and characterization of electrostatic micro-generators. Proc. Power MEMS 2008: 15.
- [6] Mide Technology. <http://www.mide.com>.
- [7] S. Boisseau, G. Despesse and B. Ahmed Seddik, Electrostatic Conversion for Vibration Energy Harvesting, Small-Scale Energy Harvesting, Intech, 2012
- [8] F. Cottone , Marie Curie Research Fellow, ESIEE Paris – University of Paris Est, [f.cottone@esiee.fr](mailto:f.cottone@esiee.fr) NiPS Energy Harvesting Summer School August 1-5, 2011.
- [9] C.B. Williams, R.B. Yates, "Analysis of a micro-electric generator for Microsystems", Sens. Actuators A: Phys 52, 8-11, 1996
- [10] E. Mustafa Qureshi. Representation-of-the-electromechanical-model-for-piezoelectric-shunt-damping. Researchgate Sept 2015.
- [11] Roundy, S., Wright, P. K. and Rabaey, J. (2003). A study of low-level vibrations as a power source for wireless sensor nodes. Computer Communications, volume 26, numéro 11, p.1131-1144
- [12] Tanner, T. (2007). Energy Harvesting Technology (Présentation PowerPoint). Adaptiv Energyè

# Table Of Contents

## Chapter II: Modelling and optimisation of energy harvesting circuit

1. Simple AC rectifier Circuit
  - 1.1. Diode
  - 1.2. Analytical Study
    - 1.2.1. At initial time  $t=0$ .
    - 1.2.2. For  $t \in ]0, \tau_1[$  The capacitor charge starts.
    - 1.2.3.  $\tau_1 < T/4$  with  $T=2\pi\omega$ .
    - 1.2.4. For  $t= \tau_1$  : The diode is on (Open circuit).
    - 1.2.5. For  $t \in [\tau_1, T/4[$  : Diode voltage decreases.
    - 1.2.6. For  $t=T/4$ : At this moment, the sign of generator voltage changes.
    - 1.2.7. For  $t=3T/4$ : The generator voltage become positive.
    - 1.2.8. For  $t= \tau_2 < T$ : The diode is off.
    - 1.2.9. For  $t \in ]\tau_2, \tau_3[$  : Capacitor charge for the second period ( $\tau_3 < 5/4T$ ).
    - 1.2.10. Energy harvesting calculation.
  - 1.3. AC rectifier circuit Simulation.
    - 1.3.1. Simulation Results of AC rectifier circuit.
    - 1.3.2. Results obtain changing resistance and capacitor values.
2. Modifications of our circuit on Simulink.
  - 2.1. Diode Bridge.
    - 2.1.1. Simulation of an RC circuit with the diode bridge.
  - 2.2. Effect of inductance.
    - 2.2.1. Theoretical study.
    - 2.2.2. Simulation Results.
3. Energy difference between AC Simple Diode Circuit, AC rectifier Circuit.
4. Circuit Synchronised Switch Damping (SSD), Synchronised Switch Harvesting (SSH).
  - 4.1. SSD and SSH presentation.
  - 4.2. SSD circuits.
    - 4.2.1. Results obtained with SSD.
  - 4.3. Recovery with RC Circuit.
  - 4.4. SSDI and SSHI Circuits.
  - 4.5. SSDV Circuit.
5. Energy comparisons between SSHI, SSHV, and RLC Circuits.
6. Mechanical System.
  - 6.1. Mechanical system Presentation.
  - 6.2. Use of the modal synthesis and condensation technique for a precise impedance's calculation.
    - 6.2.1. Technique description.
    - 6.2.2. Comsol procedure description.
  - 6.3. Frequency response function.
7. State system.
8. SSHI simulation With the piezoelectric elements
9. Applications.
  - 9.1. Tire Pressure Monitoring system (TPMS).
  - 9.2. Pacemakers.

9.3. Others application.  
References.

## 1. Simple AC rectifier Circuit

To understand the principle of charging a capacitor across a diode bridge we start by studying the charge of a capacitor using a single-wave rectifier.

This circuit consists of a series RC circuit, in series with a diode (figure 1.1). The capacitor will allow us to accumulate energy and this energy can be used when stopping the primary source. We are interested in the evolution of charge over time; the different steps of charging a capacitor how does the diode system help charge the capacitor. We will start by studying a simplified circuit RC connected in series with an alternating current generator, to study in an analytical way all the steps of the evolution of the voltages at the terminals of the generator and the diode system for a period in order to generalize. Next, we will simulate Simulink and see if the analytical model is identical to the simulations. Then we will evolve our model by adding different elements (Diode Bridge, switch, and inductor) and tell what is going on.

$$V=V_0*\cos(\omega t)$$

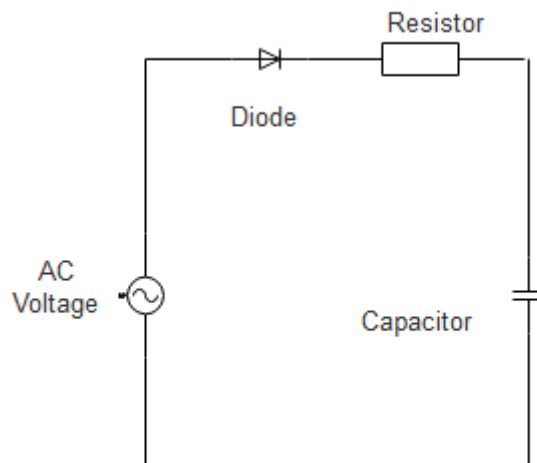


*Figure: 1.1 simple Ac rectifier circuit*

### 1.1. Diode

A diode is an electronic component that can behave like a switch in the circuit; it allows us to straighten the voltage. The ideal diode can be defined by a variable resistance resistor ( $R_d$ ) and a threshold voltage ( $V_s$ ) across the diode.

In our case, the voltage across the diode is:

$$V_d = V - (V_C + V_R)$$

$$\begin{cases} V_d = V_s & R_d = 0 & I_d = I > 0 & \text{the diode behaves as a Short circuit, diode is } \mathbf{off} \text{ or reverse biase} \\ V_d < 0 & R_d = \infty & I_d = I = 0 & \text{the diode behaves as an Open circuit, diode is } \mathbf{on} \text{ or forward biased} \end{cases}$$

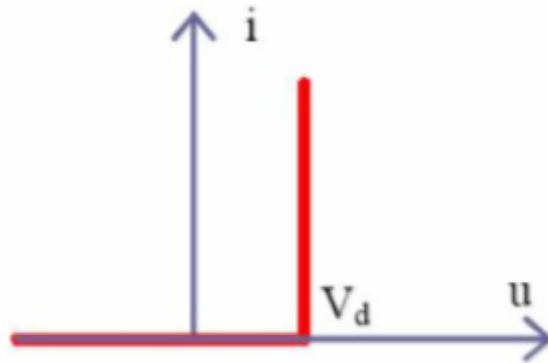


*Figure: 1.2 diode (I-U) curve*

## 1.2. Analytical study

On this part, we will divide our system into time intervals, repeated periodically. Over a period, we will see the evolution of the voltage across the capacitor ( $V_c$ ), the voltage across the diode ( $V_d$ ), at the end we will see the behaviour of the latter over time.

$$V_c = \frac{q_c}{c} \quad V_R = RI$$

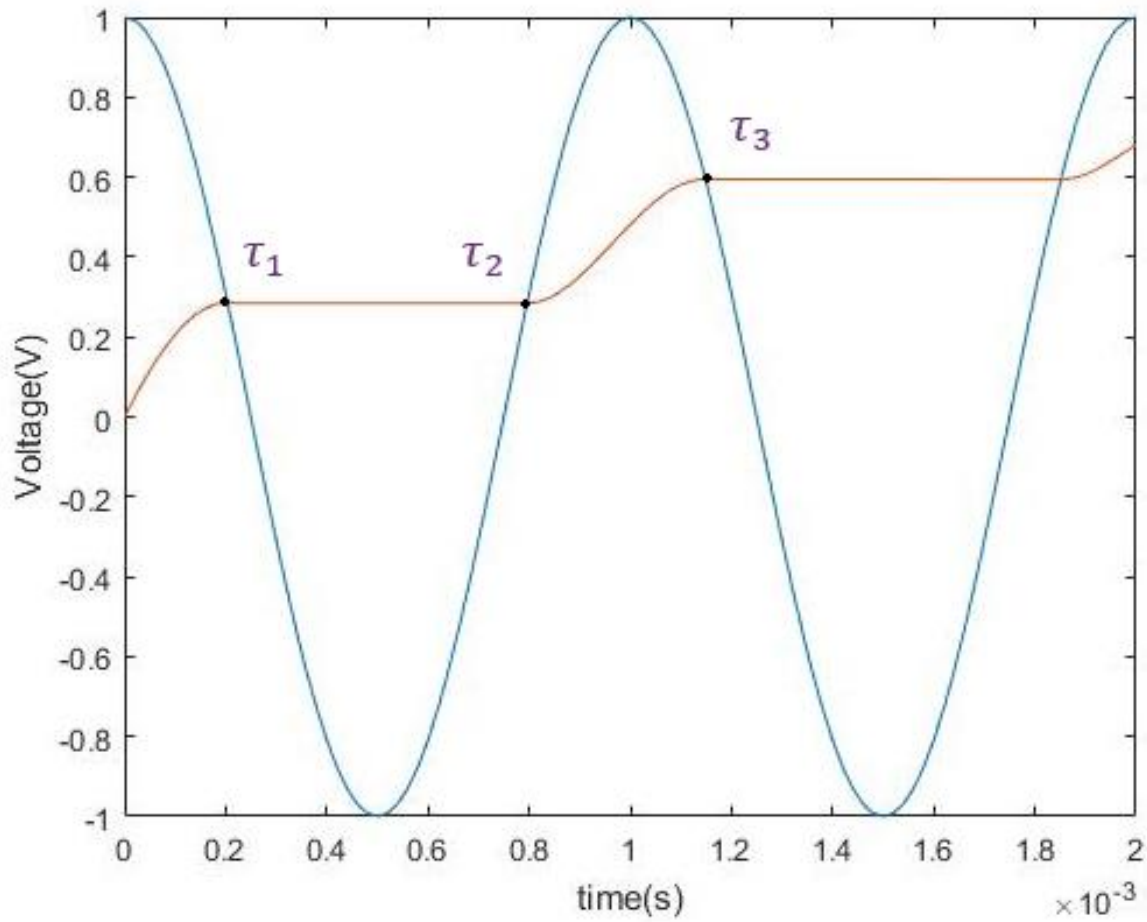


Figure 1.3 simple Ac rectifier circuit curve

### 1.2.1. At the initial time $t=0$

$$V(0) = V_0, \quad V_c(0) = 0, \quad Q_c(0) = 0, \quad V_d = V_s$$

The initial charge of the capacitor is zero; the voltage of the diode is equal to a threshold value appearing on its characteristics.

In this study we take in consideration that  $V_s = 0$  for the all process.

### 1.2.2. For $t \in ]0, \tau_1[$ : The capacitor charge starts

$$\tau_1 < T/4 \quad \text{with } T=2\pi\omega$$

$$V(t) = V_o * \cos(\omega t) > 0$$

$$V_d = V_s$$

$$V = V_R + V_c$$

$$Q_c = Q(t) + Q_k$$

$Q_k$ : Represents the amount of charge in our capacitor at the initial time.

For our case we take the capacitor discharged initially  $Q_k=0$ .

$$V_c = \frac{Q_c}{C}$$

$$V_R = RI$$

$$I = \frac{dQ}{dt} = \dot{Q}$$

$$V = V_0 \cos(\omega t)$$

$$\dot{Q} + \frac{Q}{RC} = \frac{V_0}{R} \cos(\omega t) - \frac{Q_k}{RC} \quad (1)$$

We still have to solve a first order differential equation (1) to determine the charge of the capacitor and deduce the capacitor voltage.

In order to resolve the equation, we multiply all the terms by  $e^{t/RC}$

$$e^{t/RC} \dot{Q} + e^{t/RC} \frac{Q}{RC} = e^{t/RC} \frac{V_0}{R} \cos(\omega t) - e^{t/RC} \frac{Q_k}{RC}$$

$$\frac{d}{dt}(Qe^{t/RC}) = e^{t/RC} \frac{V_0}{R} \cos(\omega t) - e^{t/RC} \frac{Q_k}{RC}$$

$$\int \frac{d}{dt}(Qe^{t/RC}) dt = \int_a^t (e^{x/RC} \frac{V_0}{R} \cos(\omega x) - e^{x/RC} \frac{Q_k}{RC}) dx$$

$$Q(t) = Ae^{-t/RC} + e^{-t/RC} \int_a^t (e^{x/RC} \frac{V_0}{R} \cos(\omega x) - e^{x/RC} \frac{Q_k}{RC}) dx$$

It is notified that  $f(x) = e^{x/RC} \frac{V_0}{R} \cos(\omega x) - e^{x/RC} \frac{Q_k}{RC}$  and when we make integration at the limit of  $f(x)$  we obtain  $F(a)=0$ .

$$Q(t) = Ae^{-t/RC} + e^{-t/RC} [Re(\int_a^t e^{x/RC} e^{i\omega x} \frac{V_0}{R} dx) - \int_a^t e^{x/RC} \frac{Q_k}{RC} dx]$$

$$Q(t) = Ae^{-t/RC} + e^{-t/RC} [\frac{V_0}{R} Re(\int_a^t e^{x(i\omega + \frac{1}{RC})} dx) - \int_a^t e^{x/RC} \frac{Q_k}{RC} dx]$$

$$Q(t) = Ae^{-t/RC} + e^{-t/RC} [V_0 C (\frac{1-ir\omega C}{1+R^2\omega^2 C^2})(\cos(\omega t) + \sin(\omega t)) - Q_k] e^{t/RC}$$

$$Q(t) = Ae^{-\frac{t}{RC}} + V_0 C (\frac{1-ir\omega C}{1+R^2\omega^2 C^2})(\cos(\omega t) + \sin(\omega t)) - Q_k$$

We resolve the problem at the initial condition to have the A value.

$$Q_c(t) = Ae^{-t/RC} + V_0 C (\frac{1-ir\omega C}{1+R^2\omega^2 C^2})(\cos(\omega t) + \sin(\omega t))$$

For  $Q_c(0) = 0$

$$A = \left( \frac{-CV_0}{1+R^2\omega^2C^2} \right)$$

$$V_c(t) = \frac{Q_c(t)-A}{C} e^{-t/RC} + V_0 \left( \frac{1-ir\omega C}{1+R^2\omega^2C^2} \right) (\cos(\omega t) + \sin(\omega t))$$

In this interval the capacitor charges.

RC and  $\omega$  values show us how fast the circuit is charging

- For very large RC values, we can see that the capacitor is charging very slowly.
- For very small RC values, the capacitor is quickly charged, and the voltage increases quickly.

### 1.2.3. For $t = \tau_1$ : The diode is on (Open circuit)

As the generator voltage decreases on time interval between 0 and  $T/4$ , there is a time  $\tau_1$  between 0 and  $T/4$  such that the voltage across the RC circuit reaches the value of the voltage of the generator. When  $t = \tau_1$  the diode is On and behaves as an open circuit.

$$V(t) = V_c(t)$$

$$V_0 \cos(\omega\tau_1) = \frac{A}{C} e^{-\frac{\tau_1}{RC}} + V_0 \left( \frac{1-ir\omega C}{1+R^2\omega^2C^2} \right) (\cos(\omega\tau_1) + \sin(\omega\tau_1))$$

We can find time  $\tau_1$  graphically or by calculation.

### 1.2.4. For $t \in [\tau_1, T/4]$ : Diode voltage decreases.

$$V(t) > 0$$

$$V_c(t) = V_c(\tau_1) = cste$$

$$V_d(t) = V(t) - (V_c(\tau_1) + RI)$$

$$I(t) = 0$$

$$V_d(t) = V_0 \cos(\omega t) - \left[ \frac{A}{C} e^{-t/RC} + V_0 C \omega \left( \frac{1-ir\omega C}{1+R^2\omega^2C^2} \right) (\cos(\omega t) - \sin(\omega t)) \right]$$

The voltage across the capacitor remains constant over this interval so the capacitor charge also remains constant and the voltage across the diode begins to change and decreases as it follows the voltage across the generator but is shifted down.

**1.2.5. For  $t=T/4$ : At this moment, the sign of generator voltage changes.**

$$V_c(t) = 0$$

$$V_c(t) = V_c(\tau_1)$$

$$V_d(t) = - \left[ \frac{A}{C} e^{-\tau_1/RC} + V_0 \left( \frac{1-ir\omega C}{1+R^2\omega^2 C^2} \right) (\cos(\omega\tau_1) + \sin(\omega\tau_1)) - \right. \\ \left. R(-A/RC) + RV_0 C \omega \left( \frac{1-ir\omega C}{1+R^2\omega^2 C^2} \right) \right]$$

At this moment, the sign of generator voltage changes from positive to negative.

**1.2.6. For  $t=3T/4$ : The generator voltage become positive.**

$$V_c(3T/4) = 0$$

$$V_c(3T/4) = V_c(\tau_1)$$

$$V_d(t) = - \left[ \frac{A}{C} e^{-\tau_1/RC} + V_0 \left( \frac{1-ir\omega C}{1+R^2\omega^2 C^2} \right) (\cos(\omega\tau_1) + \sin(\omega\tau_1)) - \right. \\ \left. R(-A/RC) + RV_0 C \omega \left( \frac{1-ir\omega C}{1+R^2\omega^2 C^2} \right) \right]$$

The generator voltage is positive, and the diode is always on.

**1.2.7. For  $t = \tau_2 < T$ : The diode is off.**

$$V(\tau_2) = V_c(\tau_1)$$

$$V_0 \cos(\omega\tau_2) = \frac{A}{C} e^{-\tau_1/RC} + V_0 \left( \frac{1-ir\omega C}{1+R^2\omega^2 C^2} \right) (\cos(\omega\tau_1) + \sin(\omega\tau_1))$$

$$\tau_2 = \omega \cos^{-1}(V_c(\tau_1)/V_0)$$

**1.2.8. For  $t \in [\tau_2, \tau_3]$  : Capacitor charge for the second period ( $\tau_3 < 5/4T$ ).**

$$V(t) > 0$$

$$V = V_R + V_c$$

$$Q_c(\tau_1) = Q_1$$

$$Q_c = Q(t) + Q_1$$

$$V_c(t) = B e^{-t/RC} + V_0 \left( \frac{1 - ir\omega C}{1 + R^2\omega^2 C^2} \right) (\cos(\omega t) + \sin(\omega t))$$

In order to have B value, we must resolve initial conditions. On that case, initial charge is not zero.

$$B e^{-\tau_2/RC} + V_0 \left( \frac{1 - ir\omega C}{1 + R^2\omega^2 C^2} \right) (\cos(\omega \tau_2) + \sin(\omega \tau_2)) = \frac{A}{C} e^{-\tau_2/RC} + V_0 \left( \frac{1 - ir\omega C}{1 + R^2\omega^2 C^2} \right) (\cos(\omega \tau_2) + \sin(\omega \tau_2))$$

The process repeats periodically until we reach a limit charge where the voltage is maximal this voltage is not more than generator voltage.

### 1.2.9. Energy harvesting calculation

During our work, we will deal with energy produced by the AC generator and we will calculate the energy harvested in the capacitor. in order to have them we need to apply these formulations:

$$P = VI$$

$$\text{provided energy} = \int_{t_i}^{t_f} V(t) i(t) dt \quad \text{Harvested energy} = \int_{V_c(t_i)}^{V_c(t_f)} C V_c dv$$

The efficiency depends on the diode because, without it, the capacitor will charge and discharge during one cycle. We are in an ideal circuit and we will not take in consideration, energy dissipated in the circuit due to the resistance during the flow of electron, and energy lose on the circuit components. We take into consideration that all the energy is transmitted to capacitor and Harvesting on it.

$$\eta = \frac{\text{Harvested energy}}{\text{provided energy}} = \frac{\int_{V_c(t_i)}^{V_c(t_f)} C V_c dv}{\int_{t_i}^{t_f} V(t) i(t) dt}$$

### 1.3. Simple AC rectifier circuit Simulation

We use Simulink as simulation software for our circuit. The purpose of this simulation is to see if the results obtained experimentally coincide with the analytical results introduced above, in this part we are interested in the different variations of the voltage curves across the capacitor, the diode, and the source. We simulate our RC circuit with an alternating voltage source of amplitude  $V = 1$  volt, connected to a resistance R that will be varied and to a

capacitor of capacitance  $C$ , which will also be varied from time to time for understanding what is happening in the circuit (Figure 1.1). In the following, we will add new elements to our circuit to understand what is happening and see the different changes. The Simulink schemes used is on the figure 1.4

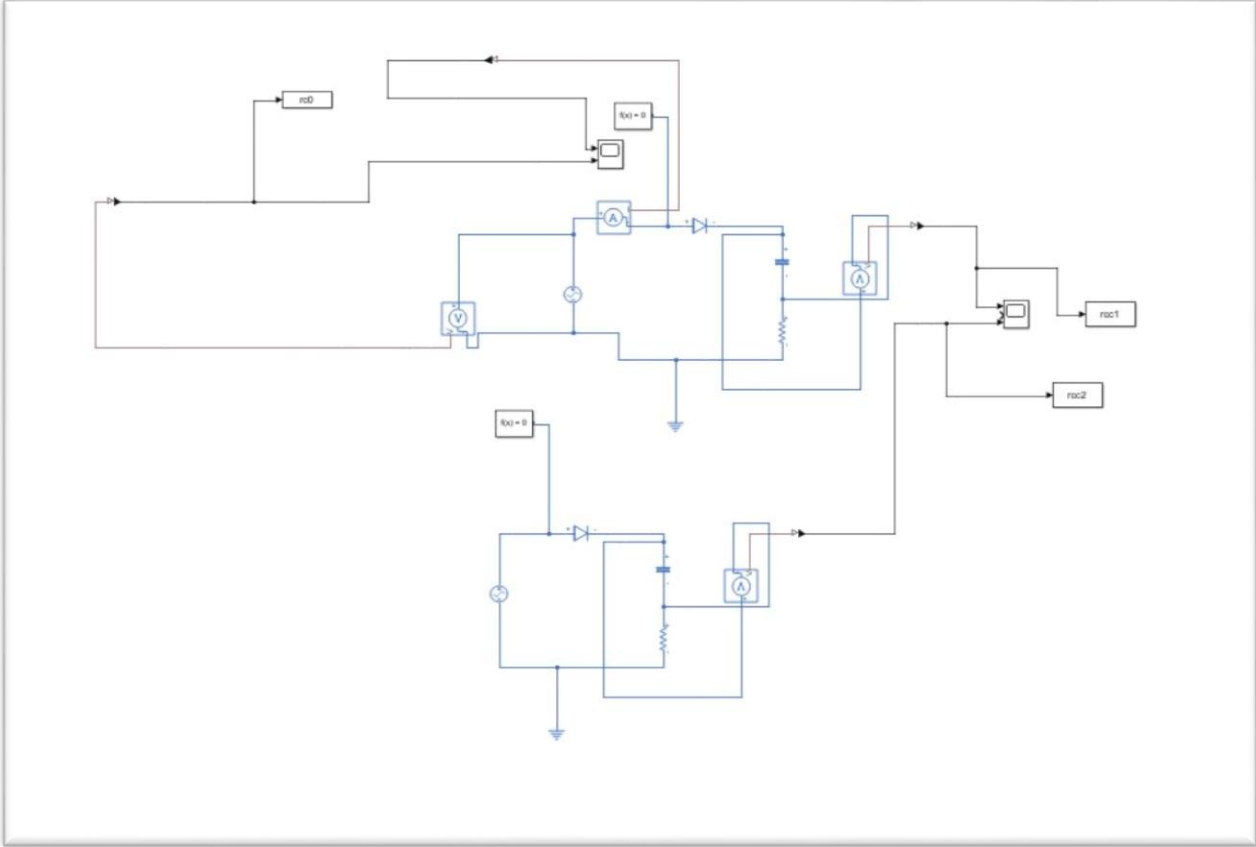


Figure: 1.4 Simulink simulation structure of simple diode RLC circuit

**1.3.1. Simulation Results of AC rectifier Circuit.**

This simulation is done for a duration  $Dt = 0.01s$  with a low resistance value  $R = 10 \text{ ohm}$  and a low capacitance value  $C = 4 \cdot 10^{-6}F$ .

After having simulated our circuit, we get the (figure 1.5) where the AC voltage across the diode and the voltage across the capacitor are represented.

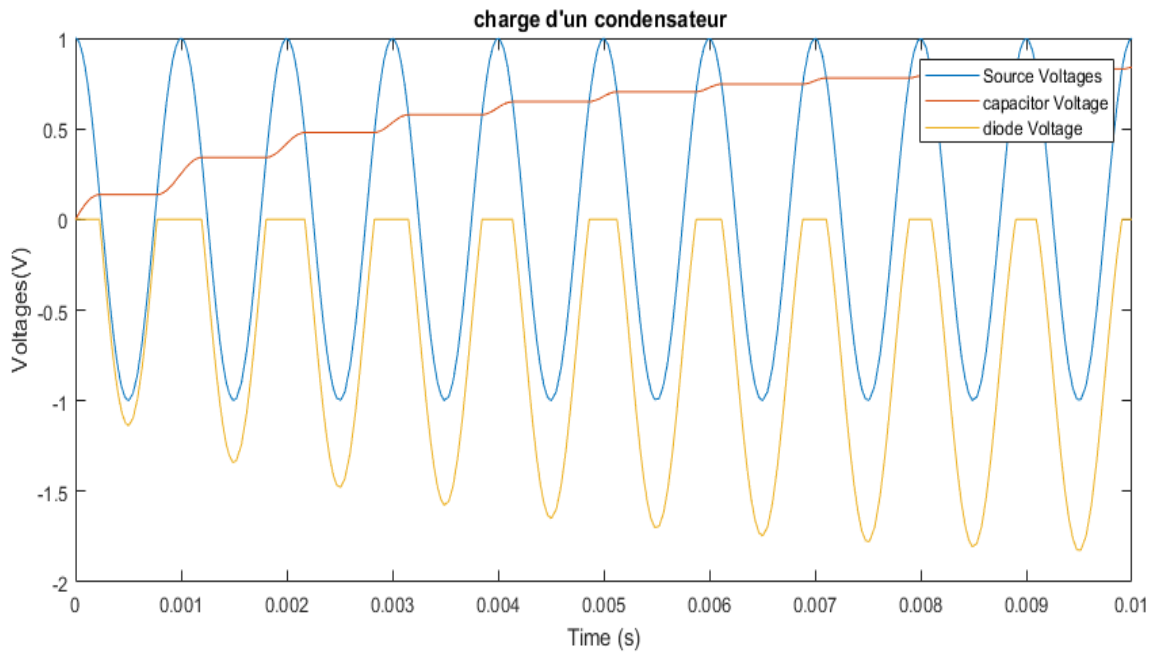


Figure 1.5 curve  $V(t)$  of an RLC simple diode circuit

After the simulation, we obtain the results predicted analytically on the first part. When our generator curve is positive, the capacitor is charged if the voltage across the capacitor is lower than the voltage across the generator.

For the rest of the time the capacitor does not charge and its voltage remains constant, the diode is blocking. When the diode is blinking all the charge sent by the capacitor is consumed in the diode. When the voltage across the capacitor reaches a threshold value equal to the maximum voltage sent by the voltage source, the capacitor stops charging.

It is possible see that for the negative curve of the generator not energy harvesting take place on the capacitor.

### 1.3.2. Results obtain changing resistance and capacitor values.

In this part, we have changed the values of the parameters  $R$  and  $C$ ; we wanted to see variation on the charge curve of the capacitor. The results are obtained in Figure 1.6. We can see that on the yellow curve we charged the capacitor using a simple alternating rectifier circuit with a resistance value  $R=1000$  Ohm and on the red curve we use a resistance value  $R = 100$  Ohm. The two curves are obtained by using a capacitor with capacitance value  $C_0 = 10^{-4}F$ , an AC current source with voltage value  $V=V_0 * \cos(\omega t)$ ,  $V_0=1V$ ,  $f=1000HZ$ , the simulation takes 5s.

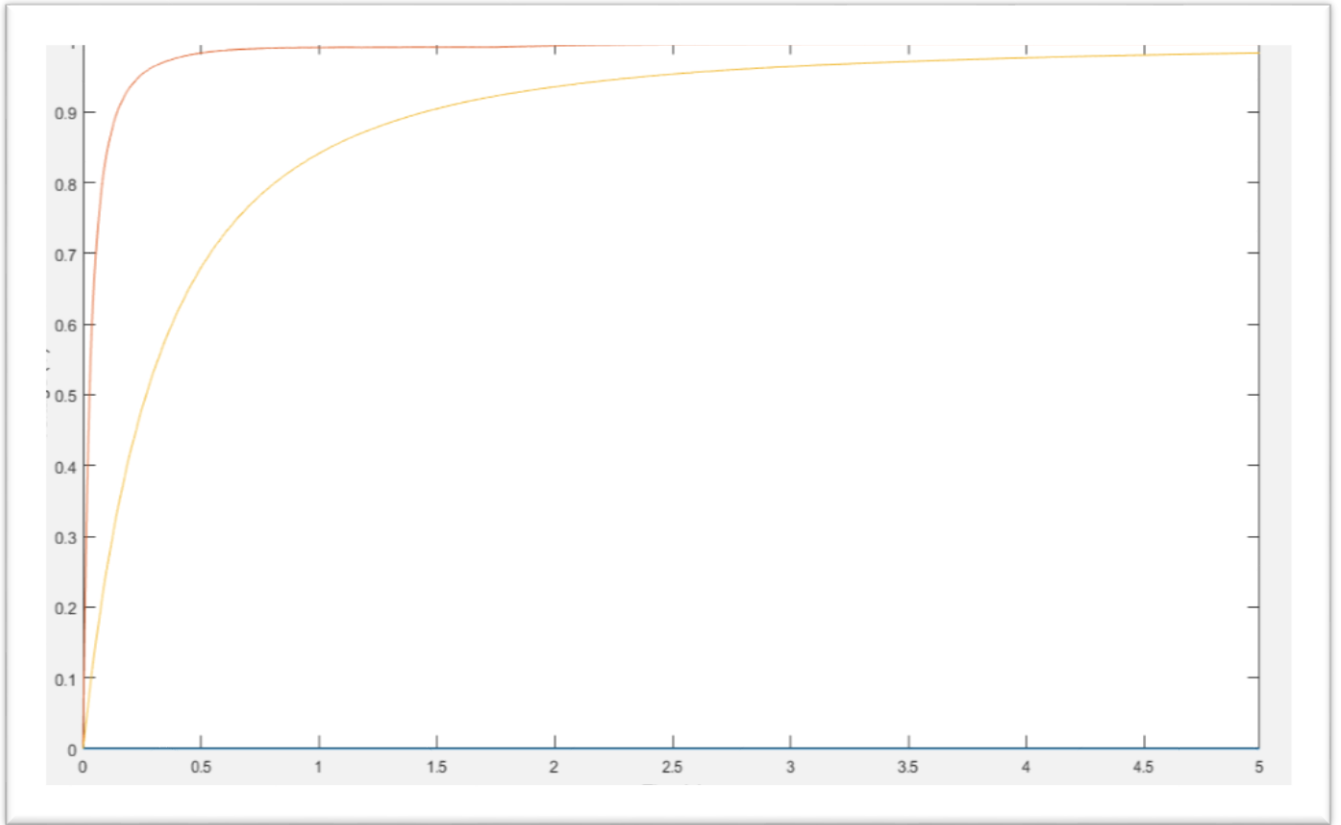


*Figure 1.6: curve  $V(t)$  of an RLC simple diode circuit by changing  $\tau$*

We can see that by changing the resistance value, the slopes of curves are not the same; the charging speed is not the same. When the parameter  $\tau = RC$  is big the capacitor charge is slow as we can see on the yellow curve (figure 1.4). However, when the parameter  $\tau$  is small, the charge of the capacitor is fast; we can see it on the red curve (figure 1.4).

The charge and the discharge of the capacitor are therefore a function of the parameter  $\tau = RC$ . The simulations have the same tendency as the results obtained with the analytical solution, so they are reliable. We will then evolve our circuit by adding several elements.

## 2. Modifications of our circuit on Simulink.

### 2.1. Diode Bridge.

The diode bridge is a full-wave voltage rectifier: its role is to restore the voltage seen by the capacitor, the latter sees only positive alternations and therefore charge at each alternation. The operation of a diode bridge is to transform our alternating current (AC) into positive alternating current at the capacitor. Figure 2.1 illustrates this phenomenon, or we can see that the sinusoidal incoming current comes out as having undergone an operation in absolute value.

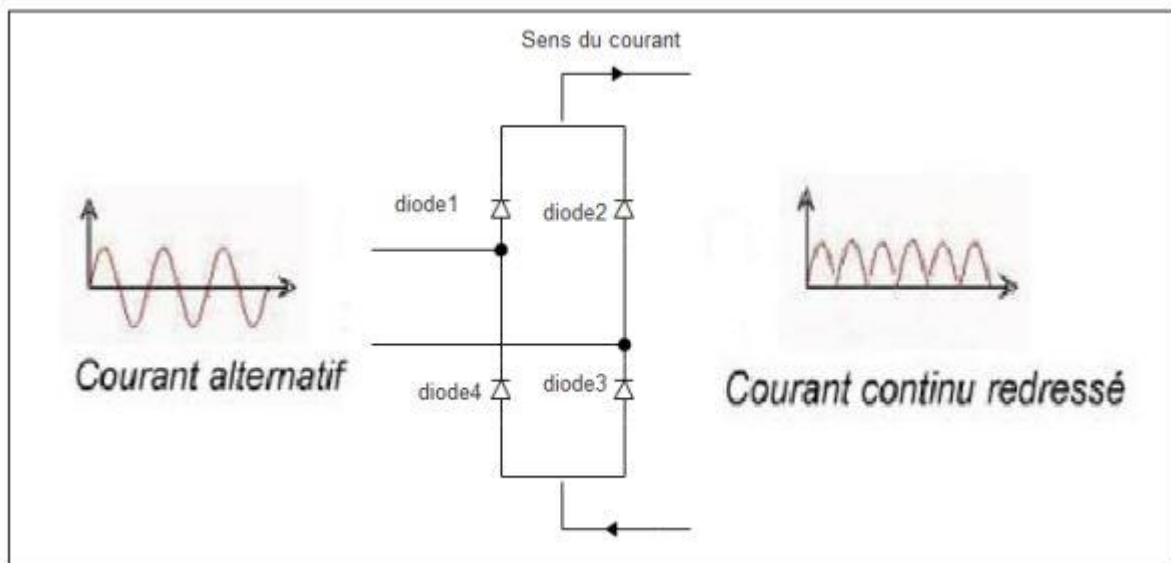


Figure 2.1: Diode bridge effect on the circuit

In the rest of our simulations, a diode bridge has replaced our diode.

We assume our diode bridge formed of identical diodes.

$$V_d = V_{diode1} = V_{diode2} = V_{diode3} = V_{diode4}$$

$$2V_d = |V| - (V_c + V_R)$$

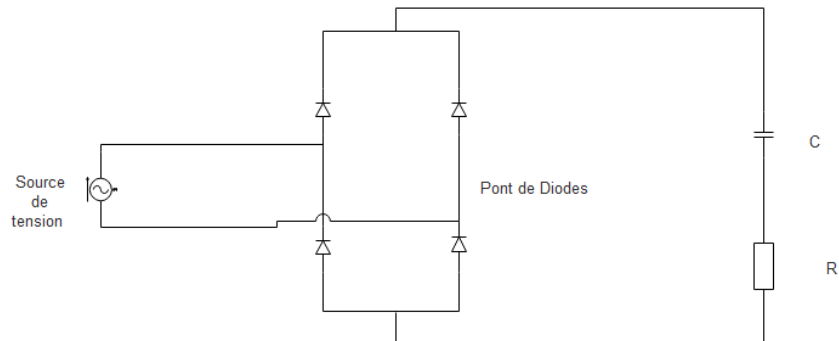
$$\text{For } \begin{cases} V_d > V_s \\ |V| > V_c \end{cases}$$

$$\text{For } \{ V \leq V_c$$

The difference at this level is that during the cycle, and on the analytic part, the positive alternation equations replaced the negative alternating parts.

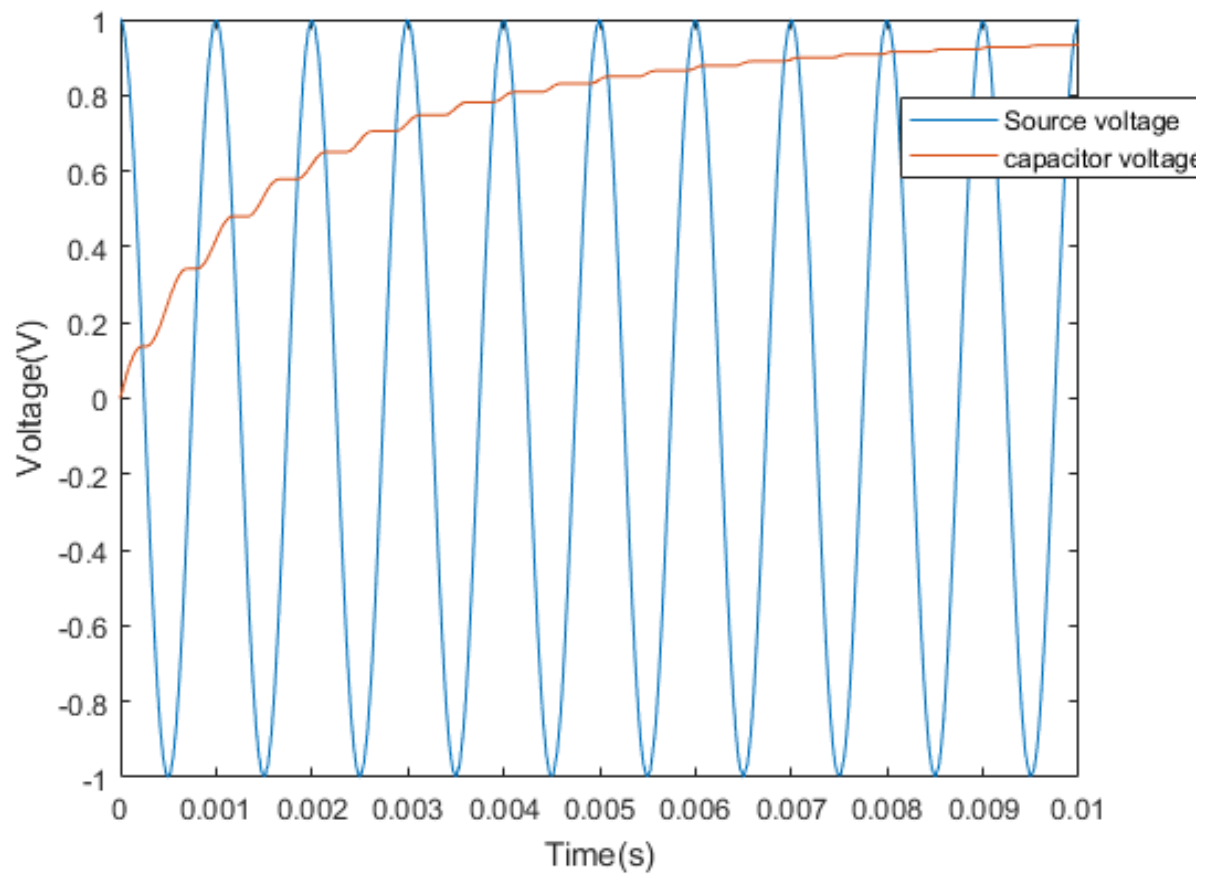
### 2.1.1. Simulation of an RC circuit with the diode bridge.

Figure 2.2 illustrates the block diagram of an RC circuit loaded via a diode bridge.



*Figure 2.2: Diode Bridge RC Circuit*

This simulation is done in order to look at the behaviour of the capacitor during its charge and for this reason we do a very short simulation for a duration  $t_f = 0.01s$  for a voltage  $V = 5v$  and a frequency  $f = 100Hz$ .



*Figure 2.3:  $V(t)$  curve result for a Diode Bridge RC circuit*

We can see that the capacitor charges at each alternation provided that the voltage across the capacitor is less than the absolute value of the voltage across the generator. The capacitor sees positive alternation at the place of negative alternation

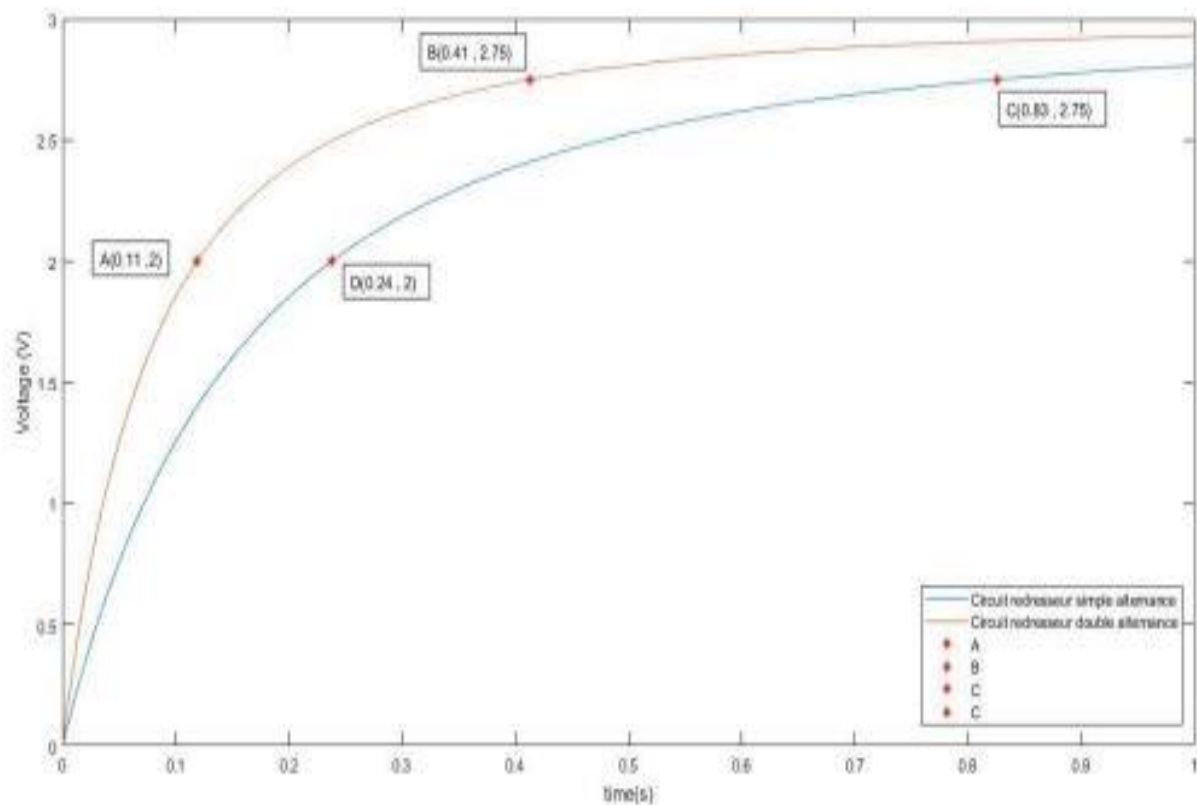


Figure 2.4:  $V(t)$  curves of simple rectifier circuit blue and Diode bridge circuit

Figure 2.4 illustrates the load curves of the capacitors of a rectifier circuit blue and the load curve of a capacitor via a diode bridge. We can see on the A and D points that gives us the times to charge and different voltages. It can be seen that the circuit consisting of the diode bridge charges almost twice as fast as the circuit without a diode bridge. We have taken the threshold voltage values of the diodes substantially equal to zero. But in reality, the diodes do not have voltage thresholds as small and we will have a lot of losses at the level of the diodes.

## 2.2. Effect of inductance.

The inductor aims to increase the current flowing in the circuit. By doing the equivalence with a mechanical circuit it plays the role of the damper, if it is well adjusted it allows us to see a load higher than that delivered by the source. We added an inductor to our RC circuit to see the different effects. We place the coil in series or in parallel as on (Figure 2.5) the goal being to see the effect of this coil for different value and depending on its positioning.

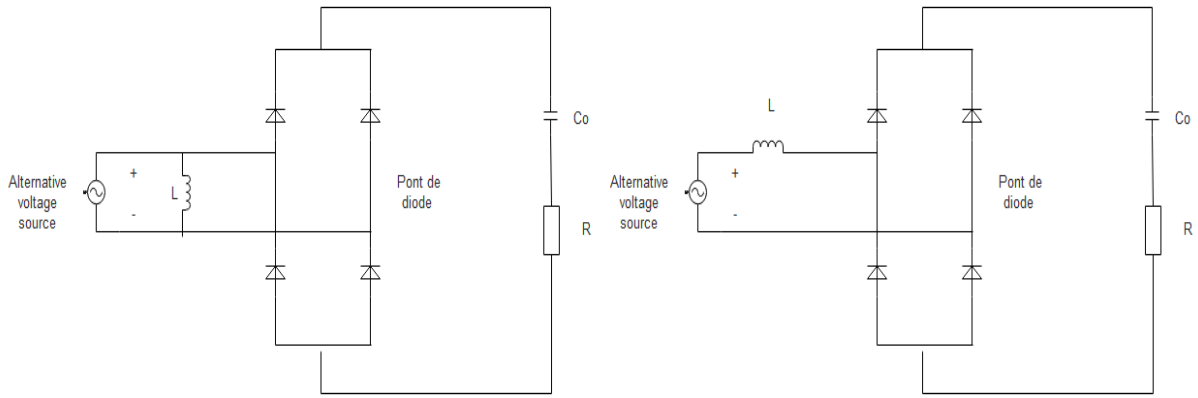


Figure 2.5: RLC parallel and RLC series circuit

### 2.2.1. Theoretical study

For an inductance parallel to the current source, the voltage across the coil is the same as the voltage across the generator.

$$V_L = V_R + V_C \quad \text{with } V = V_L = L \frac{d_i}{d_t}$$

For a series inductor, we add the damping to our system, which is a loss of energy; we would agree that our accumulated charge decreases.

$$|V + V_L| > V_R + V_C \quad \text{The capacitor is charging.}$$

$$|V + V_L| < V_R + V_C \quad \text{The capacitor is not charging.}$$

The maximal charge that our capacitor can take is  $V_{Cmax} = V_{max} + V_L$ .

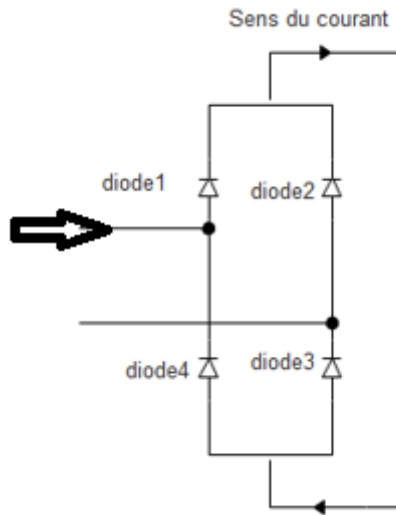
#### 2.2.1.1. For $t \in ]0, \tau_1[$ : The capacitor charge starts

$$\tau_1 < \frac{T}{4} \quad \text{With } T = 2\pi\omega$$

$$V(t) = V_o * \cos(\omega t) > 0$$

$$I(t) > 0$$

The diodes 1 and 2 are off, the diodes 2 and 4 are on.



$$V_L + V_R + V_C = V$$

$$\ddot{V}_c + \frac{R}{L} \dot{V}_c + \frac{1}{LC} V_c = \frac{1}{LC} V$$

$$Q = \frac{L\omega_0}{R} = \frac{1}{R} \sqrt{\frac{L}{C}}$$

Q= quality factor

Resolving the differential equation, we obtain.

$$\ddot{V}_c = \frac{\ddot{V}_0}{\left( \left( 1 - \left( \frac{\omega}{\omega_0} \right)^2 \right) + j \frac{\omega}{\omega_0} \frac{1}{Q} \right)}$$

$$\varphi(\omega) = \frac{Im(\ddot{V}_c)}{Re(\ddot{V}_c)}$$

The type of damping we will have solving this differential equation depend on Q.

### 2.2.1.2. For $t \in ] \tau_1, \tau_2 ]$ , the diodes are on (open circuit).

$$|V + V_L| < V_R + V_C$$

$$i(t) = 0$$

The capacitor no longer charges, and its voltage remains constant because of open circuit.

### 2.2.1.3. For $t \in ]\tau_1, \tau[$ , The capacitor is charging.

$$V(t) = V_o \cdot \cos(\omega t) < 0$$

The diodes 2 and 4 are Off, the diodes 1 and 3 are On.

$$i(t) < 0$$

$$-V_L + V_R + V_c = -V$$

$$-\dot{V}_c + \frac{R}{L} \dot{V}_c + \frac{1}{LC} V_c = |V|$$

It is the same than what we resolve for the first charge of the capacitor.

During all these steps, we will each time have an interval where the capacitor charges, an interval where the charge of the capacitor remains constant, until we reach the threshold voltage which is  $V_s$ .

$$V_s = V_{max} + V_L$$

### 2.2.2. Simulation Results.

We have done the simulation of our circuits of the figure 2.5 in order to be able to validate our theoretical study of the model and we obtained the results of simulation in figure 2.7. In this figure in yellow, we have the voltage across the capacitor connected in parallel, in red the voltage recovered at the capacitor when there is no coil connected, in purple the voltage when the coil connected in series. It should be noted that the yellow curve charge more for time less than 0,15s means that for very short period of time when coil are in parallel we recover a big voltage. In blue, we have the voltage at the terminals of the source and finally in purple we have the voltage across the capacitor for the coil connected in series.

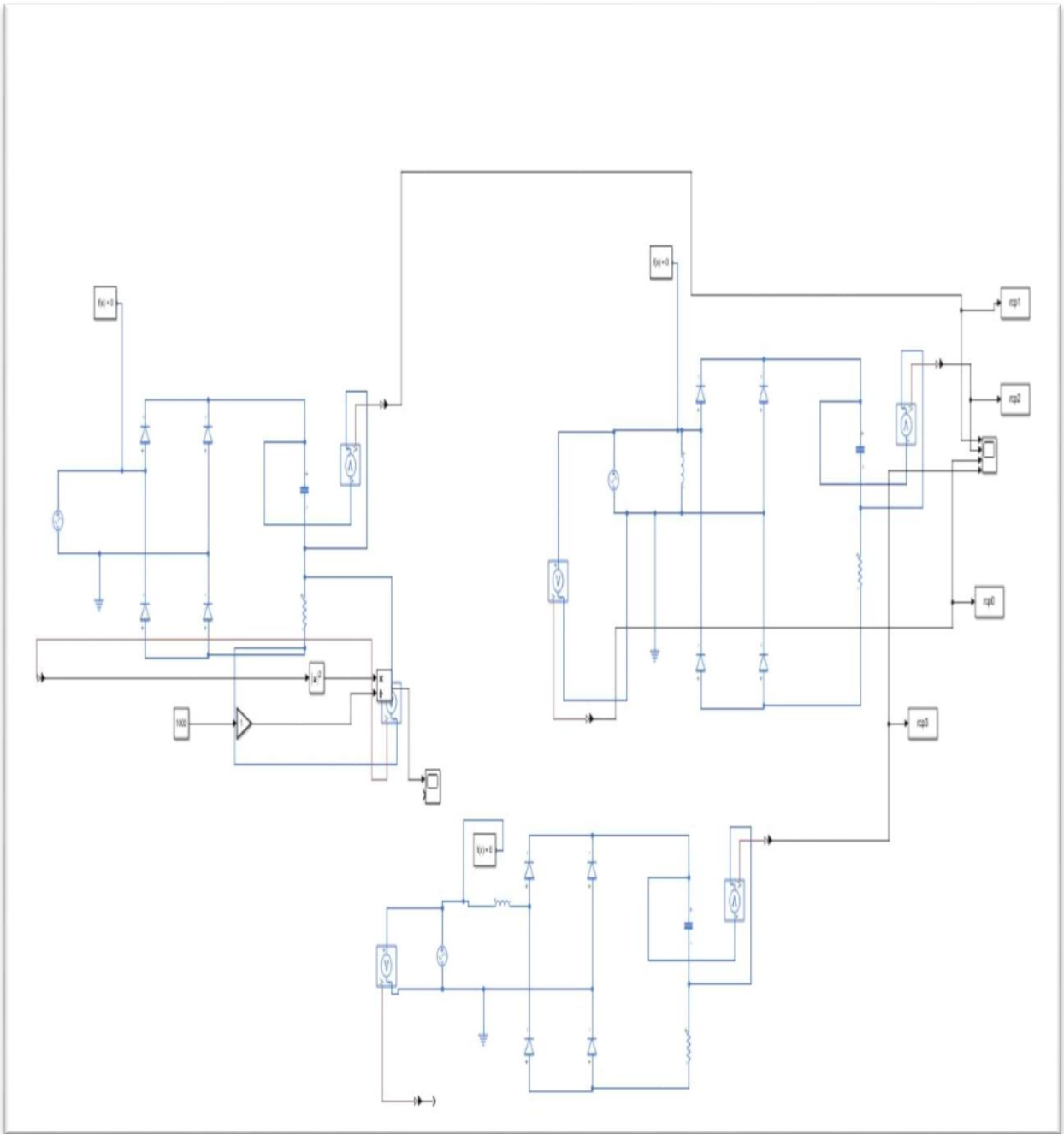


*Figure 2.6: Simulink circuit of Diode bridge RLC circuit*

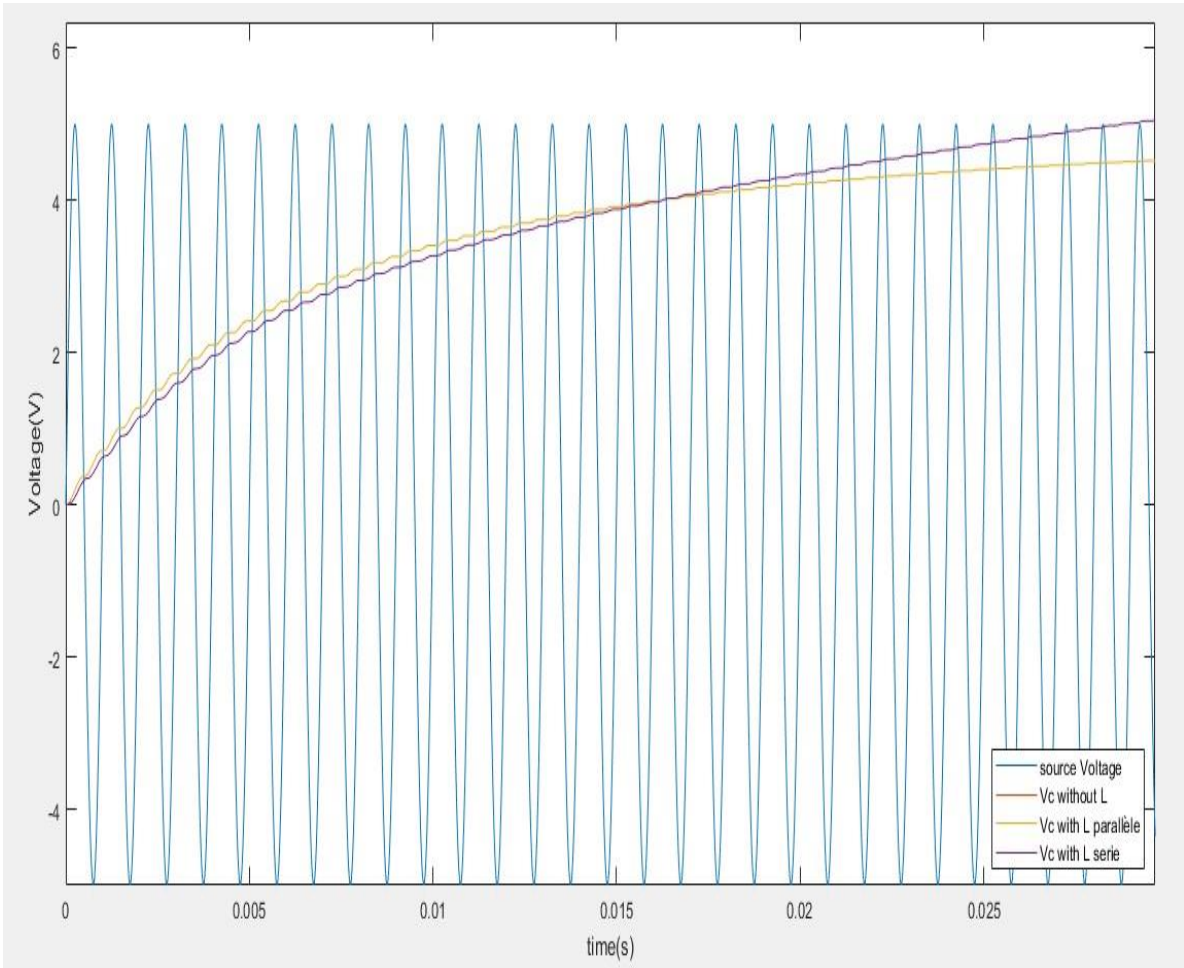
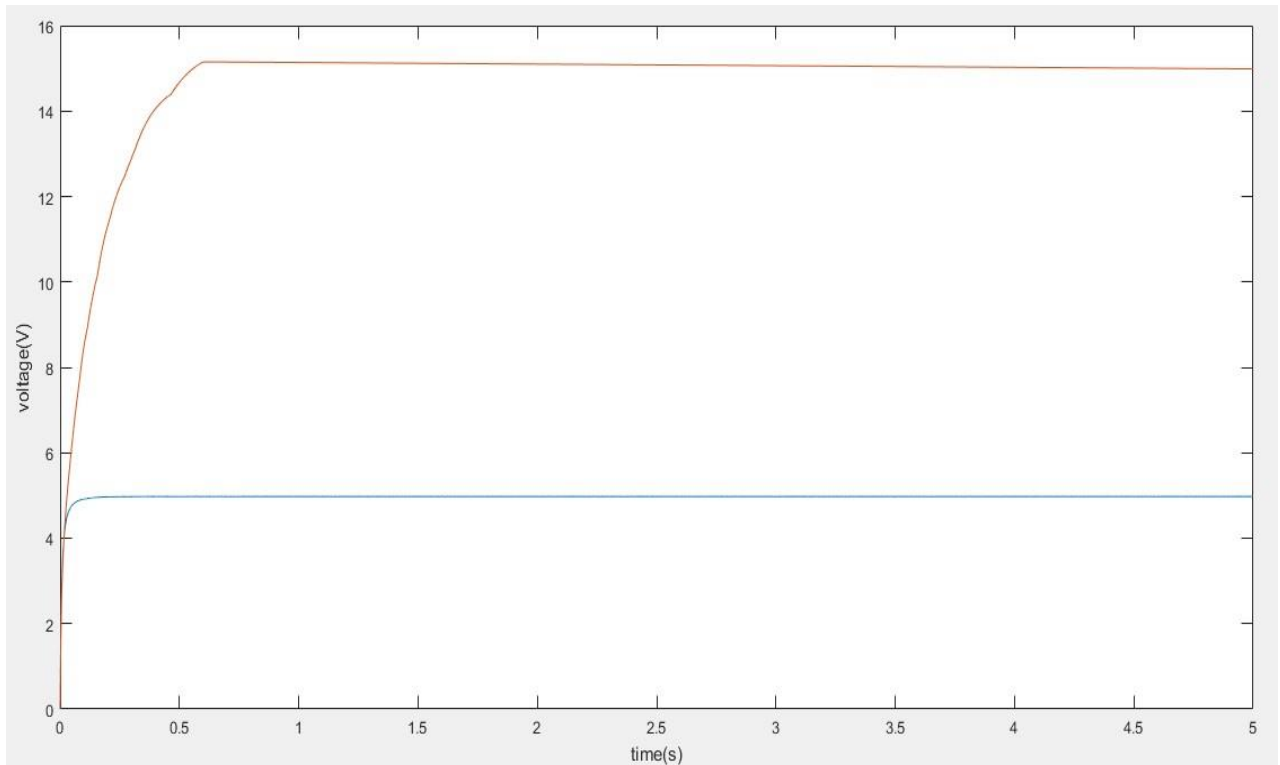


Figure 2.7: curve  $V(t)$  of RC, RLC series, RLC parallel circuits



*Figure 2.8: curve  $V(t)$  of RC, RLC series, RLC parallel circuits*

When we connect a coil in parallel with our circuit for a long period of time 4s as in our case illustrated in figure 2.8, the charge curve of the capacitor remains the same as when there was no coil connected, that is to say that the coil connected in parallel does not influence the charge seen by the capacitor during the different cycles this is illustrated by the yellow curve of Figure 2.8. But connecting a coil in series the charge level is increased, for an inductance  $L = 0.11\text{H}$  the charge level is increased, and the capacitor now sees a larger voltage value. The new voltage is  $V'_{\text{max}} = 15.5\text{V}$ . In the case of series coil, the inductance allows us to increase the accumulated voltage level (purple curve figure 2.8).

It is also important to precise that during our simulation, for low values of inductance there is no variation in the capacitor charge curve.

### 3. Energy difference.

In order to see the quantities of energy involved and harvested in capacitor with diode or diode bridge, we did simulation for a period  $\Delta T=5s$ , with voltage value  $V=5V$  from the AC generator. In our circuit, at the capacitor capacitance we take  $C_0=10^{-4}$ , the coil inductance is  $L=0.11H$ .

$$\text{Energy harvested} = 1/\Delta T \sum_{i=1}^n \frac{1}{2} C_o V_i^2 dt$$

With:  $dt=1/f/50$  simulation step

$\Delta T=5s$  duration of simulation

$T = 1/f= 0.001s$  simulation period

Energy Harvested with R=100 ohm / simple diode.	3.373557717987885 <sup>e</sup> (-08) KWh
Energy harvested with R=1000 ohm / simple diode.	2.804689221347982 <sup>e</sup> (-08) KWh
Energy harvested with R=1000 ohm / diode Bridge.	3.425882101386861 <sup>e</sup> (-08) KWh
Energy harvested with R=1000 ohm / diode Bridge / parallel coil L=0,11H.	3.425882101386861 <sup>e</sup> (-08) KWh
Energy Harvested with R=1000 ohm / diode Bridge / coil in series L=0,11H.	3.025844377989255 <sup>e</sup> (-07) KWh

*Table 1: Energy comparison*

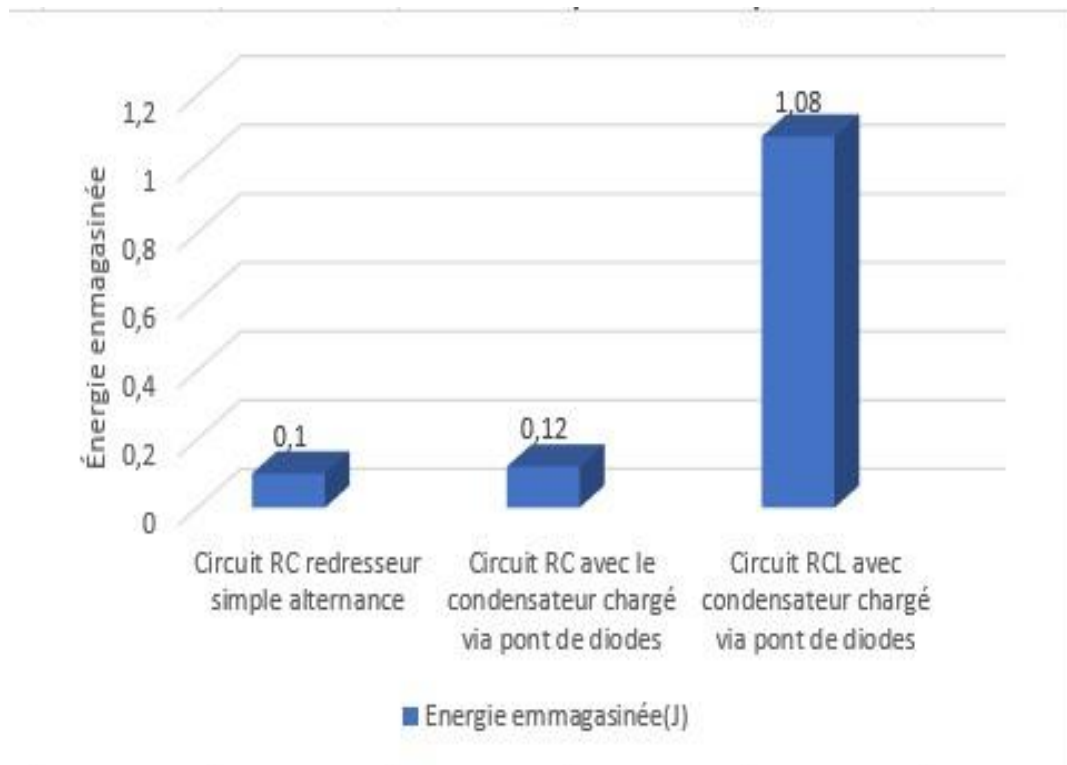


Figure 3: energy diagram of AC simple rectified circuit, Diode Bridge RC circuit, RLC Diode Bridge Circuit

On figure 3 we have the graph where we compared the energies harvested by RC circuit with a simple diode, by RC circuit with a diode bridge, by RLC circuit with diode bridge. We can see that when we charge with a simple diode, we have a small amount of energy harvested by with a diode bridge; this is because we just take positive part of wave's energy. We can also see that with the diode bridge the amount of energy is not two-time the energy accumulated with simple diode. We can also see that adding a coil energy harvested is more increased.

On that first part, we wanted to understand the charging process of a capacitor, by analytical studies after simulation, we verified the theories. By adding another element like diode bridge, coil, we see that it was possible increase energy harvested by our capacitor. We see that it is more important the way we insert these elements in our circuit. For example, adding a parallel coil our circuit is no longer changed, but adding series coil increase energy harvested. In addition, we see that capacitor is limited for energy harvesting because it can take a big amount of Energy.

For the next part, we will make simulation to study systems that are more complex. We will make complex system by adding a switch, we will change the source from the AC voltage source to piezoelectric system and at the end of all see, and how we can recover vibratory energy.

## **4. . Circuit Synchronised Switch Damping (SSD), Synchronised Switch Harvesting (SSH).**

### **4.1. Presentation**

The Synchronized Switch Damping (SSD) is a technique used to damp a dynamic system, this technique is between a passive damper and an active damper that both differ in that the passive damper is good, but it adds the mass to the system and the latter also has a problem due to the fact that it is limited by the change in rigidity of the system on which it operates. An active damper consumes a lot of energy; it can dissipate large vibrations over wide frequency bands. SSD uses piezoelectric elements to transform mechanical energy into electrical energy and vice versa, and to dissipate energy in the form of heat. The advantage of SSD techniques over active dampers is that they are energy independent. Our goal is to recover some of this energy during system vibration instead of dissipating it.

During the oscillations, when the displacement of our vibratory system is at the extremities, we close the electric circuit for a very short time (one half of the period of the mechanical system considered for an optimal recovery), and the rest of the time the electrical circuit remains open. During this period, the charge stored in the piezoelectric element is transmitted to the electric circuit. Depending on the elements connected to our circuit, we will have the Synchronized Damping Switch on Short (SSDS) when the shunt circuit has a resistor that dissipates the load, the Synchronised Switch Damping on Inductance (SSDI) when the circuit has an inductance that accumulates the load then sends it back to the system to dampen the vibrations, and the Synchronised Damping Switch on Voltage (SSDV) when the circuit has an additional DC voltage source to help dampen the vibrations.

The Synchronized Switch Harvesting (SSH) is the name given to the techniques of energy recovery, the operating principle is based on that of the SSD techniques. The difference is that instead of dissipating energy, it is instead stored in a capacitor.

### **4.2. SSD Circuits**

We first represent our piezoelectric material by an ideal current generator (0.001mA) connected in parallel to a capacitor of low capacitance (40nF). By using an ideal current generator, we do not consider the fact that our circuit imposes a voltage on the piezoelectric element before receiving an electric current from it, the feedback of the electrical system on the mechanical behavior is not taken into account. The circuits representing the SSDS and an RC circuit connected to the terminals of the piezoelectric element through a bridge of diodes are represented on the following figure (Figure 4.1):

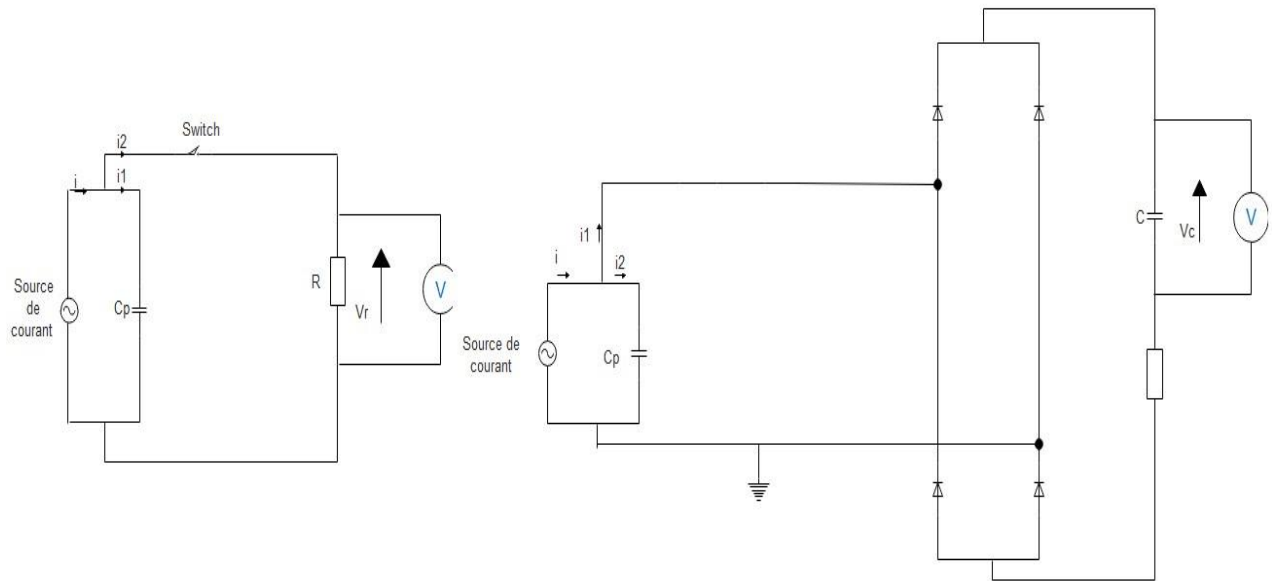


Figure 1.4: a) SSDS Circuit b) RC Diode Bridge Circuit

In figure 4.1 (a), we have a switch between the piezoelectric and resistor (our resistor has a low value, 7 Ohm), which serves to dissipate the current accumulated in the capacitance  $C_p$  of the piezoelectric allowing us to dissipate the energy in the field electric. The switch remains open for the most part during the operation of the circuit, its closing is for very short time intervals that is 10 to 50 times lower than the period of mechanical oscillations.

For the control of the switch, the voltage is measured at the terminals of the piezoelectric, and a circuit is used which makes it possible to detect the extremity amplitude. At each extreme, the controlled switch is closed for a short time. On the figure 4.2, we can see the SSDS circuit simulation

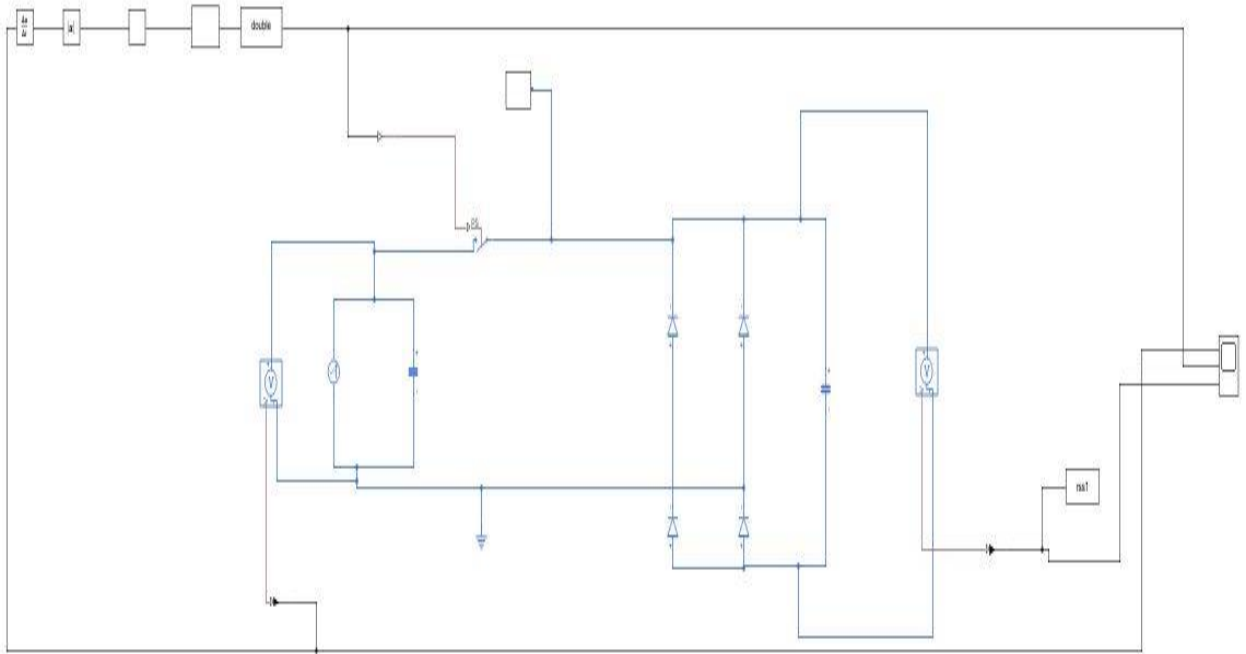
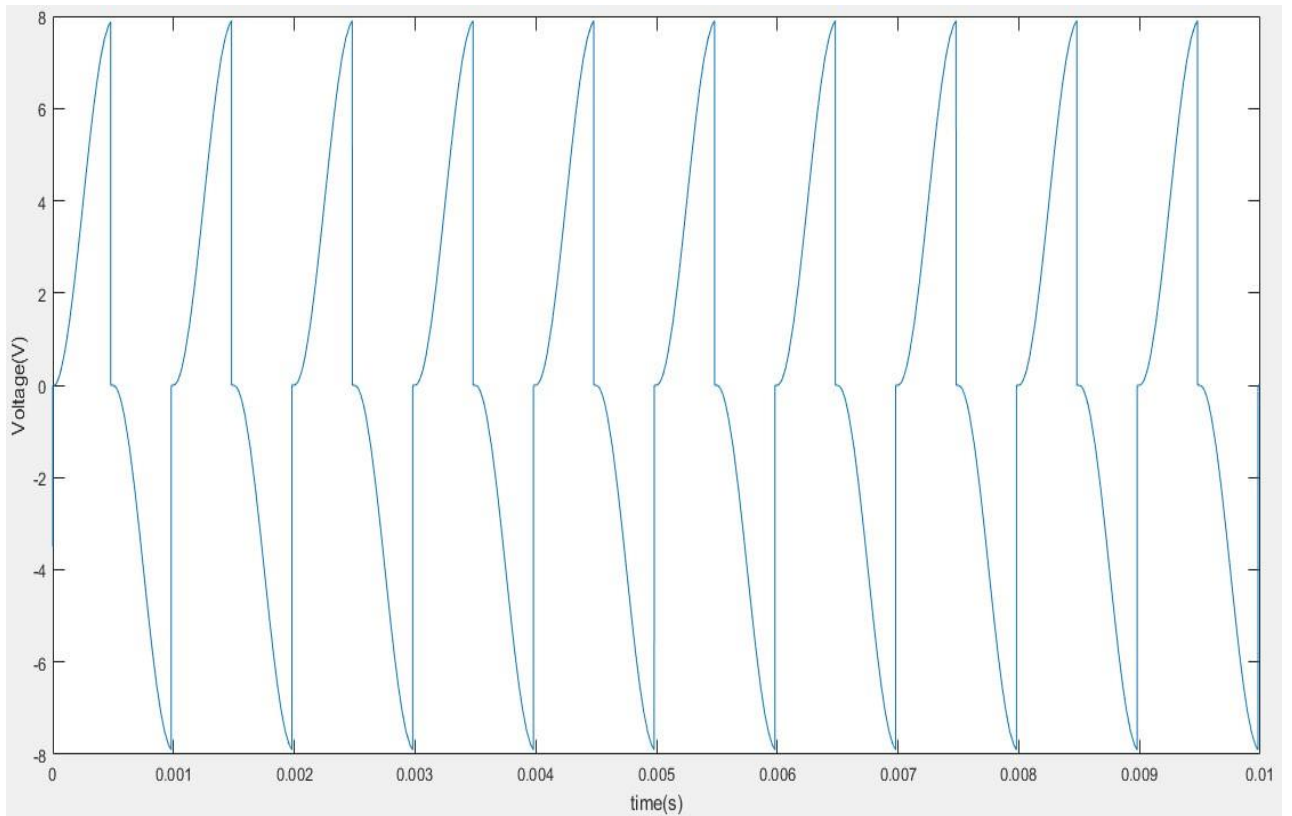


Figure 4.2: Sketch of SSDS circuit on Simulink

#### 4.2.1. Results obtained

The simulations are carried out over a duration  $DT = 0.001s$ , with an alternating current source of amplitude  $I_o = 0.001 A$ , of frequency  $f = 1000 Hz$ ,  $R = 700hm$ . After simulation, we obtain the following results:



*Figure 4.3 Voltage curve at the terminals of and SSDS circuit.*

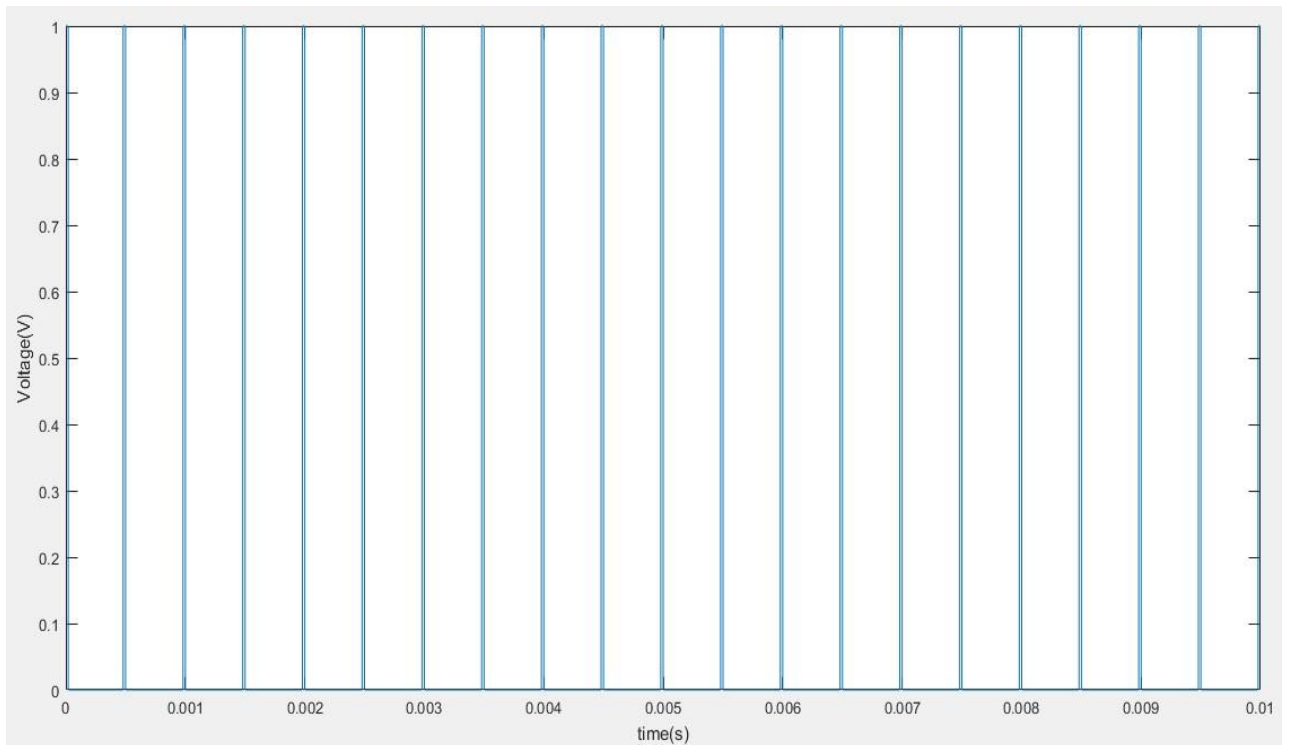


*Figure 4.4: Switch control voltage curve.*

Figure 4.4 shows the closing time of the switch. Closing and opening are done periodically, each time the extremity voltage is reached in the piezoelectric element for a duration  $t = 1 / f / 50$ . Figure 4.3 shows the voltage generated by the electrical circuit during the deformation of the piezoelectric. During this deformation, the energy is accumulated in the piezoelectric and this is represented by its capacitance  $C_p$ . During the first semi period, once the piezoelectric element has moved and reached the extremity, the switch is activated for a time  $\tau$  and the electrical circuit is connected, the charge accumulated in the piezoelectric element is recovered in the circuit. The time constant  $\tau$  of an RC circuit is the discharge time of a capacitor  $C_p$  in a resistor  $R$ . This time constant is equal to the product of the resistor  $R$  and the capacitance  $C$  of the RC circuit considered. For a fast discharge, it is necessary to have a low value of the resistance. This explains the fact that we took  $R = 7 \text{ Ohm}$ . Then, during the next half-period, the piezoelectric charge again (with reversed polarity) and once the extremity reaches the load is once again sent to the circuit. In our case, this charge is dissipated in the resistance. We can recover the electrical energy by connecting a capacitor on our circuit.

### 4.3. Recovery with RC Circuit.

We add a capacitor to our resistor in order to recover the energy instead of dissipating it, we remove the switch and use a diode bridge the diagram illustrating the operation of the energy recovery circuit thus formed is presented in (figure4. 2b). After simulation, we can see in Figure 4.5 how the capacitor charge varies over the different periods.

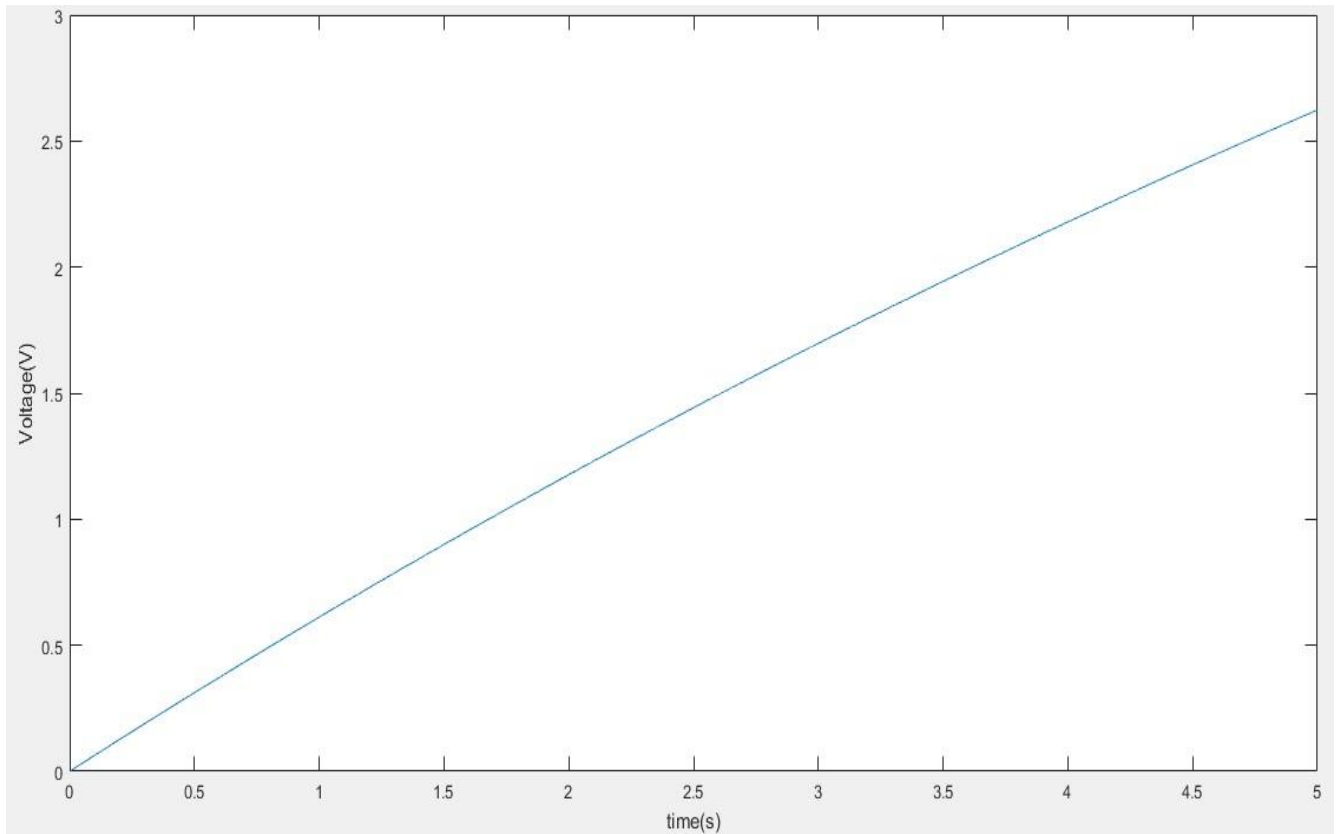


*Figure 4.5: Capacitor charge curve for an RC circuit connected to the piezoelectric via a diode bridge.*

In this part, we saw that it is not possible to realize an SSHS circuit, the diode bridge plays the role of the switch, and to recover the energy of such a system a full-alternation RC circuit was enough.

#### 4.4. SSDI and SSHI Circuits.

Note: By changing the values of  $C_p$  or the values of the inductance  $L$ , the voltage across the piezoelectric element changes.

We simulate an SSDI circuit, then a SSHI circuit with which we recover energy. The SSDI circuit is shown in Figure 4.5.a, and the SSHI circuit in Figure 4.5. b. These circuits remain open during their operation, the closure is for a short time equivalent to half of the period of equivalent electrical circuits [4], in our case the closing time is:

$$t = \pi \sqrt{L C_{equivalente}}$$

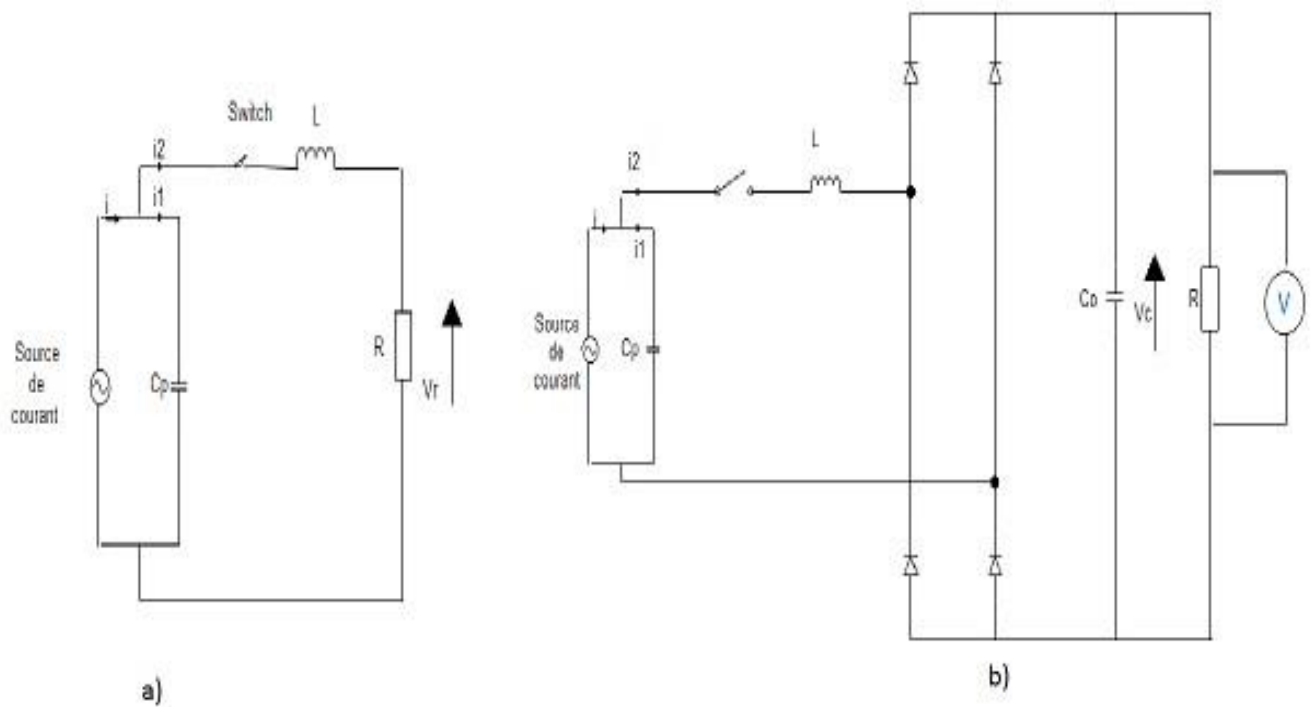


*Figure 4.6: Representation of SSDI and SSHI circuits (a) SSDI circuit, b) SSHI circuit*

We use the same current source, the same capacity and the same resistance as in SSDS and an inductance value  $L = 0.11\text{H}$ . Figure 4.6 is obtained. In this figure we can first notice that the maximum voltage is higher than that obtained in SSDS. This increase in voltage can be explained by the creation of the current induced in the coil which increases the voltage level across the piezoelectric.

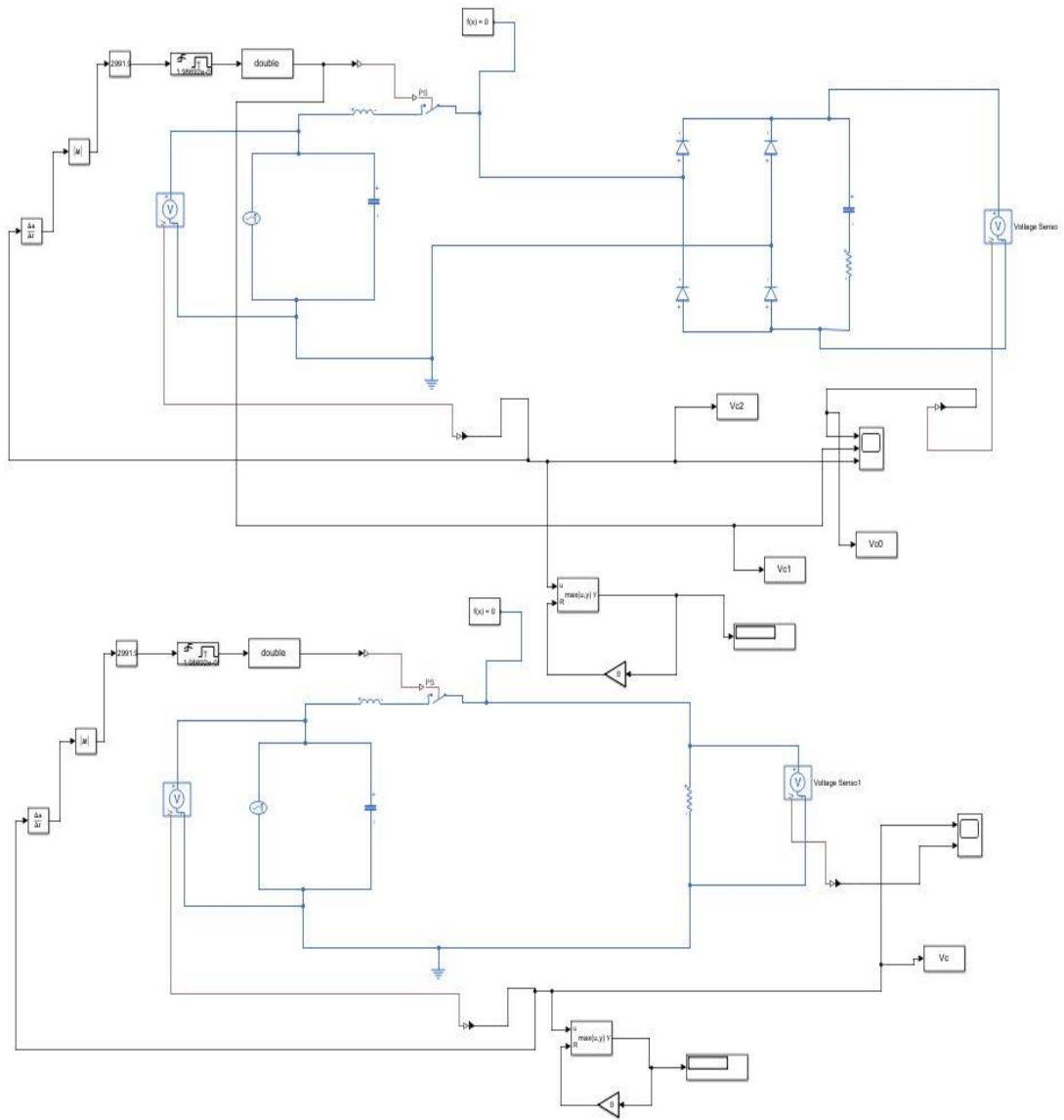


**Figure 4.6:** SSDI and SSHI circuits Simulink simulation sketch

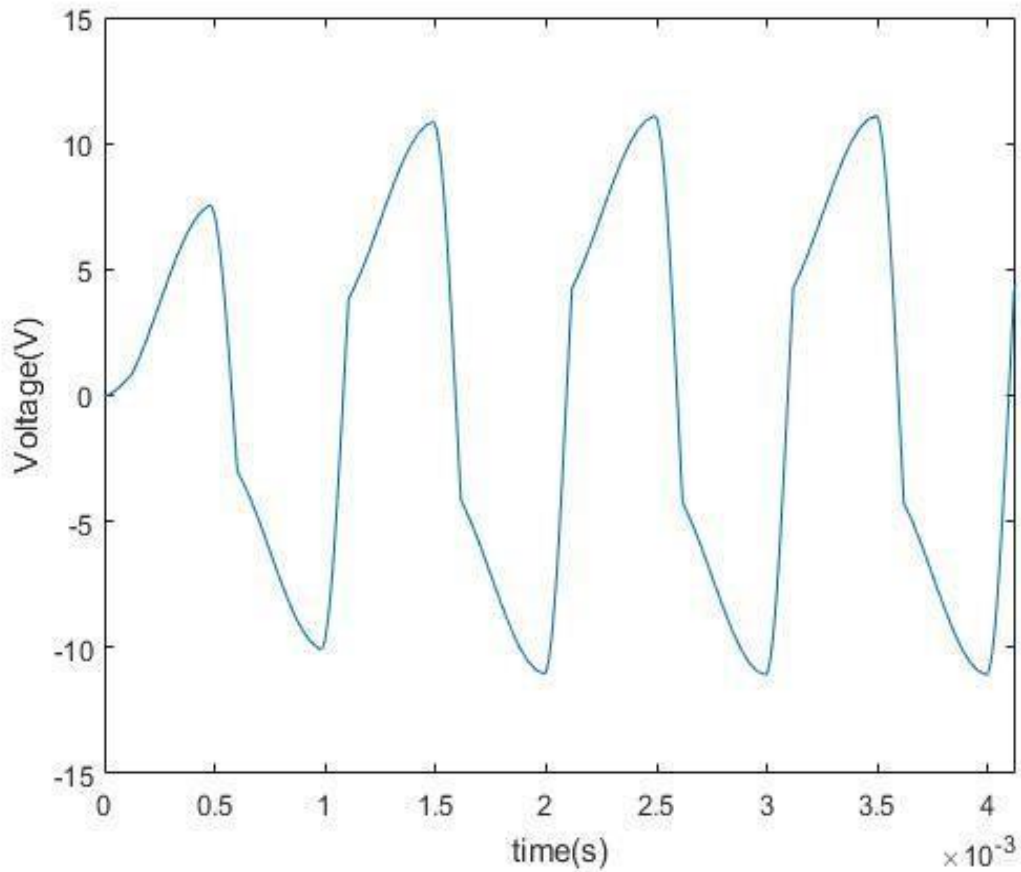


**Figure 4.7** Curve representing the voltage at the terminals of an SSDI circuit

On the curve of the figure 4.7, we can see that the first swing does not reach the maximum level as the others; this can be explained by the fact that we are in the transitional phase. Once the voltage on the extremity is reached, the switch is closed and the piezoelectric element discharges. The load does not start again at zero but at a limit  $V = 3.5 \text{ V}$  and with this last circuit, we have a higher voltage level in our piezoelectric element.

It should be noted that the voltage values at the terminals of the element representing our piezoelectric element vary if we vary the parameters of the circuit such as the capacities of the piezoelectric and the accumulator, the value of the inductance of the coil. Because of all this, it is difficult to control the openings and closings of our circuit, and it is necessary to adjust the values of inductance, of capacities in a scrupulous way to reach the maximum performance.

The closing time of the circuit in SSHI is substantially equal to the closing time of the SSDI circuit.

$$t = \pi \sqrt{LC_{\text{equivalent}}} \quad C_{\text{equivalent SSDI}} = C_p, \quad C_{\text{equivalent SSHI}} = \frac{C_p}{C_0 + 1}, \text{ but } C_p / C_0 \sim 0$$

Simulations are then made on a duration  $DT = 1 \text{ sec}$ , with an alternating current source amplitude  $I_o=0.001 \text{ A}$ , frequency  $f=1000 \text{ Hz}$ , inductance value for a coil is  $L = 0.11 \text{ H}$ , capacity  $C_o = 4F$ .

The accumulation capacity value is  $C_o = 4F$  with a sampling frequency value  $dt = 1/f/5$ ,  $R = 70\Omega$ . We took a very high-quality factor  $Q = 22$  after simulation, we get the curve of figure 4.6 on which we can see our dynamic damped system.

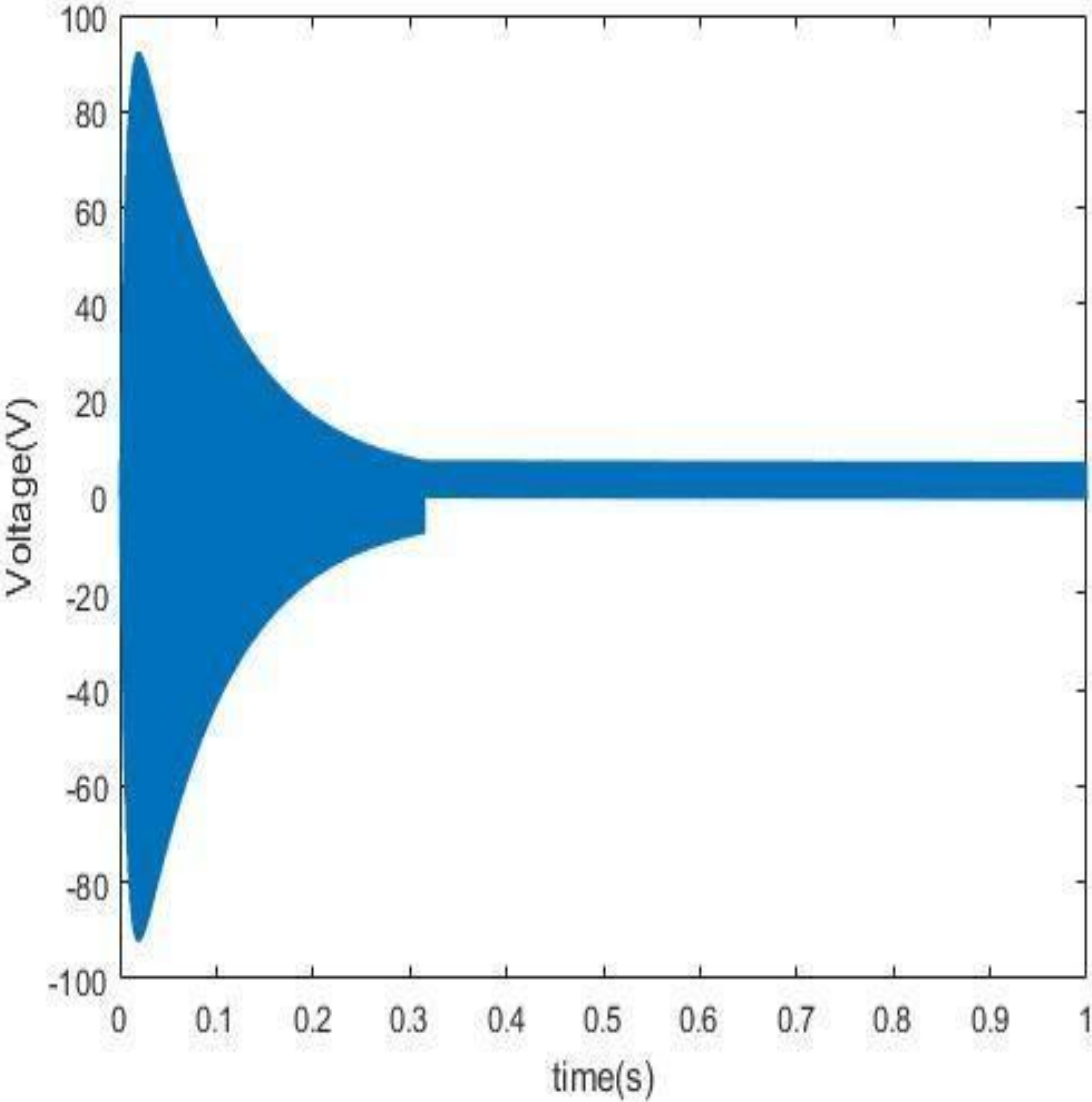


*Figure 4.8: curve representing the voltage at the terminals of an SSHI circuit*

## 4.5. SSDV CIRCUIT

In the SSDV, we increase the system voltage not external sources of voltage. The operating principle is the same as in SSDI: when our circuit reaches to the extremity, it closes and adds a DC voltage  $V_{cc}$  to the latter, so that the voltage level across the battery is increased. All this is done during very short time intervals. The circuit illustrating its operation is in figure 4.9.

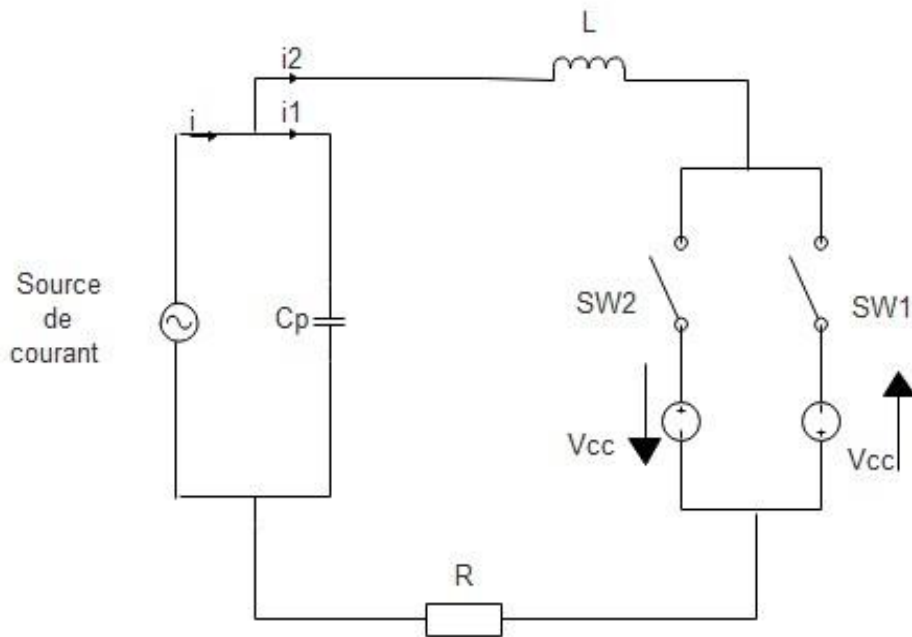


*Figure 4.9: SSDV Circuit*

Figure 4.9 was obtained by adding a voltage value  $V_{cc} = 2 V$  to our SSDV circuit. Wanting to have a higher voltage than SSDI, the Switch does not work well under the same conditions. It is therefore necessary to modify the parameters of the circuit to have a higher voltage than in SSDV.

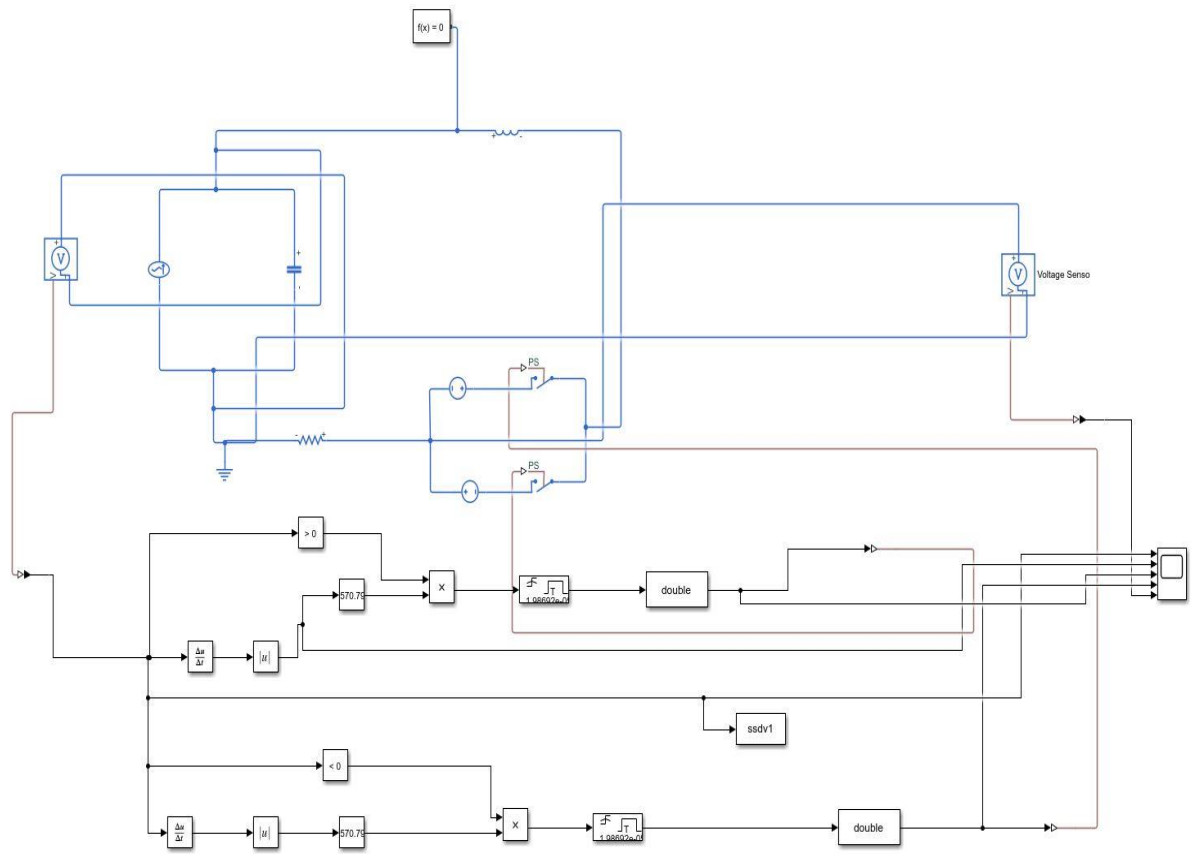
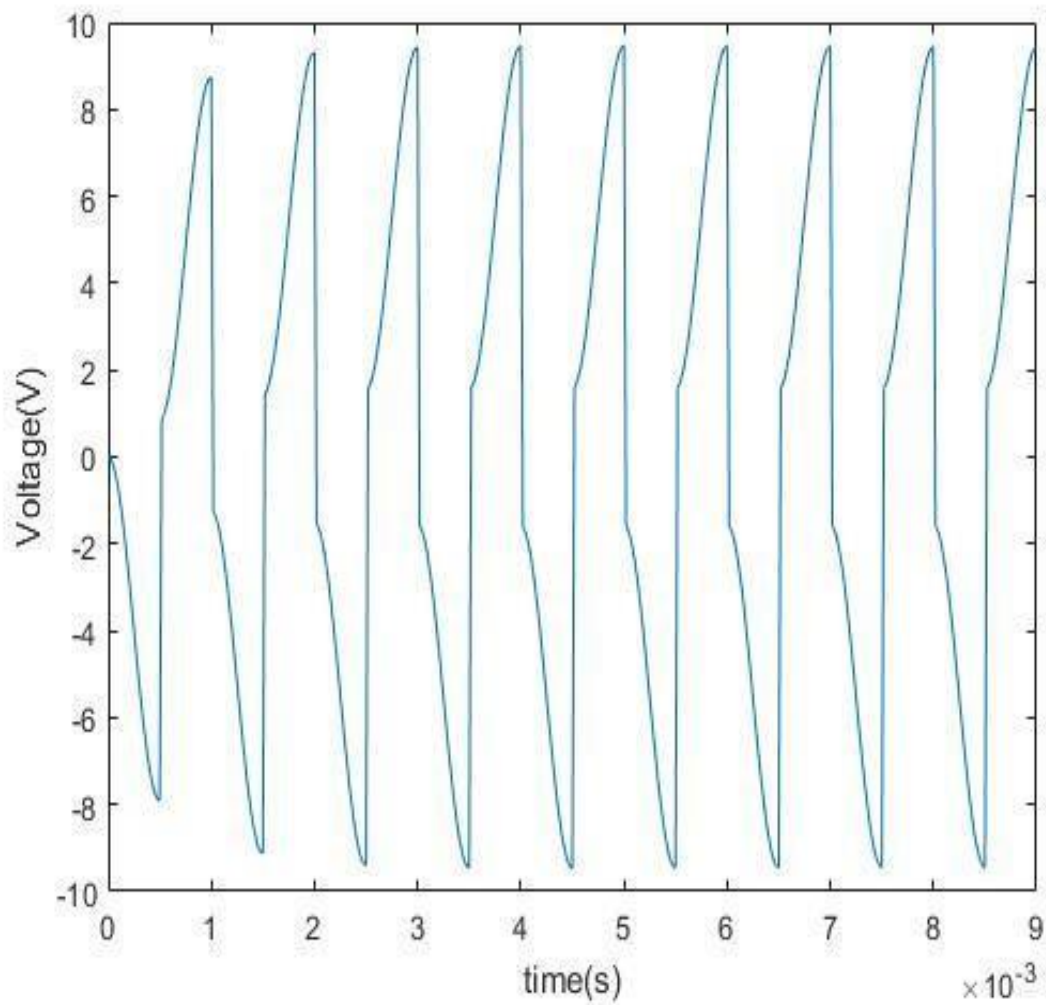
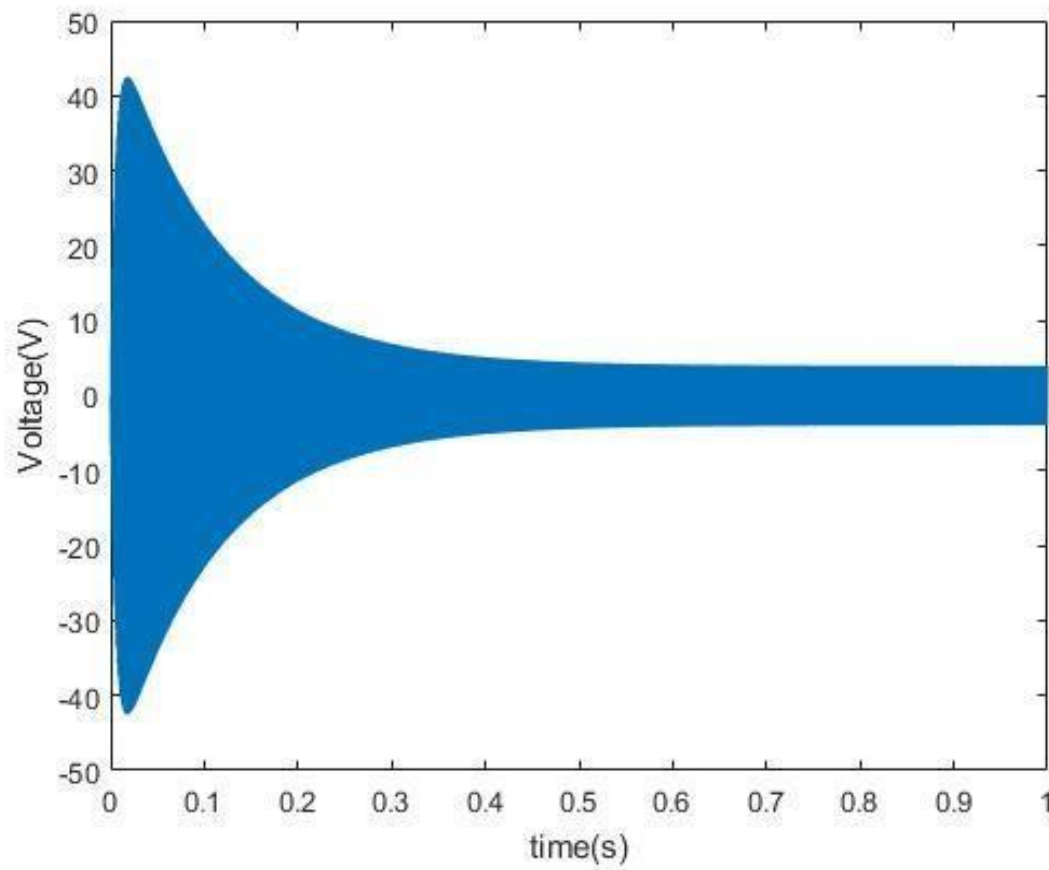


Figure 4.5 SSDV Simulink simulation sketch



*Figure 4.11 curve representing the voltage at the terminals of an SSDV circuit*

By adding a capacity to the system to recover energy via the diode bridge we get the SSHV circuit and we can see how the system is damped over time in Figure4.10



*Figure 4.11: Curve representing the variation of voltage at the terminals of an SSHV circuit*

Our system is quickly depreciated because we took a very high-quality factor  $Q = 22$  for this simulation.

## 5. Energy comparisons between SSHI, SSHV, and RLC Circuits.

In order to see the quantities of energies involved in accumulating with our different systems, we did a simulation for a duration  $\Delta T = 1\text{s}$ , for a current of intensity  $i(t) = 0.001\sin(\omega t)$ ,  $C_0 = 4 \times 10^{-4}$ ,  $L = 0.001\text{H}$ ,  $C_p = 4 \times 10^{-8}\text{F}$

$$\text{Accumulated energy} = \frac{1}{\Delta T} \sum_{i=1}^n \frac{1}{2} C_0 V_i^2 dt$$

With:  $dt = 1 / f /$  step of 50 simulation  
 $\Delta T = 1\text{s}$  duration of simulation  
 $f = 1000\text{HZ}$  frequency of simulation

For an RLC circuit the quality factor  $Q$  is define by  $= \frac{1}{R} \sqrt{\frac{L}{C}}$ , the capacity of our circuits is substantially equal to  $C_p$ .

For the different values of  $Q$  ( $Q = 2$  and  $Q = 22$ ). Obtained by just changing the value of the resistance  $R = 7\text{ Ohm}$  and  $R = 70\text{ Ohm}$ , we obtain the following graphs:

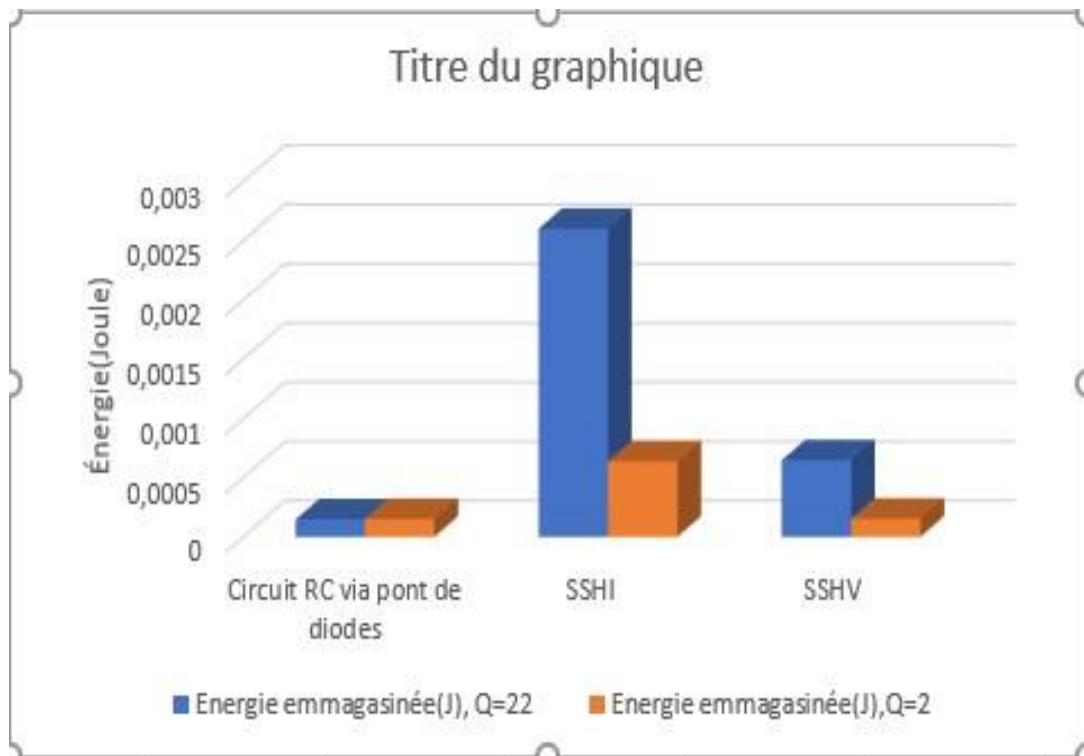


*Figure 5 energy comparison diagram of different energy accumulation techniques SSHV, SSHI, full-alternation RC circuit.*

We can see in Figure 5 that by setting the values of the different parameters and varying the value of the circuit resistance and quality factor, the SSHI allows us to accumulate more energy than the SSHV and a simple RC load circuit via a diode bridge.

## 6. Mechanical System.

We use the simulation software COMSOL to do the mechanical system calculations. In this part, it is a question for us to represent our material in terms of dimension, to find the characteristic matrices making it possible to solve the equations of the constituted mechanical system. Since the coupling problem is one of the most important factors in energy recovery, we will use the modal synthesis and dynamic condensation reduction technique, which ensures a good representation of the coupling matrix.

### 6.1 Mechanical system presentation .

Piezoelectric materials are materials that have property to be electrically polarized under the action of a mechanical stress and reciprocally to deform when an electric field is applied to them. In the case of energy recovery, the piezoelectric effect direct will be exploited by coupling a PZT to a resonant structure which imposes a deformation. The mechanical structure is in most cases an embedded beam, on which one or more ceramics are bonded. The vibrations of the beam induce a deformation of the piezoelectric material, thus creating its polarization. To optimise our energy harvesting system, it was possible for us to deal with all the types of piezoelectric materials to determine which one we will use for the project. However, in this work is not made on this study because simulation take much more time, but we can present what is use for many simulation.

Material type	Peak power ( $\mu W$ )	Volume	Frequency (Hz)	Excitation (acceleration or force or pressure)	Reference
PVDF	2	28 modules of $16.5 \times 9.5 \times 0.15 \text{ cm}^3$ film	2	0.1 or 0.2 G	69
PVDF	0.0005	$30 \times 12 \times 0.005 \text{ mm}^3$	2	3-point bending at 3 N	70
PVDF	610	$72 \times 16 \times 0.41 \text{ mm}^3$	3	Wind speed of 4 m/s	15
PVDF	2.75	$10.94 \times 22 \times 0.354 \text{ mm}^3$	104	1 G	8
PVDF	2	$20 \times 16.1 \times 0.2 \text{ mm}^3$	146	Acoustic pressure: 9 Pa	71
PZT ceramic	47	$25 \times 10 \times 0.8 \text{ mm}^3$ bimorph	1	Shook by hand. Ball	14

				hits piezo beams	
PZT ceramic	265	$1 \times 1 \times 2 \text{ cm}^3$	1	1900 N	13
PZT ceramic	2000	$45 \times 20 \times 0.3 \text{ mm}^3$	20	1 N	12
PZT ceramic	40	$31.8 \times 6.4 \times 0.51 \text{ mm}^3$	36	0.2G	72
PZT ceramic	30000	$63.5 \times 60.3 \times 0.27 \text{ mm}^3$	50		11
PZT ceramic	39 000	$1 \text{ cm}^3$	100	7.8N	9
PZT ceramic	52 000	$1.5 \text{ cm}^3$	100	70N	10
PZT ceramic	60	$1 \text{ cm}^3$	100	0.23G	7
PZT ceramic		$1 \text{ cm}^3$	120	0.25G	6
PZT ceramic	1800		2580	2G	73
PZT ceramic	144	$90.4 \times 14.5 \times 0.79 \text{ mm}^3$	2.5		74
PZT fiber	75		180		16
PZT fiber	120 000	$2.2 \text{ cm}^3$		Dropping a 33.5 g steel ball from 10 cm	75
PMN-PT single crystal	14.7	$20 \times 5 \times 0.5 \text{ mm}^3$	1744		67
PMN-PT single crystal	3700	$25 \times 5 \times 1 \text{ mm}^3$	102	3.2 G	66
PMN-PT single crystal	6.7	$1.7 \times 1.7 \times 0.00084 \text{ cm}^3$	0.3	Bending motion at a strain of 0.36%	17

Take from [27] [Table 2: Some piezoelectric energy harvesters reported in the literature and their performances.](#)

By studying the data presented in this table, we can see that the piezoelectric ceramics work on a frequency close to 50 HZ and have higher output power. Their problem lies in the fact that they cannot withstand heavy mechanical stress because they are brittle. On the other hand, the polymeric piezoelectric materials work on frequencies <10HZ producing low power with respect to piezoelectric ceramics but bearing great mechanical constraints because of their flexibilities. Piezoelectric single crystal materials produce greater output power, but they are little used because they are very expensive.

There are many configurations of piezoelectric materials, for the entire configuration, it is possible see that the form factor is always small. With small form factor, our system is not too heavy, and it is possible to put it in the place where access is difficult. For this case of study,

we will use a cantilever beam. The characteristics and dimensions are giving in the table3. The beam is locked at one of his end. Our beam is composed of several materials, namely a metal support or we deposit our piezoelectric material, it is also constituted of a fine electrode in Titanium above our piezoelectric one or we have our potential difference. We also add a Tungsten mass to make t1he counterweight. Our system is a mechanical auxiliary.

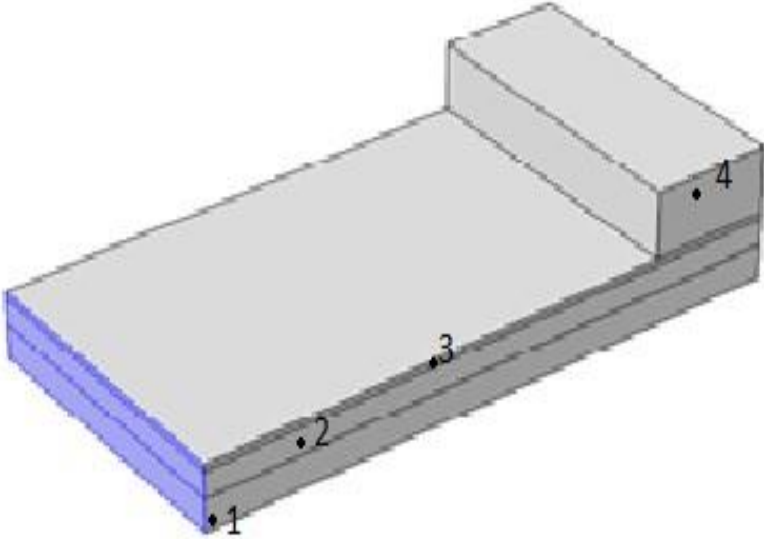


*Figure 6.1: Mechanical structure*

Blocks	1	2	3	4
Widths (m)	0.01	0.01	0.01	0.02
Depths (m)	0005	0005	0005	0005
Heights (m)	0.0005	0.0004	0.0001	0001
Materials	Structural Steel	lead zirconate titanate (PZT-2)	Ti (Titanium)	W Tungsten

*Table 3: Geometric data of the mechanical system.*

## 6.2 Use of the modal synthesis and condensation technique for a precise impedance's calculation.

For the calculation of piezoelectric materials, there are several finite element models. The document [1] presents us the limits of use of the various models and proposes us a new approach allowing to have a good matrix of electromechanical coupling. The matrices being very large and difficult to calculate, the condensation techniques used in the past introduced a lot of error which prevented to have precise impedances. By having a good representation of the electromechanical coupling matrix, we can optimize our vibratory energy recovery system based on piezoelectric materials.

### 6.2.1 Technique description

We use the condensation technique proposed in [1] and used in [5] in reduced form to represent our dynamic system. The voltages on our piezoelectric element (block2 figure 6.1) are divided into surface Voltages  $V_s$  and internal voltages  $V_o$  to the piezoelectric. We will just consider as surface tensions  $V_s$  the tensions on the separation surfaces of blocks 1 and 2 (Figure 6.1), and the surface tension on the separation surface of blocks 2 and 3 (Figure 6.1), all other surface tensions will be neglected. The voltage from below is on our metal base or the material deposit has been made. The metal base on which the piezoelectric element has been deposited constitutes the mass of the system. Therefore, the voltage on this surface is considered to be zero. We will remain the internal voltages of the piezoelectric represented by the block 2 of figure 6.1 and that the surface bound to our electrode. The charge inside the piezoelectric element is zero, the only charge that will remain us is the surface charge. We also have degrees of freedom related to displacement  $W$ . We consider displacement in the direction where we apply our force.

By balancing forces, we get the following system:

$$\begin{bmatrix} M & 0 & 0 \\ 0 & 0 & 0 \\ 0 & 0 & 0 \end{bmatrix} \begin{bmatrix} \ddot{W} \\ \ddot{V}_s \\ \dot{V}_o \end{bmatrix} + \begin{bmatrix} K & E_{WV_s} & E_{WV_o} \\ -E_{WV_s}^T & C_{V_sV_s} & E_{V_sV_o} \\ -E_{WV_o}^T & E_{V_oV_s}^T & C_{V_oV_o} \end{bmatrix} \begin{bmatrix} W \\ V_s \\ V_o \end{bmatrix} = \begin{bmatrix} F \\ q_o \\ 0 \end{bmatrix} \quad (1)$$

Article [5] proposes a simplified reduction method, for this part the same procedure is used.

$$[V] = [V_s \quad V_o]^T \quad [E] = [E_{WV_s} \quad E_{WV_o}] \quad [Q] = [q_o \quad 0]^T \quad [Cv] = \begin{bmatrix} C_{V_sV_s} & E_{V_sV_o} \\ E_{V_oV_s}^T & C_{V_oV_o} \end{bmatrix}$$

Replacing all these terms in (1) we obtain the following equation system:

$$\begin{cases} M\ddot{W} + KW + EV = F \\ -E^T W + C_v V = Q \end{cases}$$

By doing the modal decomposition of the displacement we get

$$W = \Psi \cdot \eta$$

$$\text{Where } \Psi = [\Psi_1, \Psi_2, \dots, \Psi_n]$$

To obtain the values of the different elements constituting the matrix  $\Psi = [\Psi_1, \Psi_2, \dots, \Psi_n]$ , we solve the eigenvalue problem for  $F = 0$  and  $V = 0$

$$(-\omega_i^2 [M] + [K])\Psi_i = 0$$

By replacing the expression of the displacement and multiplying by the transpose we can write our equation as follows:

$$\begin{cases} [\Psi]^T [M] [\Psi] \ddot{\eta} + [\Psi]^T [K] [\Psi] \eta + [\Psi]^T [E] V = [\Psi]^T [F_r] \\ -[E]^T [\Psi] \eta + C_v V = Q \end{cases}$$

$$M_a = [\Psi]^T [M] [\Psi] = Id \quad K_a = [\Psi]^T [K] [\Psi] \quad L_a = [\Psi]^T [F_r] \quad K_{adv} = [\Psi]^T [E]$$

We get the following reduced equation system:

$$\begin{cases} M_a \ddot{\eta} + K_a \eta + K_{adv} V = L_a \\ -K_{adv}^T \eta + C_v V = Q \end{cases} \quad (2)$$

This system of equation represents the behaviour of the mechanical system in figure 5.1, the latter is a mechanical auxiliary. In the following we will add depreciation to our system, and we will find all the elements of the matrix using COMSOL simulation software.

## 6.2.2 COMSOL procédure description

From COMSOL we have to obtain the different matrices of the equations representing the mechanical system in order to use them on our Simulink model. We will start from the model with geometry defined above, in this part it will be question of giving the reasoning adopt on the software to obtain the different matrices  $M_a$ ,  $K_a$ ,  $C_p$ ,  $K_{adv}$ ,  $F_a$ . To fully understand the procedure, it is important to look at our COMSOL model which is given with documents in annexes.

- From our materials select, on COMSOL we have all the characteristic properties of the material, by summing the densities integrated on the volumes of the constituent blocks of figure 6.1 one obtains the matrix of mass. Once the latter obtained, it is transformed to have an identity matrix:  $M_a = [\Psi]^T [M] [\Psi] = Id$

- To obtain the stiffness matrix we solve the problem with the following eigenvalues:

$$(-\omega_i^2 [Ma] + [Ka])\Psi_i = 0$$

$$Ka = \Omega^2 \quad \Omega^2 = \begin{bmatrix} \omega_1^2 & 0 & 0 \\ 0 & \cdot & 0 \\ 0 & 0 & \omega_n^2 \end{bmatrix}$$

- To obtain the  $C_v$  capacitance of the piezoelectric material, we make a static study in low stress condition  $F_a = 0$  by applying a voltage  $V = 1$ , we manage to find  $C_v^*$  in Simulink and we will have to correct to have  $C_v$ .

$$\begin{cases} K_a \eta + K_{adv} V = 0 \\ -K_{adv}^T \eta + C_v V = Q \end{cases}$$

$$C_v = C_v^* - K_{adv}^T K_a^{-1} K_{adv}$$

- To obtain the coupling matrix  $K_{adv}$ , we study at  $V = 0$  and the eigenvalues.

### 6.3 Frequency response function.

In order to validate our model, we propose to plot the various frequency response functions on COMSOL and MATLAB. On COMSOL, we make a study in the frequency domain with frequencies going from 1000 to 100000 Hz and taking a step of 1000. By applying a sinusoidal force of amplitude  $F = 0.5$  on the 2 ends (figure 6.2) of the tops above of the mass and in open circuit condition and such that  $L_a = [\Psi]^T \{F\}$ .

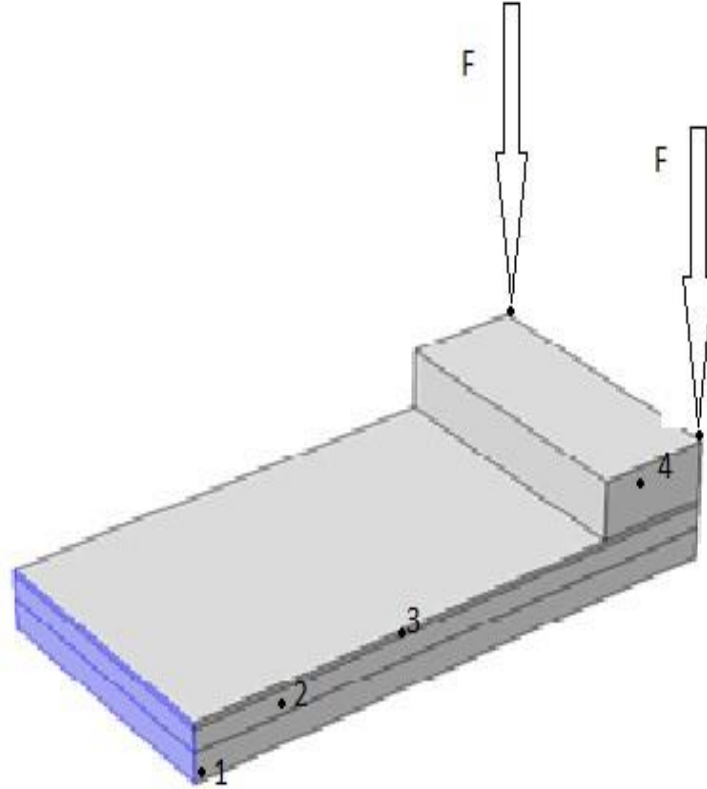


*Figure 6.2: Structure solicitation*

Using the matrices obtained on COMSOL, we plot the open-circuit frequency response function according to the equation below.

$$\begin{cases} M_a \ddot{\eta} + K_a \eta + K_{adv} V = L_a \\ -K_{adv}^T \eta + C_v V = 0 \end{cases}$$

By doing Fourier transform we get:

$$\tilde{\eta} = (-\omega_i^2 * M_a + K_a)^{-1} * L_a$$

$$\tilde{V} = K_{adv}^T * \tilde{\eta} / C_v$$

It should be noted that the graph obtained on COMSOL in displacement is that  $\tilde{W} = [\Psi] \tilde{\eta}$ , for simplicity reasons, we traced our graph according to the voltage V.

But it is also possible to do a very simple operation to have the displacements multiplied by the force  $L^T \eta$ .

Figure 6.3 is the result obtained by putting the two curves obtain from COMSOL and MATLAB on the same graph, the one in blue is the frequency response function taking in consideration the voltage (V) obtained on MATLAB by using the modal mass matrix, the stiffness matrix, the corrected capacitance, the electromechanical torque matrix. And the red one come from COMSOL.

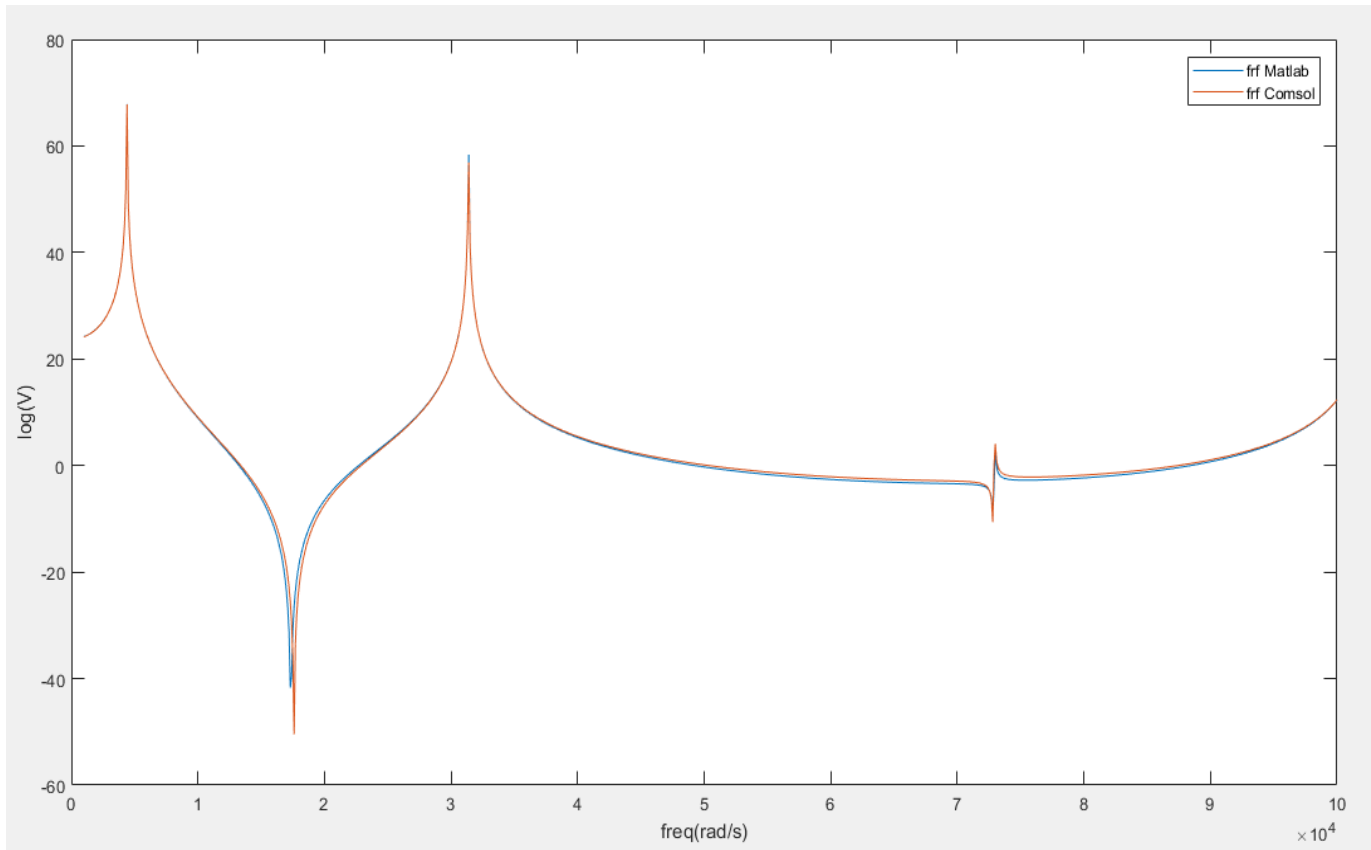


**Figure 6.3** Frequency response functions as a function of the voltage  $V$  (when the load is zero  $Q = 0$  and the structure is biased by two sinusoidal forces of the same amplitude at the ends of the structure) for a frequency range [1000, 100000] HZ.

We can observe that the 2 curves are superimposed, the different problems at the level of the anti-resonance peak which is not equal is due to a problem of resolution of the different graphs. So, we can validate our model and use it for our SSH circuits.

## 7. State system.

In this part we take the matrices we had and the goal here is to implement it in our Simulink software. Given the equation system defined below, this equation system defines the dynamic behaviour of our piezoelectric.  $x(t)$  represents the state of the system and will be the state of our electrical circuit. The state of a system at a moment  $t$  represents the minimum memory of the past necessary for the determination of the future.  $U(t)$  represent the input of our system at the input we will have the force  $L_a$  and at the output  $y(t)$  we will have the tension.

$$\begin{cases} \dot{x} = Ax + Bu(t) \\ y = Cx + Du(t) \end{cases}$$

Taking our system of equation (1) deriving from the mechanical system to which one adds damping and by deriving the second equation, one obtains the following system, of this system, one will find the various parameters of the system of state.

$$\begin{cases} M_a \ddot{\eta} + 2\epsilon\omega_n \dot{\eta} + K_a \eta + K_{adv} V = L_a \\ K_{adv}^T \dot{\eta} - C_v \dot{V} = I \end{cases} \quad \dot{x} = \begin{bmatrix} 0 & 1 \\ -K_a/M_a & -2\epsilon\omega_n \end{bmatrix} \begin{Bmatrix} \eta \\ \dot{\eta} \end{Bmatrix} + \begin{bmatrix} 0 & 0 \\ 1 & -K_{adv} \end{bmatrix} \begin{Bmatrix} L_a \\ V \end{Bmatrix}$$

$$\dot{x} = \begin{bmatrix} 1 & 0 \\ 0 & 1 \end{bmatrix} \begin{Bmatrix} \eta \\ \dot{\eta} \end{Bmatrix} \quad I = I_1 - I_2 = K_{adv}^T \dot{\eta} - C_v \dot{V}$$

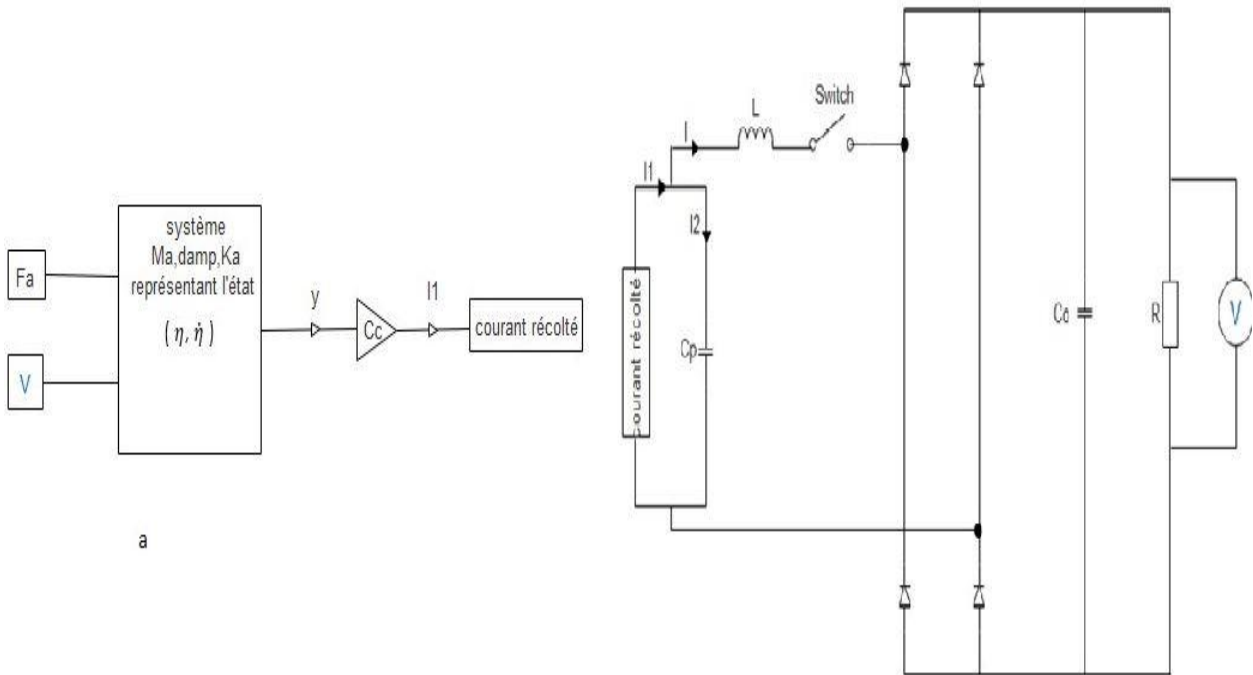


**Figure 7.1 a) State system representing the mechanical behaviour of our piezoelectric, b) SSH recovery circuit**

During the deformations of our mechanical system, the piezoelectric element produces electric current (I1) while receiving a voltage imposed by the circuit. Part of this current is sent capacitor within the piezoelectric (I2) and a part is transmitted to the circuit (I). Figure 7.1 illustrates this process perfectly.

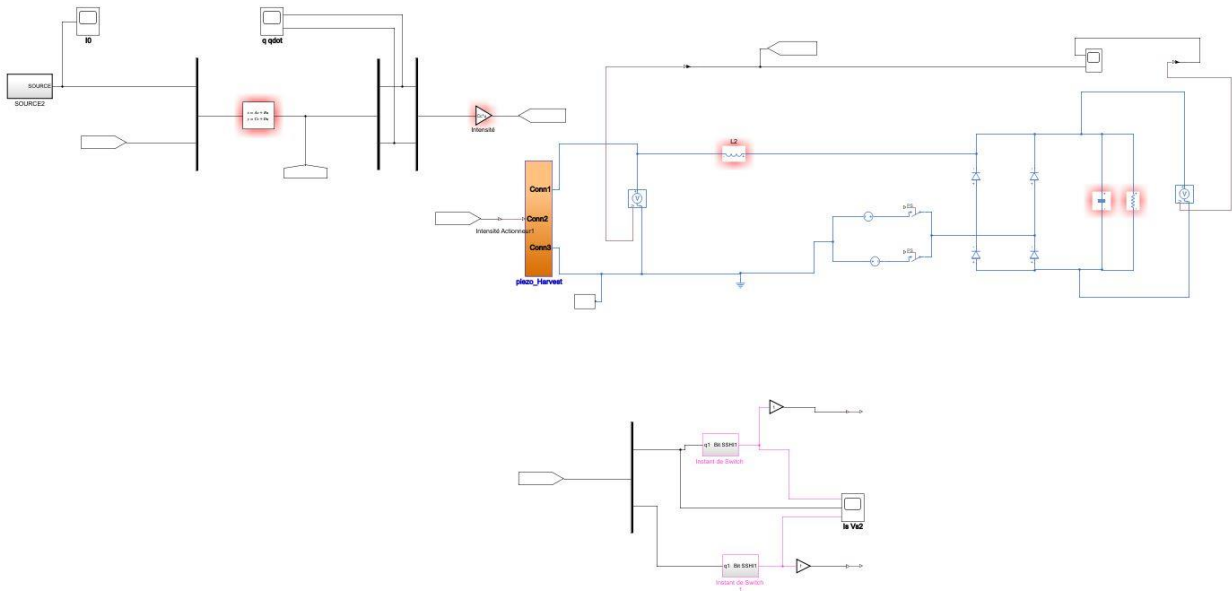


*Figure 7.2 : Simulink simulation sketch of SSH recovery circuit*

## 8. SSHI simulation with the piezoelectric element.

In this part, we use the results obtained under COMSOL to make the simulations. The voltage of the piezoelectric element is that obtained by making the correction. The current feeding our electrical circuit now comes from the piezoelectric element. The latter is represented via the state system. We add a little damping to our system  $2\varepsilon\omega_n$ , with  $\varepsilon = 5 * 10^{-3}$ .

$$\begin{cases} M_a \ddot{\eta} + 2\varepsilon\omega_n \dot{\eta} + K_a \eta + K_{adv} V = L_a \\ K_{adv}^T \dot{\eta} - C_v \dot{V} = I \end{cases}$$

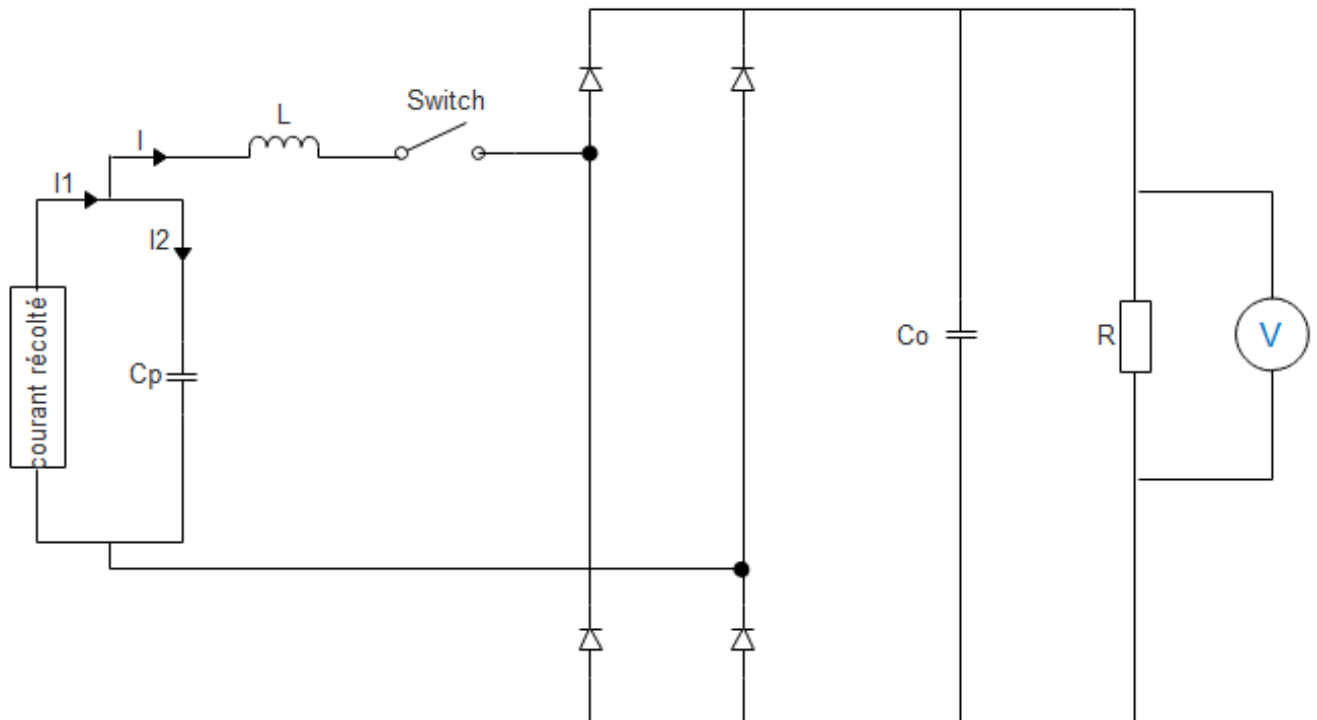


*Figure 8.1 SSHI circuit representation*

The simulation parameters are detailed on the MATLAB program delivered to the LTDS. Because of the small simulation step  $\text{dut} = 6 * 10^{-8}$  s, we do a simulation for a duration of  $\text{DT} = 0.3$  s, the goal being to see the shape of the curve. Then we will simulate for a little longer and see the amount of energy accumulated. The frequency  $f = 200$  Hz.

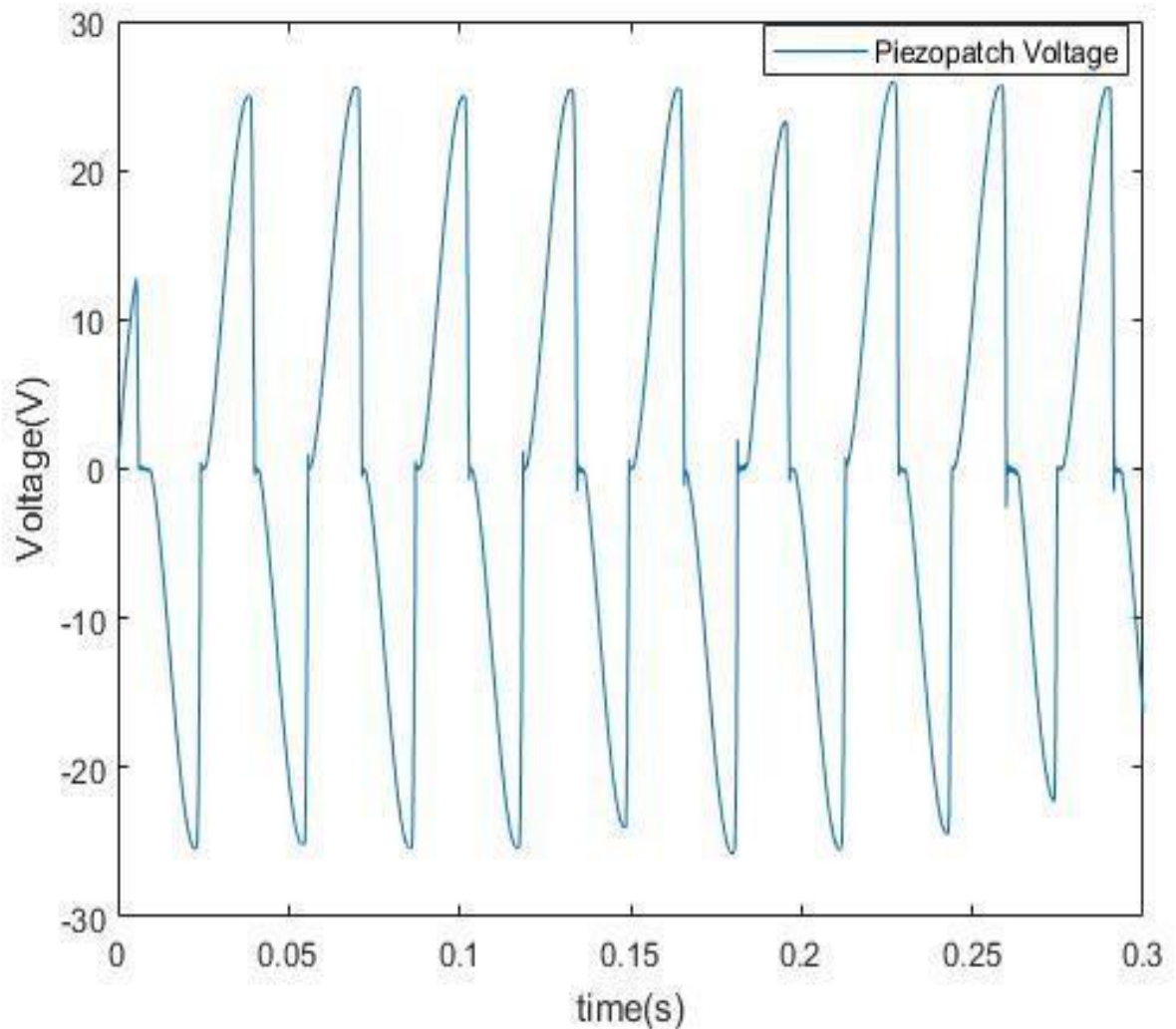


*Figure 8.2 Curve representing simulation results from SSHI.*

The curve in blue represents the simulation result with our piezoelectric material excited by a harmonic force of amplitude  $F = 1\text{N}$  distributed at the upper ends of our structure as in figure 5.2. We can notice small instabilities of the system at the level of the intervention of the switch. This is due to the setting of the switch. The simulation step is small because after this step of time the program is stop working, we can explain this by the fact that our switch is not well setting.

For  $Dt=0,3\text{s}$  we take  $1,13 \times 10^{-8}\text{W}$ .

We can always see that is it not good to harvest energy using capacitor because of his limitation.

## 9 Applications

Driven by the need for energy self-sufficiency in some low-power applications and lower consumption of electronic components, energy micro sources based on the recovery of vibration energy using piezoelectric elements have emerged. Energy retrieval, which transforms ambient energy into electrical energy, is very attractive in applications where the battery cannot be replaced easily.

### 9.1 Tire Pressure Monitoring system (TPMS)

Driven by increasingly stringent standards on Fuel consumption. Fuel consumption increases by 1% every 2,9 psi / 0.2 bar the tire is under-inflated. - 0,4 bar under-inflation  $\Rightarrow$  2% increase in fuel consumption - 0,6 bar under-inflation  $\Rightarrow$  3% increase in fuel consumption. Tire wear increases by 5% every 2,9 psi / 0.2 bar the tire is underinflated. - 0,4 bar under-inflation  $\Rightarrow$  10% increase in tire wear - 0,6 bar under-inflation  $\Rightarrow$  15% increase in tire wear. According to NHTSA: Tire wear increases by 15% every 2,9 psi / 0.2 bar the tire is under-inflated., we are developing more and more hybrid cars, self-guided, electric cars. Nowadays in a car, it is possible have 60 sensors that must all be connected to transmit the signal. By choosing a signal transmission with wiring, we are limited by the lengths of wiring that according to research [28] are 4 km in modern cars, which becomes heavy. At this time, we must fall back on the use of wireless connections that consume a lot of energy. Because of the location of the sensor, it is difficult to change the batteries and for this reason, we think about use of energy harvested systems. Using energy harvested systems it is possible increase batteries.

It is important to know the pressure in the tires of a car for better energy consumption and for a longer life of the tire. To measure the pressure in the tires, we use the tire pressure measurement systems (TPMS). These TPMS are existing on the market, there are many TPMS systems with different characteristics.



*Figure 9.1: Pressure measurement transmission via wireless*

The TPMS (Tire Pressure Monitoring System) is a device that allows the driver of the vehicle to know the tire pressure state permanently during the operation of the vehicle. The pressure is obtained using sensors implanted in the tires or a measurement electronics (figure 9.2). A TPMS includes an IC sensor, a low frequency interface, an RF transmitter, an antenna and a main battery. The IC sensor incorporates a low power MCU, an ADC module, a pressure sensor, a temperature sensor and an accelerometer. The accelerometer activates the standby mode when the car is idling for a preset period. During operation, tire pressure is measured and transmitted wirelessly one or more times per minute (figure 9,1). The overall power consumption of a TPMS module strongly depends on the number of transmissions of the RF transmitter in one minute and the length of time that the TPMS module remains in sleep mode. The capacity of TPMS batteries is approximately 220 to 600 mAh and their typical lifespan is 5 to 10 years according to the references [29] [30].

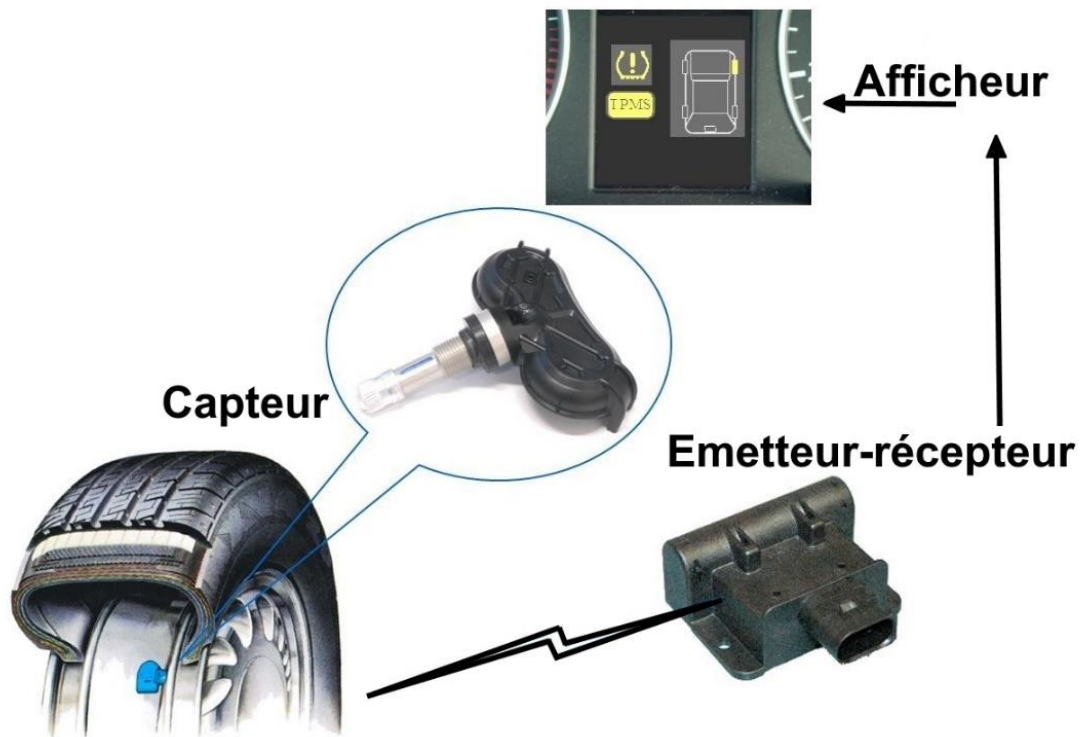


*Figure 9.2: TPMS systems location on tire*

on the table below we find the TPMS chips most commonly used on the market and their energy consumption. The RF transmitter consuming the most energy, needs one to be powered by a current of 10 mA. In standby mode, it consumes 1  $\mu$ A of current. Overall, it is estimated that an average of 450  $\mu$ W is required to achieve a transmission rate of 1 Hz for a TPMS238 module. Current cars are unused more than 90% of the time and most of the energy stored in the battery is consumed by the current of sleep.

Company	IC Solutions	Typical Current Consumption Run mode + RF Transmission
Infineon	SP370	run mode: 2 mA RF: 10 mA sleep current: 0.7 $\mu$ A
Freescale	FXTH870x	run mode: 2 mA RF: 6 mA sleep current: 0.5 $\mu$ A
Texas Instruments	TPIC82010	run mode: 1.53 mA RF: 10.5 mA sleep current: 0.1 $\mu$ A

Melexis	MLX91801/2 + MLX72013	run mode: 1 mA RF: 3.8–16.8 mA sleep current: 0.25 $\mu$ A
---------	-----------------------	--

All data are from the [datasheets](#) of the ICs. Operation voltage of the ICs is about 1.8–3.6 V

*Table 4: TPMS module and on the market*

During the rolling of a car tire, several forces can be used to deform our piezoelectric system, so we can take advantage of vibration energy from gravity, periodic and random vibrations of tire-road interaction and the variation of the periodic acceleration of the centripetal force.

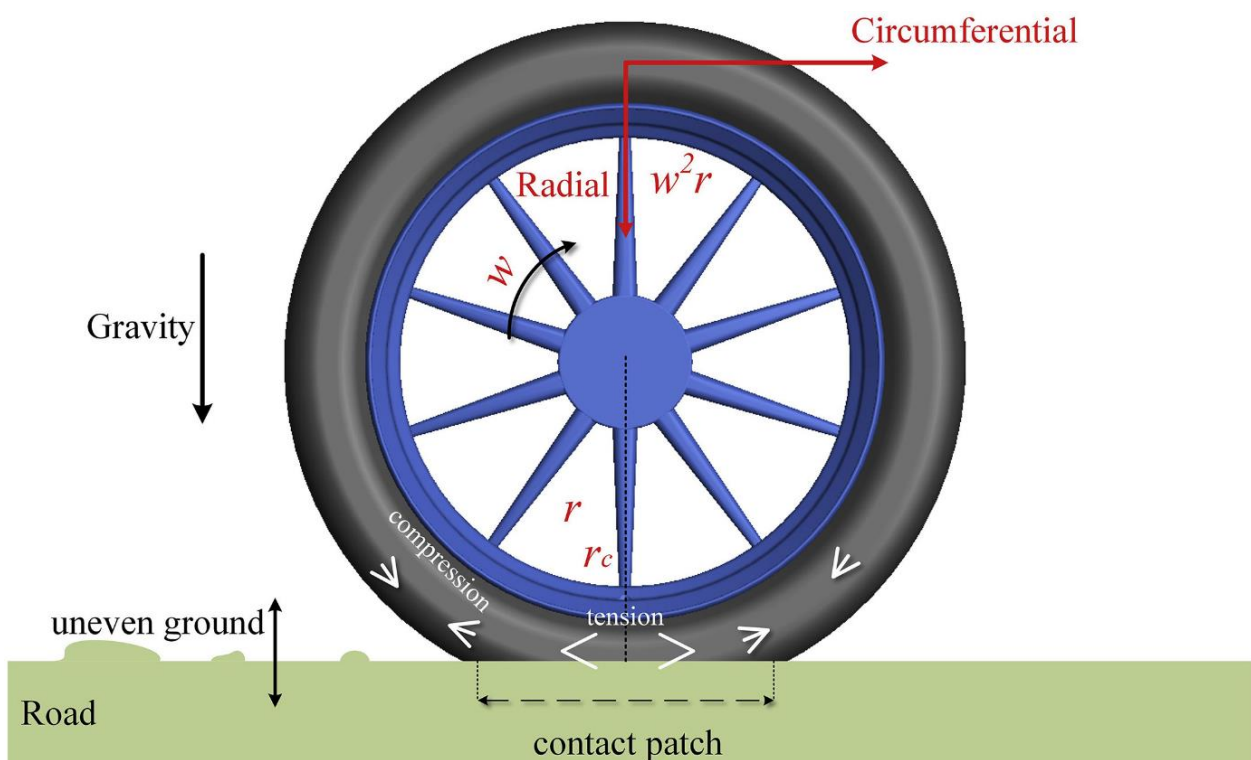


*Figure 9.4 Different forces applying on tires*

The vibration of the tire-road interaction is unpredictable and random it will depend on the type of road and its coating. The radial acceleration keeps at a constant value  $\omega^2r$  ( $\omega$  angular velocity of the wheel;  $r$  radius of the tire). Gravity is always in a direction towards the ground, but the structures fixed on a wheel can undergo a periodic acceleration change of  $\pm 1$  g due to the rotation of the wheel. Looking at the analyzes made by Löhndorf et al on a set of tangential acceleration data recorded at the lining of a tire at 50 km h<sup>-1</sup>, they found that power exists mainly in a low frequency range of 5 to 20 Hz, corresponding to the rotation period of the wheel. also shows several peaks around 100 Hz, which should come from the tire-ground interaction. To harness the energy of the vibrations from the tire-road interaction and the periodic acceleration, the energy recuperations must be designed with a large bandwidth. On the market and on the literature, we have a lot of harvesting systems base.

Material type	Volume	Speed	Frequency (Hz)	power	Reference
PZT elements	11 × 5 × 0.18 mm <sup>3</sup>	64.4 km hr <sup>-1</sup>		298 μW	32
PZT-ZNN	25 × 5 × 0.4-mm <sup>3</sup>	acceleration of 0.4 g	62.5Hz	15 μW	33
AlN	3 × 3 × 1.7-mm <sup>3</sup>	~70 km hr <sup>-1</sup>	1,011 Hz	~30 μW	34
PZT-5A	8 × 5 × 0.5-mm <sup>3</sup>	~50 mph	11 Hz-470 Hz	47 μW	35
PZT-5H	70 × 7 × 0.32-mm <sup>3</sup>	50 km hr <sup>-1</sup>		140 μW	36
PZT	35 × 35 × 25 mm <sup>3</sup>	60 km hr <sup>-1</sup>		88 μW	38
PVDF	25 X 1 2 X 0,1 mm <sup>3</sup>	90 km hr <sup>-1</sup>		5,6 μW	39
PVDF	9X1,3X0,14 mm <sup>3</sup>		10–22 Hz	10 μW	40

*Table 5: Energy harvesting system based on piezoelectric materials results on literature*

For the study as we can see on table 5, many research used PZT, PVDF, piezoelectric polymer, the dimensions are small. Speed is between 50-90 km. hr<sup>-1</sup> for the test. Frequency are between 1-400Hz. And power is between 5,6 - 300 μW. With these result it is possible see that it is impossible think about use of piezoelectric material as primary source of energy.

## 9.2 Pacemakers

The wide diffusion of implantable medical devices has been raising the quality of life and life expectancy. The artificial pacemaker, for example has saved over 3 million lives to date, and every year 600,000 new pacemakers are implanted inpatients. Ideally, implantable electronic devices are expected to work automatically inside bodies for years without maintenance. However, the commonly used electrochemical batteries cannot constantly supply power for long enough. It is therefore useful to find practical methods to increase the energy density and lifespan of power sources. By harnessing energy from the nonstop body motions, energy harvesters supply a perpetual approach to achieve lifelong autonomous operations of medical implants. Powering medical implants by harvesting a small part of energy from body motions without any side effects is a true possibility. To secure years of autonomous operations, low

power consumption has become one of the most critical requirements for the design of biomedical implants. And most of these implants require power less than 1 mW, and the artificial cardiac pacemaker only consumes 5–10 mW. The required microwatt level power is trivial compared with the rich mechanical energy associated with body motions. The artificial cardiac pacemaker is an interesting application for energy harvesters and has attracted much attention from both the engineering and medical fields. The longevity of pacemakers is mainly decided by the battery lifespan. Currently pacemakers are powered by lithium-iodine cells, which theoretically can support pacemakers to operate uninterruptedly for up to 10 years. However, the lifespan of a pacemaker depends upon the frequency of use, and is usually less than 7 years, which is not satisfactory especially for the increasing number of young patients (as young as 2 years old). Also, new functions, such as biventricular pacing (three electrodes), consume more energy than current pacemakers (one electrode). Energy harvesters hold therefore great potential to prolong the lifespan of pacemakers and supply extra power for new functions.

Design of energy harvesters for pacemakers is much more challenging than that for industrial applications because of the very limited space, which is typically less than  $1\text{ cm}^3$ . Furthermore, human motion is most of the time in a low frequency range under 10 Hz. As a rule of thumb, the smaller the size of the harvester, the higher will be the resonant frequency. This means it is necessary to develop a compact energy-harvesting system that can work under ultra-low-frequency excitations with an ultra-high efficiency. Both the electromagnetic effect and piezoelectric effect have been explored to harvest energy for pacemakers. The mass imbalance oscillation generator in automatic wristwatches has been tested, and generated a power of 16.7mW from the cardiac wall motion of a sheep. Due to the very limited space, PEHs are supposed to show better performance than electromagnetic counter-parts. We will mainly have focused on powering pacemakers using PEHs.

There are mainly three excitation sources that have been studied for energy harvesters in pacemakers: heart beats, blood pressure gradients, and arterial wall deformation.

The cyclic heart beat causes vibration and deformation of the myocardium at a frequency of 1-3Hz. The frequency depends on a person's activity and morphology. The induced strain on the myocardium is 15%–23% in the radial direction and 9%–12% in the circumferential direction. The blood pressure gradient, in a healthy body, varies with amplitude of about 20–100 mmHg (2.7–13.3 kPa) in right and left ventricles, and about 40 mmHg (5.3 kPa) in the arterial system.

For arterial wall deformation, it has been reported that the diameter of the distal abdominal aorta varies between 15.8 mm (blood pressure 118 mmHg) and 17.3 mm (blood pressure 64 mmHg) at a heart rate of 66 beats per minute. The diameter variation of the carotid artery is about 10% between the diastolic and systolic period. The human brachial artery experiences a diameter distension of 3.7%.

Blood flow is also a possible energy source for energy harvesters. However, concerns such as the blood cell damage from rotating blades and the risk of vortex-induced thrombi impede research endeavors on flow-based energy harvesters for pacemakers.

Talking about energy harvesters that use the heart motions, in early 2011, Inman's group (reference 42,43) started to explore the possibility of utilizing the heartbeat-induced vibration energy inside the chest to power pacemakers. A battery roughly occupies two-thirds of the volume of a pacemaker ( $\sim 42 \times 51 \times 6 \text{ mm}^3$  of Biotronik's device), and thus an inserted harvester should not be designed to be larger than the battery volume. Within such a small space and restricted weight, linear PEHs will have resonant frequencies much higher than that of the heartbeat excitation. To lower the resonant frequency, in 2017 Ansari and Karami (44) proposed a fan-folded structure that consists of bimorph beams folding on top of each other. A  $1\text{-cm}^3$  prototype was constructed with three bimorph beams (PZT-5A layer:  $20 \times 5 \times 0.19 \text{ mm}^3$ ) and a tip mass of 18.4 g. The prototype was excited by a normal heartbeat waveform from a feedback-controlled shaker, and generated 16mW power on average. As well as the fan-fold, structure.

In addition to rigid mechanical devices encapsulated in the solid pacemaker case, researchers have also tried to develop soft energy harvesters that can be directly attached to hearts and extract energy from the deformation of the myocardium. In 2014, Dagdeviren et al. (45) proposed a strain-based harvester for conformal energy harvesting from the contraction and relaxation motions of the heart. The Figure below shows schematically the PZT thin-film harvester.

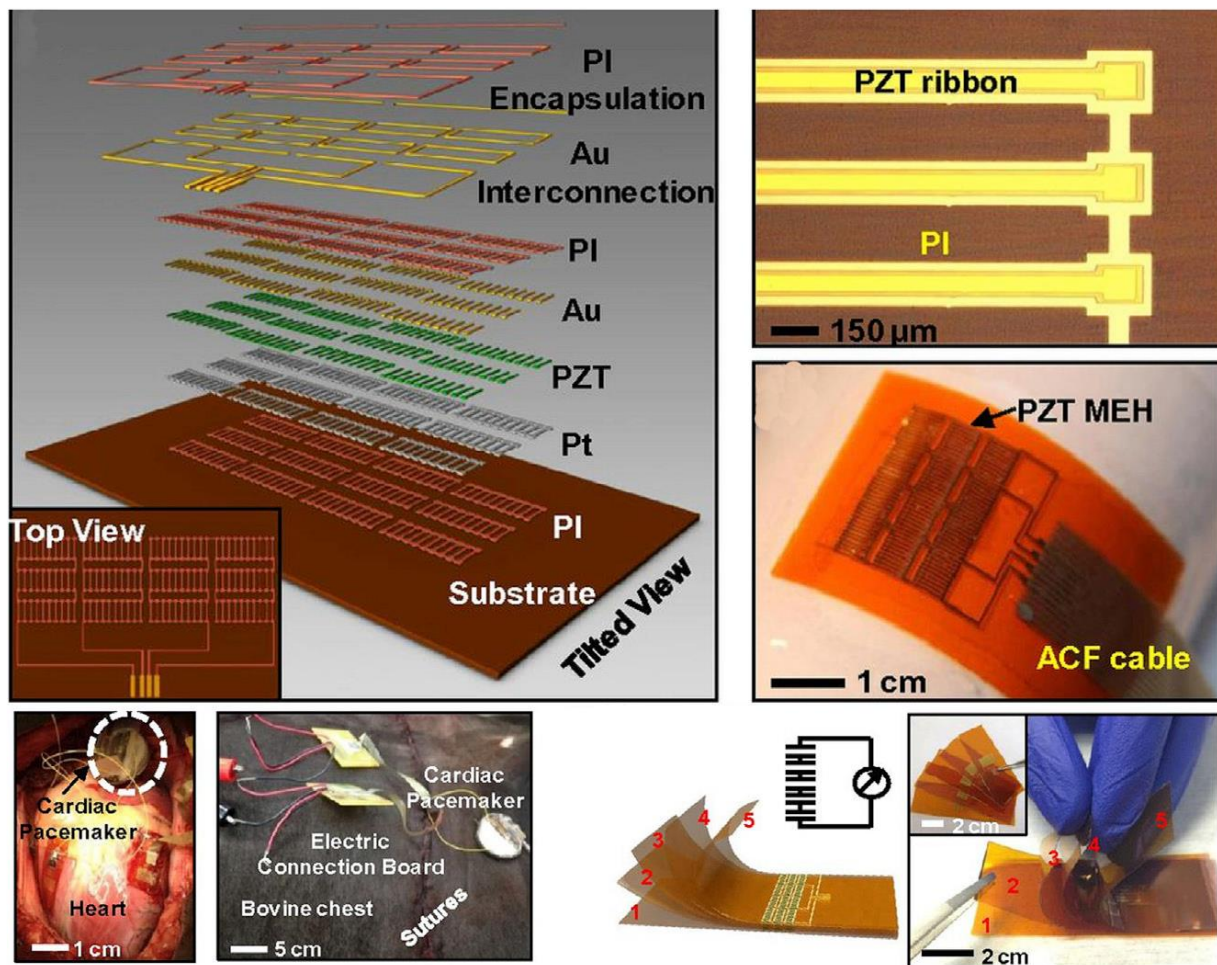


*Figure 9.5: Conformal Piezoelectric Energy Harvesting and Storage from Motions of the Heart, lung and diaphragm.*

Thin PZT ribbons (500 nm in thickness) were sandwiched between metal electrodes, fixed on a thin spin-cast PI substrate layer, and encapsulated with biocompatible materials. The harvester was further integrated with a bridge rectifier and a millimeter-scale battery for simultaneous power generation and storage. The thin PZT ribbon composite showed a superior stability and was sustained after 20 million bending cycles. The flexible piezoelectric patch was affixed on the surface of the ventricles of bovine and ovine hearts. The thin-film harvester generated a maximum open-circuit voltage of 4–5 V and its maximum power density could reach  $1.2 \mu\text{Wcm}^{-2}$  when using multi-layer stacks.

Regarding methods to harvest energy from blood pressure gradients, the piezoelectric diaphragm is the most widely studied structure in this application. As shown in the figure below, the harvester typically consists of a substrate layer with a thin piece of piezoelectric element attached on one side. The other side is exposed to the low-frequency blood pressure variation.

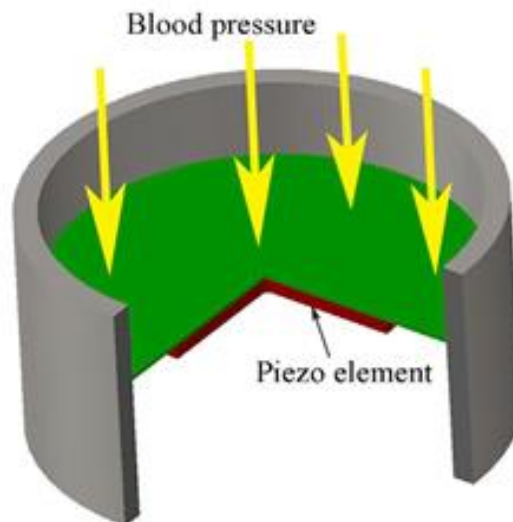


*Figure 9.6: Schematic of piezoelectric diaphragms to harvest energy from blood pressure variations.*

It has been shown that a prototype made of a  $\Phi 25 \times 0.11$  mm PZT layer on  $\Phi 45 \times 0.1$  mm brass diaphragm generated a maximum voltage of 10 V and maximum energy per cycle of  $25 \mu\text{J}$  under a 50 mmHg air pressure variation (2 Hz). This equates to average power output of about  $50 \mu\text{W}$ . The energy per cycle refers to the highest energy stored in the piezoelectric elements. It is calculated via the equation: half of capacitance of the piezoelectric element times squared maximum voltage over the electrodes. This calculation overestimates the harvester performance because, in an energy-harvesting system, the effective energy that can be finally consumed by a target electric load is much less than the energy stored in the piezoelectric elements. No in vivo tests have been performed. As these diaphragm harvesters need one side of the diaphragm structure to be exposed to the blood flow, possible installation sites may be located along the endocardium and the endothelium of large arteries. Another structure to harvest energy from blood pressure gradients is a micro-spiral piezoelectric transducer associated with a novel micro-fabricated packaging that captures energy from blood pressure variations in the cardiac environment. This is intended for use as a leadless pacemaker that resides inside a heart. As shown in Figure 9.8, the system consists of an ultra-flexible electrodeposited micro-bellows ( $21 \text{ mm}^3$  volume), a micro-machined spiral-shaped piezoelectric bimorph, and a 1-mm diameter coupling rod.

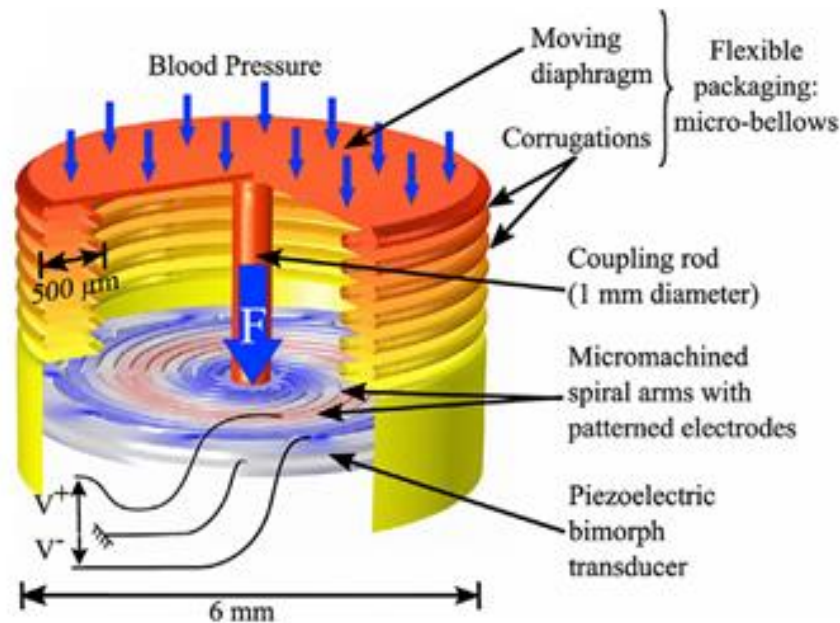


*Figure 9.7: A micro-spiral piezoelectric transducer that captures energy from blood pressure variations.*

The coupling rod is fixed on a spiral-shaped bimorph on one end, and connects the top surface of the micro-bellows on the other end. The top surface is only 12  $\mu\text{m}$  in thickness so that we can regard it as a diaphragm. Both the top diaphragm and deformable bellows contribute to the total flexibility of the harvester.

Regarding methods to harvest energy from arterial wall deformations, harvesters on blood vessels are prohibited to hamper blood flow and arterial movement. Therefore, soft piezoelectric materials such as PVDF films are preferred in this application. It has been designed in 2008 a PVDF cuff surrounding arterial blood vessels. A small  $25 \times 8 \times 0.028 \text{ mm}^3$  PVDF film was embedded inside a  $0.25 \text{ cm}^3$  self-curling silicone cuff. The harvester was tested on a mock artery (latex tubing). On average, 6 nW power was generated from  $\sim 80 \text{ mmHg}$  blood pressure variation through the  $\Phi 12.7 \text{ mm}$  latex tubing. In 2015, a similar PVDF harvester was tested on the ascending aorta of a pig heart, as shown in Figure 9.8.

They first evaluated the performance of the flexible PVDF harvester on a latex tube. A  $25 \times 56 \times 0.2 \text{ mm}^3$  prototype showed a maximum output power of 681 nW and a maximum voltage of 10.3 V, respectively, under a pressure variation of 80 mmHg, 160 beats per minute. When wrapping the PVDF film around the ascending aorta of a porcine heart, a maximum voltage of 1.5 V was achieved under the heart rate of 120 beats per minute and blood pressure of 160/105 mmHg. The implanted harvester is able to charge a 1-mF capacitor to 1.0 V within 40 s. It is roughly estimated that the average power output is about 12.5 nW.

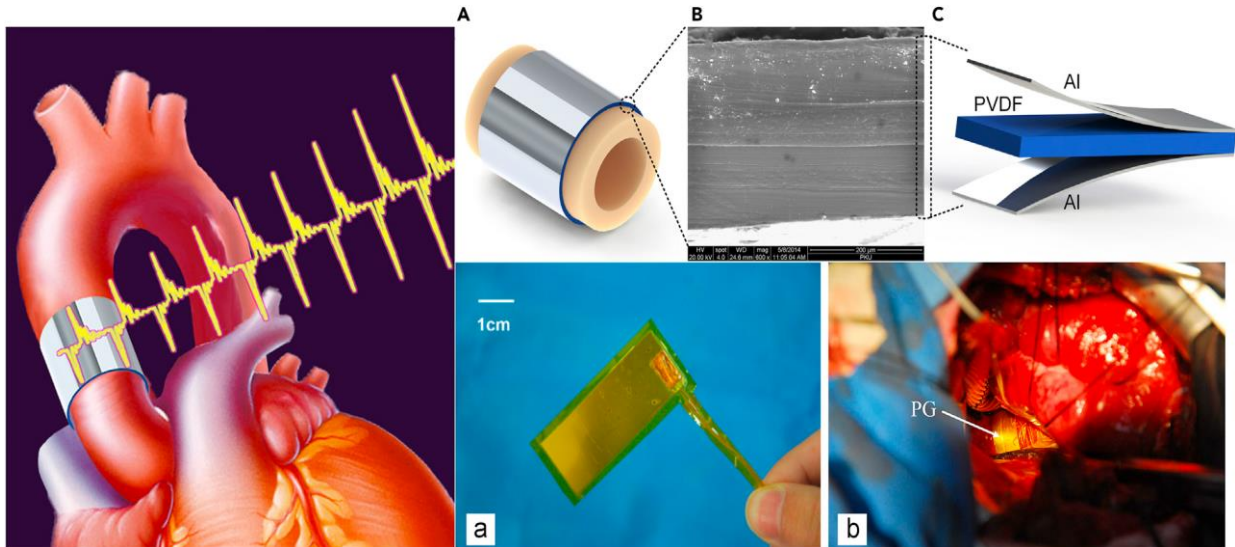


*Figure 9.8: A PVDF Harvester that Captures Energy from the Arterial Wall Deformation*

## 9.3 Others applications

### 9.3.1 Building and Bridges

In the field of high-rise buildings and long-span bridges, structural monitoring systems are used for maintenance, early-stage degradation detection and alarm warnings (eg notification earthquakes). Compared with other applications there is almost no space limitation for bridges and buildings. Therefore, relatively large-size harvesters can be designed to meet the power requirements from sensors. The power output of the developed PEHs ranges from several microwatts to several mill watts.

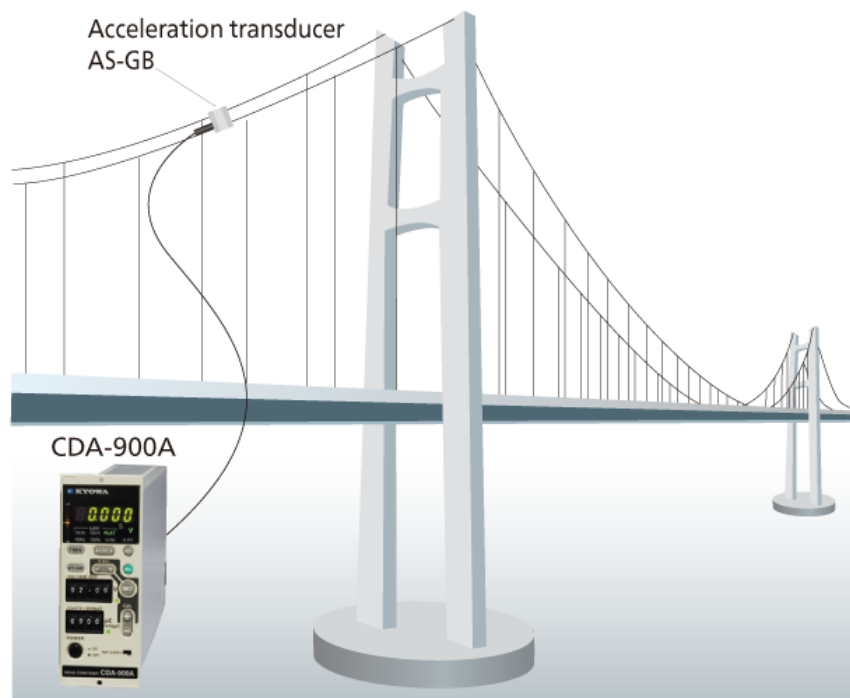
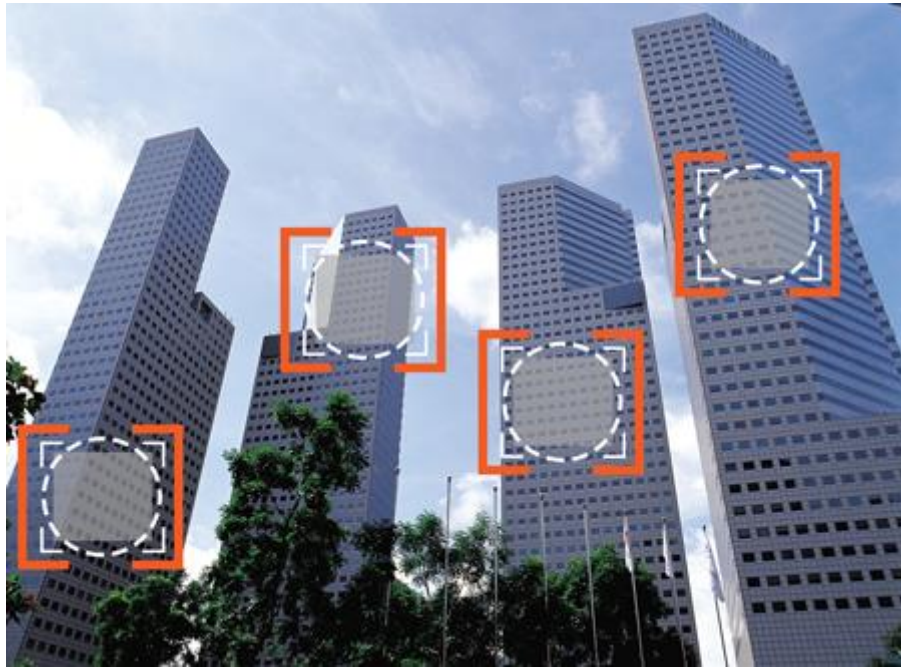


*Figure 9.9: Building and walk energy harvesting systems*

### 9.3.2 Industrial applications

The control of the operation of industrial machinery and the prevention is one of the factors contributing to the continuity of service and therefore to the productivity of a factory. It is therefore imperative to consider this before the installation of any equipment, particularly in the case of equipment located in hostile and inaccessible places. The implantation of systems ensuring permanent

monitoring is confronted with the cabling stress, the limited life of batteries, and in some circumstances the inability to access sensors to replace the battery, this is the case of speed sensors, implanted in rotating machines, hence the advantage of using systems for recovery of ambient energy and vibration energy in particular.

## Conclusion

During this work, which aimed at optimizing a system of energy recovery using piezoelectric material, we first studied the most basic capacitor charging circuits that we developed in introducing each time new elements to understand the role of each element that we can add. We have seen that the energy recovery circuits on which a series-connected inductance coil was added allowed us to considerably increase the voltage level at the source voltage as seen by the capacitor. By increasing this voltage, we can, thanks to our capacitor, produce a current with a greater voltage, thus increasing the current seen by the user at the terminals of the capacitor, the low intensity of the currents produced by the piezoelectric elements is one of the main problems. energy recovery systems.

Then at the time of the study of the mechanical system using the dynamic condensation method proposed by [1] we have a reduced model in which we have a coupling matrix well made without too much error. It should be noted that with the condensation methods used previously, did not allow to have an exact coupling matrix, which was a problem for the calculation of piezoelectric elements. But with the new model ensuring a good coupling matrix we have an optimal system.

At the end of the first part study it emerges that the SSHI with the series coil is better technique than all the technique we study to recover the energy of our vibratory system by means of piezoelectric elements. Using SSHI with coil series to simulate a PZT cantilever beam, we recovered  $1,13 \times 10^{-8} \text{W}$ .

Studying piezoelectric energy harvesting application for TPMS devices, we see that many research used PZT, PVDF, and piezoelectric polymer, with small's dimensions. Speed of car is between  $50\text{-}90 \text{ km. hr}^{-1}$  for the test. Frequency are between  $1\text{-}400\text{Hz}$ . And power is between  $5,6 - 300 \mu\text{W}$ . We see that there are also many applications using energy harvesting systems based on piezoelectric material like on the building and bridge for maintenance, early-stage degradation detection and alarm warnings.

## General Conclusion

During this work, which aimed to optimize a vibratory energy recovery system using piezoelectric materials, the problem is to design and optimize a vibratory energy recovery system based on piezoelectric materials for the purpose of feed a TPMS.

We first made a bibliographic study, bringing it closer to our case each time. In this study, we quoted the energy sources in the environment as well as the problems related to their use for our energy recovery system thus demonstrating the choice of vibratory energy that has a good power to power the MEMS. It is all the more available in large quantities in the tire and easily accessible for its use. Then doing a quick study on the various energy recovery systems and their characteristics, in particular the electromagnetic recovery system, the electrostatic recovery system, and the piezoelectric recovery system because of the large voltages of currents at the outputs of the piezoelectric element, and also because of the ease of miniaturization we chose the piezoelectric device. Finally, we chose a beam structure for our system presenting the equations allowing to calculate theoretically the power as well as the factors influencing the mechanical model.

Then we studied the capacitor charge circuits starting with the most basic recovery circuits powered by a DC voltage source. We have developed the circuits by introducing each time new elements to understand the role of each element, and also to see the limits of use of each element in our circuits. We have seen that the energy recovery circuits on which a series-connected inductance coil was added allowed us to significantly increase the voltage level at the source as seen by the capacitor, thus the losses were damped. By increasing the current induced by the coil, we can, thanks to our capacitor, produce a current with a higher tension, and a greater intensity. We then saw that our circuit was charging just for short while then was discharging. We then used the SSD circuits that connect the piezoelectric element to the load circuit for now when we are at the levels of the spades on the mechanical system. Among the vibratory energy recovery circuits that we developed by comparing the accumulated energy, we saw that the SSHI recovery circuits were the best but we faced the problem of setting the switch. The SSHI with the serial coil was of all the circuits we designed the best energy recovery circuit. The simulation of the SSHI circuit with coil in parallel was difficult because I did not know how to properly adjust the switch.

After we made the choice of a mechanical structure that of a beam with a mass above to amplify the vibrations perceived by the piezoelectric element, By choosing the piezoelectric element, we looked at what is used by other researchers, we chose the PZT-2 because of its ability to work in a wide frequency range and can produce a great energy efficiency with the only defect that is fragile and cannot bear large load. The simulation on the Comsol software allowed us to have the mass matrix, the stiffness matrix, the piezoelectric element capacity, and the coupling matrix using the dynamic condensation method proposed in the article [1]. It should be noted that with the condensation methods used previously, it had the drawback of not giving an exact coupling matrix, which posed a great problem for the calculation of the coupling matrices of the piezoelectric device. However, with the new model ensuring a good coupling matrix, we have an optimal system. After we have used the data acquired from the Comsol simulation of our piezoelectric element to use it as a source in our previously simulated SSHI circuit, we obtain for an excitation frequency of 1000HZ a power of 113 $\mu$ W.

In studying piezoelectric energy recovery applications for TPMS devices, we found that many searches used PZT, PVDF, and a small piezoelectric polymer. The speed of the car is between 50 and 90 km. hr-

1 for the test. The frequency is between 1 and 400 Hz. And the power is between 5.6 and 300  $\mu\text{W}$ . We find that there are also many applications that use piezoelectric material-based energy recovery systems, such as building and bridge, for maintenance, early-stage degradation detection, and alarm warnings. . Comparing the energy obtained by our system and the energy recovery systems presented on the market, our vibratory energy recovery system is not the best but we are on a good way to be able to apply it to TPMS. We have been able to understand that the main constraint induced by the use of a piezoelectric material is the management of the reactive energy due to the intrinsic capacity and the high voltage levels involved. This specificity of the piezoelectric elements therefore has consequences on the conversion structures in which they are immersed as well as on their control modes. In general, the intrinsically capacitive character leads to having to manage reactive energies in the structure, which contribute either to degrade the power factor or to complicate the structure.

## References

- [1] JIMSS\_Piezo 2008; Mr. Collet and K. A. Cunefare
- [2] (Carrera, 1997, Chattopadhyay, 1997, Bernadou, 2003, Fernadez, 2004, Maurini and dell'Isola, 2004
- [3] (Lin and Abatan 1994, Varadan and Lim 1996, Tzou 1997)
- [4] D. Guyomar, Y. Jayet, L. Petit, E. Lefeuvre, T. Monnier, C. Richard, and M. Lallart, " Synchronized Switch Harvesting Applied to Self-Powered Smart Systems: Piezoactive Microgenerators for Autonomous Wireless Transmitters, " *Sensor. Actuat. A: Phys.*, Vol.138, no.1. pp. 151-160, Jul. 2007.
- [5] Yi, K., Monteil, M., Collet, M., & Chesne, S. (2017). Smart metacomposite-based systems for transient elastic wave energy harvesting. *Smart Materials and Structures*, 26 (3), 035040.
- [6] S. Roundy and P. K. Wright, *Smart Mater. Struct.* **13**(5), 1131–1142(2004). <https://doi.org/10.1088/0964-1726/13/5/018>, [\*\*Google ScholarCrossref\*\*](#)
- [7] S. Roundy, P. K. Wright, and J. Rabaey, *Comput. Commun.* **26**(11), 1131–1144 (2003). [https://doi.org/10.1016/S0140-3664\(02\)00248-7](https://doi.org/10.1016/S0140-3664(02)00248-7), [\*\*Google ScholarCrossref\*\*](#)
- [8] D. Shen, Ph.D. dissertation, Auburn University, 2009. [\*\*Google Scholar\*\*](#)
- [9] H. W. Kim, A. Batra, S. Priya, K. Uchino, D. Markley, R. E. Newnham, and H. F. Hofmann, *Jpn. J. Appl. Phys., Part 1* **43**(15), 6178 (2004). <https://doi.org/10.1143/JJAP.43.6178>, [\*\*Google ScholarCrossref\*\*](#)
- [10] H. W. Kim, S. Priya, K. Uchino, and R. E. Newnham, *J. Electroceram.* **15**(1), 27–34 (2005). <https://doi.org/10.1007/s10832-005-0897-z>, [\*\*Google ScholarCrossref\*\*](#)
- [11] H. A. Sodano, G. Park, D. J. Leo, and D. J. Inman, *Proc. SPIE* **5050**, 101–108 (2003). <https://doi.org/10.1117/12.484247>, [\*\*Google ScholarCrossref\*\*](#)
- [12] J. Yuan, T. Xie, and W. Chen, *IEEE Ultrason. Symp.* **1–4**, 1397–1440(2008). [\*\*Google Scholar\*\*](#)
- [13] S. R. Platt, S. Farritor, K. Garvin, and H. Haider, *IEEE/ASME Trans. Mechatron.* **10**(4), 455–461 (2005). <https://doi.org/10.1109/TMECH.2005.852482>, [\*\*Google ScholarCrossref\*\*](#)
-

- [14] M. Renaud, P. Fiorini, R. van Schaijk, and C. Van Hoof, *Smart Mater. Struct.* **18**(3), 035001 (2009). <https://doi.org/10.1088/0964-1726/18/3/035001>, **Google ScholarCrossref**
- [15] S. Li, J. Yuan, and H. Lipson, *J. Appl. Phys.* **109**(2), 026104 (2011). <https://doi.org/10.1063/1.3525045>, **Google ScholarScitation**
- [16] D. L. Churchill, M. J. Hamel, C. P. Townsend, and S. W. Arms, *Proc. SPIE* **5055**, 319–327 (2003). <https://doi.org/10.1117/12.483591>, **Google ScholarCrossref**
- [17] G.-T. Hwang, H. Park, J.-H. Lee, S. Oh, K.-I. Park, M. Byun, H. Park, G. Ahn, C. Jeong, K. No, H. Kwon, S.-G. Lee, B. Joung, and K. J. Lee, *Adv. Mater.* **26**(28), 4880–4887 (2014). <https://doi.org/10.1002/adma.201400562>, **Google ScholarCrossref**
- [18] C. Xu, B. Ren, W. Di, Z. Liang, J. Jiao, L. Li, L. Li, X. Zhao, H. Luo, and D. Wang, *Appl. Phys. Lett.* **101**(3), 033502 (2012). <https://doi.org/10.1063/1.4737170>, **Google ScholarScitation**
- [19] A. Erturk, O. Bilgen, and D. J. Inman, *Appl. Phys. Lett.* **93**(22), 224102 (2008). <https://doi.org/10.1063/1.3040011>, **Google ScholarScitation**
- [20] E. Bischur and N. Schwesinger, *Proc. SPIE* **8688**, 868804 (2013). <https://doi.org/10.1117/12.2009610>, **Google ScholarCrossref**
- [21] R. Shukla, S. A. Qaisar, and A. J. Bell, *IEEE Int. Symp. Appl. Ferroelectr.* **2010**, 1–4. <https://doi.org/10.1109/ISAF.2010.5712228>, **Google ScholarCrossref**
- [22] B. Li, A. J. Laviage, J. H. You, and Y. J. Kim, *Appl. Acoust.* **74**(11), 1271–1278 (2013). <https://doi.org/10.1016/j.apacoust.2013.04.015>, **Google ScholarCrossref**
- [23] L. Dhakar, H. C. Liu, F. E. H. Tay, and C. Lee, *Sens. Actuators, A* **199**, 344–352 (2013). <https://doi.org/10.1016/j.sna.2013.06.009>, **Google ScholarCrossref**
- [24] M. Ericka, D. Vasic, F. Costa, G. Poulin, and S. Tliba, *J. Phys. IV* **128**, 187–193 (2005). <https://doi.org/10.1051/jp4:2005128028>, **Google ScholarCrossref**
- [25] A. Couture, B. Goodman, F. Z. Mahhou, and M. F. Tariq, University of Limerick, 2012. **Google Scholar**
- [26] F. Mohammadi, A. Khan, and R. B. Cass, in *Electronics on Unconventional Substrates- Electrotexiles and Giant-Area Flexible Circuits*, edited by M. S. Shur, P. M. Wilson, and D. Urban (Mater. Res. Soc. Symp. Proc., 2003), Vol. 736, pp. 263–268. **Google Scholar**
- [27] Huidong Li, Chuan Tian, and Z. Daniel Deng, *Applied Physics Reviews* **1**, 041301 (2014); <https://doi.org/10.1063/1.4900845>
- [28] Wikipedia <https://fr.wikipedia.org/wiki/Pi%C3%A9zo%C3%A9lectricit%C3%A9>
- [29] F. Auzanneau Wire troubles hooting and diagnosis: review and perspectives

Prog. Electromagn. Res. B, 49 (2013), pp. 253-279

[30] C. Bowen, M. Arafa **Energy harvesting technologies for tire pressure monitoring systems**  
Adv. Energy Mater., 5 (2015)

[31] Löhndorf, M., Kvisterøy, T., Westby, E., and Halvorsen, E. (2007). Evaluation of energy harvesting concepts for tire pressure monitoring systems. Proceedings of Power MEMS, p. 331–334.

[32] K.H. Mak, S. McWilliam, A.A. Popov **Piezoelectric energy harvesting for tyre pressure measurement applications**

J. Automobile Eng., 227 (2013), pp. 842-852

[Cross Ref](#) [View Record in Scopus](#) [Google Scholar](#)

[33] K.B. Singh, V. Bedekar, S. Taheri, S. Priya **Piezoelectric vibration energy harvesting system with an adaptive frequency tuning mechanism for intelligent tires**

Mechatronics, 22 (2012), pp. 970-988

[34] Elfrink, R., Matova, S., de Nooijer, C., Jambunathan, M., Goedbloed, M., van de Molengraft, J., Pop, V., Vullers, R.J.M., Renaud, M., and van Schaijk, R. (2011). Shock induced energy harvesting with a MEMS harvester for automotive applications. In Electron Devices Meeting (IEDM), 2011 IEEE International. IEEE.

[35] Q. Zheng, H. Tu, A. Agee, Y. Xu **Vibration energy harvesting device based on asymmetric air-spaced cantilevers for tire pressure monitoring system**

Proceedings of Power MEMS (2009), pp. 403-406

[36] B. Zhu, J. Han, J. Zhao, W. Deng **Practical design of an energy harvester considering wheel rotation for powering intelligent tire systems**

J. Electron. Mater., 46 (2017), pp. 2483-2493

[37] Y. Zhang, R. Zheng, K. Shimono, T. Kaizuka, K. Nakano **Effectiveness testing of a piezoelectric energy harvester for an automobile wheel using stochastic resonance**

Sensors, 16 (2016), p. 1727

[38] Jousimaa JO, Parmar, M et Lee, D,W. (2016). Système de récupération d'énergie par capteurs de pneus intelligents dans le Symposium sur les véhicules intelligents (IV), 2016 IEEE.

[39] X. Wu , M. Parmar , D.-W. Lee **Un récupérateur d'énergie structuré à bascule avec une bande passante très étendue pour l'application TPMS** IEEE / ASME

Trans. Mechatronics , 19 ( 2014 ) , pp. 1514 - 1522

[40] proche Tang, Q., Xia, X., et Li, X .. Capteur d'énergie sans conversion, à conversion de fréquence ascendante pour application TPMS automobile durable et à large bande. in Micro

Electro Mechanical Systems (MEMS), 25ème conférence internationale IEEE 2012. 2012. IEEE.

[41] Zhengbao Yang, Shengxi Zhou, Jean Zu, Daniellnman High-Performance Piezoelectric Energy Harvesters and Their Applications

Science direct: Joule Volume 2, Issue 4, 18 April 2018, Pages 642-697 Show more  
<https://doi.org/10.1016/j.joule.2018.03.011>

[42] M.A.Karami, D.J. Inman Powering pacemakers from heartbeat vibrations usins linear and nonlinear energy harvesters. Appl.Phys.Lett, 100 (2012),p. 042901.

[43] Karami, M.A, and Inman, D.J. (2011). Linear and nonlinear enrgy harversters for powering pacemakers from heart beat vibrations. In Active and Passive Smart Structures and Integrated Systems 20122. International Society for Optics and Photonics.

[44] M. Ansari, M.A. Karami Experimental investigation of fan-folded piezoelectric energy harvesters for powering pacemakers Smart Mater. Struct, 26 (2017), p. 065001

[45] C. Dagdeviren, B.D. Yang, Y. Su, P.L. Tran, P. Joe, E. Anderson, J. Xia, V. Doraiswamy, B. Dehdashti, X. Feng, et al.Conformal piezoelectric energy harvesting and storage from motions of the heart, lung, and diaphragm Proc. Natl. Acad. Sci. USA, 111 (2014), pp. 1927-1932 CrossRefView Record in ScopusGoogle Scholar

# Annex

## Matlab Script

```
clear
% close all
clc

%% Param modÃ¨le - Badel JIMSS - 2006
f0=35.34;
f1=35.52;
xi=0.001;
lambda=6.33e4;
C0=55.8e-9;
Ke=2.17e4;
M=0.440;
Cdamp=0.216;

alph=lambda*C0;

Qi=2.6;
gamma=exp(-pi/(2*Qi));

%omega0=2*pi*f0;

% law coupling
omega0=sqrt(Ke/M);

% strong coupling
% Ã modifier pour trouver la "bonne" frÃ©quence de rÃ©sonance dans le cas du
%ftest=35.512
%omega0=2*pi*ftest

f0=omega0/2/pi

um=.001;
I0=sqrt(omega0^2*um^2*Cdamp^2);
Plim=I0^2/8/Cdamp;

%% Param simu

Rostand = 1/4/f0/C0;
Ropara = 1/2/(1-gamma)/f0/C0;
```

```

Roserie = 1/4/f0/C0 * (1-gamma)/(1+gamma);

RoparaFcste = pi/C0/(1-gamma)/omega0;

[A,B,C,D,C_Courant]=SystemeEtat(M,Cdamp,Ke,alph,C0);
C_Tension = [alph/C0, 0];

%R_SSHI=Rostand;
%R_SSHI=Ropara;
%R_SSHI=Ropara;
%R_SSHI=Roserie
%R_SSHI=RoparaFcste;
R_SSHI=1.8e4;

C_SSHI=10/R_SSHI;
tau = R_SSHI * C_SSHI

[C_SSHI,R_SSHI,L2,r2,r_switch,delta_SSHI]=Param_SSHI(C_SSHI,R_SSHI,gamma,f0,C0
);

%% Paramètres de simu
% -----
dt=1e-5;
%dt=1e-4;
A_sinus1=I0;
Omega_source = 2*pi*f0;
T0=1/f0;
ech=T0/dt;

```

```

%% SSHI
% -----

function
[C_SSHI,R_SSHI,L2,r2,r_switch,delta_SSHI]=Param_SSHI(C_SSHI,R_SSHI,gamma,f0,C0
)

% inversion time Lalart page 66
tI=(1/f0)/50;
L2=(tI/pi)^2 / C0;

% r2
% gama=Vpar/s/Vavant < 1 : 0.75=valeur standard
%gama=.75;
% facteur de qualite
Qi=1/log(gamma)*(-pi) /2;
%%r2 = (1/Qi)* sqrt(L2/C0)
% Calcul des capac en serie
C_ssh_serie=C_SSHI*C0/(C_SSHI+C0);
% valeur de la resistance de la bobine dans SSHI
r2=(1/Qi)*sqrt(L2/C_ssh_serie);

r2=1.05e3
%r2=1.16e3

% r_switch
r_switch=1e-20; % valeur standard entre 1 et 10

% damping factor of SSHI
e_boost_sshi=0.5*r2*sqrt(C_ssh_serie/L2);
% Période du circuit
Periode_SSH=2*pi*sqrt(L2*C_ssh_serie)/sqrt(1-e_boost_sshi^2);
delta_SSHI=Periode_SSH/2;

```

```
%% State system
```

```
% -----
```

```
function [A,B,C,D,Cc]=SystemeEtat(M,C,Ke,alph,C0)
```

```
% Matrice d'evolution
```

```
A = [0 1 ; -Ke/M -C/M];
```

```
% Matrice d'activation
```

```
B = [0 0 ; 1/M -alph/M];
```

```
% Matrice d'observation
```

```
C = eye(2,2);
```

```
% Matrice d'action directe
```

```
D = zeros(size(B));
```

```
% Recomposition de la sortie en courant
```

```
Cc = [0,alph];
```